

$R(D^{(*)})$ in a general two Higgs doublet model

Syuhei Iguro¹ and Kazuhiro Tobe^{1,2}

¹*Department of Physics, Nagoya University, Nagoya, 464-8602, Japan*

²*Kobayashi-Maskawa Institute for the Origin of Particles and the Universe,
Nagoya University, Nagoya, 464-8602, Japan*

Abstract

Motivated by an anomaly in $R(D^{(*)}) = \text{BR}(\bar{B} \rightarrow D^{(*)}\tau^{-}\bar{\nu})/\text{BR}(\bar{B} \rightarrow D^{(*)}l^{-}\bar{\nu})$ reported by BaBar, Belle and LHCb, we study $R(D^{(*)})$ in a general two Higgs doublet model (2HDM). Although it has been suggested that it is difficult for the 2HDM to explain the current world average for $R(D^{(*)})$, it would be important to clarify how large deviations from the standard model predictions for $R(D^{(*)})$ are possible in the 2HDM. We investigate possible corrections to $R(D^{(*)})$ in the 2HDM by taking into account various flavor physics constraints (such as $B_c^{-} \rightarrow \tau^{-}\bar{\nu}$, $b \rightarrow s\gamma$, $b \rightarrow sl^{+}l^{-}$, $\Delta m_{B_{d,s}}$, $B_s \rightarrow \mu^{+}\mu^{-}$ and $\tau^{+}\tau^{-}$, and $B^{-} \rightarrow \tau^{-}\bar{\nu}$), and find that it would be possible (impossible) to accommodate the 1σ region suggested by the Belle's result when we adopt a constraint $\text{BR}(B_c^{-} \rightarrow \tau^{-}\bar{\nu}) \leq 30\%$ ($\text{BR}(B_c^{-} \rightarrow \tau^{-}\bar{\nu}) \leq 10\%$). We also study productions and decays of heavy neutral and charged Higgs bosons at the Large Hadron Collider (LHC) experiment and discuss the constraints and implications at the LHC. We show that in addition to well-studied production modes $bg \rightarrow tH^{-}$ and $gg \rightarrow H/A$, exotic productions of heavy Higgs bosons such as $cg \rightarrow bH^{+}, t + H/A$ and $c\bar{b} \rightarrow H^{+}$ would be significantly large, and the search for their exotic decay modes such as $H/A \rightarrow t\bar{c} + c\bar{t}$, $\mu^{\pm}\tau^{\mp}$ and $H^{+} \rightarrow c\bar{b}$ as well as $H/A \rightarrow \tau^{+}\tau^{-}$ and $H^{+} \rightarrow \tau^{+}\nu$ would be important to probe the interesting parameter regions for $R(D^{(*)})$.

I. INTRODUCTION

The standard model of elementary particles has been very successful to explain phenomena in nature. Recently, however, there are several observables in experiments, which may be suggesting the existence of new physics. For example, measurements of $b \rightarrow c$ transition processes $\bar{B} \rightarrow D^{(*)}l^{-}\bar{\nu}$ at BaBar [1, 2], Belle [3–5] and LHCb [6, 7] indicate a discrepancy between the experimental and theoretical values of

$$R(D^{(*)}) = \frac{\text{BR}(\bar{B} \rightarrow D^{(*)}\tau^{-}\bar{\nu})}{\text{BR}(\bar{B} \rightarrow D^{(*)}l^{-}\bar{\nu})}, \quad (1)$$

where $l = e$, or μ . Measurements of $b \rightarrow s$ transition process $B \rightarrow K^{*}\mu^{+}\mu^{-}$ at Belle [8], ATLAS [9], CMS [10], BaBar [11] and LHCb [12] also suggest an anomaly in the angular observable and moreover the LHCb has reported deviations from the SM predictions in $R_K^{(*)} = \text{BR}(B \rightarrow K^{(*)}\mu^{+}\mu^{-})/\text{BR}(B \rightarrow K^{(*)}e^{+}e^{-})$ [13]. A discrepancy between experimental and theoretical values of the muon anomalous magnetic moment has been also well-recognized [14]. These anomalies may indicate some hints of new flavor structure beyond the standard model.

One of the simplest extensions of the standard model is a two Higgs doublet model (2HDM). When both Higgs doublets couple to all fermions, it is notorious that the Higgs bosons have flavor violating interactions even at tree level, and it tends to induce the large flavor violating phenomena. Therefore, without any experimental supports, it would be difficult to justify this kind of extension. As we mentioned above, however, currently there are several indications which may support the extra flavor violation beyond the standard model, and hence we seriously consider a general type of two Higgs doublet model as a possibility to explain some of the anomalies mentioned above. In Refs. [15–17], it has been pointed out that $\mu - \tau$ flavor violations in the general 2HDM may be able to explain the muon $g - 2$ anomaly.¹ In this paper, we concentrate on $R(D^{(*)})$ in the general 2HDM.

¹ Although recently the CMS collaboration reported a stronger constraint on the lepton flavor violating Higgs boson decay $h \rightarrow \mu\tau$ [18], the $\mu - \tau$ flavor violations in the general 2HDM can still explain the muon $g - 2$ anomaly, which is consistent with the recent CMS constraint, as seen in Refs. [16, 17].

The current status of $R(D^{(*)})$ measurements is summarized in Table I. Although results are not conclusive, the current measured average values deviate from the SM prediction about 4σ .

Experiment	$R(D^*)$	$R(D)$	References
BaBar	$0.332 \pm 0.024 \pm 0.018$	$0.440 \pm 0.058 \pm 0.042$	[1, 2]
Belle	$0.293 \pm 0.038 \pm 0.015$	$0.375 \pm 0.064 \pm 0.026$	[3]
	$0.302 \pm 0.030 \pm 0.011$	—	[4]
	$0.270 \pm 0.035^{+0.028}_{-0.025}$	—	[5]
LHCb	$0.336 \pm 0.027 \pm 0.030$	—	[6]
	$0.285 \pm 0.019 \pm 0.029$		[7]
Average	$0.304 \pm 0.013 \pm 0.007$	$0.407 \pm 0.039 \pm 0.024$	[19]

TABLE I: Current status of experimental measurements of $R(D^{(*)})$. The SM prediction for $R(D^*)$ is $R(D^*) = 0.252 \pm 0.003$ [20], The SM predictions for $R(D)$ based on recent Lattice calculations are $R(D) = 0.299 \pm 0.011$ [21], $R(D) = 0.300 \pm 0.008$ [22] and $R(D) = 0.299 \pm 0.003$ [23]. See also Refs. [24, 25].

In order to study the anomaly, a model-independent effective operator approach [26–28, 30–32] is very useful to understand what type of interaction is relevant to the anomaly. On the other hand, to identify the new physics model and to know constraints from other processes and possible correlation among other phenomena, it is necessary to study the anomaly in a model-dependent way. Furthermore, the anomaly would be explained by the new particles whose masses are of $O(1)$ TeV scale. The current Large Hadron Collider (LHC) experiment is powerful to investigate such $O(1)$ TeV scale physics as stressed in Refs. [33, 34]. Therefore the interplay between the flavor physics and LHC physics would be also very helpful to probe a source of the anomaly.

Several studies on $R(D^{(*)})$ have been done in the general 2HDM (for example, see Refs. [26, 35–40]), and it seems difficult for the 2HDM to explain the anomaly of $R(D^{(*)})$ within 1σ of the current world average. However, it has not been clear how large deviations from the SM predictions of $R(D^{(*)})$ are possible when the

various constraints from other processes are taken into account, and hence we would like to clarify the predictions of $R(D^{(*)})$ in the general 2HDM. Since the current experimental results and SM predictions are subject to improve in future, it is important to understand the possible predicted values of $R(D^{(*)})$ in the general 2HDM. Furthermore, we would like to show how the LHC experiment can probe the source for the anomaly of $R(D^{(*)})$, and thus the interplay between flavor physics and LHC physics would be very important to test the new physics model.

This paper is organized as follows: In section II, we briefly review a general 2HDM. In section III, we summarize a formula for $\bar{B} \rightarrow D^{(*)} l^- \bar{\nu}$ ($l = e, \mu, \tau$) in a general 2HDM. In section IV, to study $R(D^{(*)})$ in the general 2HDM, we consider three typical scenarios and show the allowed regions of $R(D^{(*)})$ which are consistent with various flavor physics constraints such as $B_c^- \rightarrow \tau^- \bar{\nu}$, $B_{d,s} - \bar{B}_{d,s}$ mixing, $b \rightarrow s\gamma$, $b \rightarrow sl^+ l^-$, $B_{d,s} \rightarrow \mu^+ \mu^-$, $\tau^+ \tau^-$ and $B^- \rightarrow \tau^- \bar{\nu}$ in each scenario. We also show the result of the type II 2HDM as a comparison. In section V, we study the productions and decays of heavy Higgs bosons at the LHC, and discuss the constraints from the LHC results and implications at the LHC searches. In section VI, we summarize our studies.

II. GENERAL TWO HIGGS DOUBLET MODEL

In a two Higgs doublet model, when the Higgs potential is minimized in the SM-like vacuum, both neutral components of Higgs doublets get vacuum expectation values (vevs) in general. Taking a certain linear combination, we can always consider a basis (so called Higgs basis or Georgi basis [41, 42], and see also, for example, [43–47]) where only one of the Higgs doublets has the vev as follows:

$$H_1 = \begin{pmatrix} G^+ \\ \frac{v+\phi_1+iG}{\sqrt{2}} \end{pmatrix}, \quad H_2 = \begin{pmatrix} H^+ \\ \frac{\phi_2+iA}{\sqrt{2}} \end{pmatrix}, \quad (2)$$

where G^+ and G are Nambu-Goldstone bosons, and H^+ and A are a charged Higgs boson and a CP-odd Higgs boson, respectively. CP-even neutral Higgs bosons ϕ_1

and ϕ_2 can mix and form mass eigenstates, h and H ($m_H > m_h$),

$$\begin{pmatrix} \phi_1 \\ \phi_2 \end{pmatrix} = \begin{pmatrix} \cos \theta_{\beta\alpha} & \sin \theta_{\beta\alpha} \\ -\sin \theta_{\beta\alpha} & \cos \theta_{\beta\alpha} \end{pmatrix} \begin{pmatrix} H \\ h \end{pmatrix}. \quad (3)$$

Here $\theta_{\beta\alpha}$ is the mixing angle. Note that when $\cos \theta_{\beta\alpha} \rightarrow 0$ ($\sin \theta_{\beta\alpha} \rightarrow 1$), the interactions of ϕ_1 approach to those of the SM Higgs boson. In this paper, we adopt Higgs basis. In Appendix A, we summarize a relation between the Higgs basis and the general basis.

If any discrete symmetries are not imposed, both Higgs doublets can couple to all fermions.² In the mass eigenbasis for the fermions, the Yukawa interactions are expressed by

$$\begin{aligned} \mathcal{L} = & -\bar{Q}_L^i H_1 y_d^i d_R^i - \bar{Q}_L^i H_2 \rho_d^{ij} d_R^j - \bar{Q}_L^i (V^\dagger)^{ij} \tilde{H}_1 y_u^j u_R^j - \bar{Q}_L^i (V^\dagger)^{ij} \tilde{H}_2 \rho_u^{jk} u_R^k \\ & - \bar{L}_L^i H_1 y_e^i e_R^i - \bar{L}_L^i H_2 \rho_e^{ij} e_R^j. \end{aligned} \quad (4)$$

Here i, j represent flavor indices, $Q = (V^\dagger u_L, d_L)^T$ and $L = (V_{\text{MNS}} \nu_L, e_L)^T$, where V and V_{MNS} are Cabbibo-Kobayashi-Maskawa (CKM) and the Maki-Nakagawa-Sakata (MNS) matrices, respectively. Here we have assumed the neutrino masses are explained by the seesaw mechanism introducing super-heavy right-handed neutrinos, so that in the low-energy effective theory, the left-handed neutrinos have a 3×3 Majorana mass matrix, which is diagonalized by the V_{MNS} matrix. Note that Yukawa couplings y_f are expressed by the fermion masses m_f , $y_f = \sqrt{2}m_f/v$, on the other hand, Yukawa couplings ρ_f^{ij} are unknown general 3×3 complex matrices and can be sources of the Higgs-mediated flavor violation.

In mass eigenstates of Higgs bosons, the Yukawa interactions are given by

$$\begin{aligned} \mathcal{L} = & - \sum_{f=u,d,e} \sum_{\phi=h,H,A} y_{\phi ij}^f \bar{f}_{Li} \phi f_{Rj} + \text{h.c.} \\ & - \bar{\nu}_{Li} (V_{\text{MNS}}^\dagger \rho_e)^{ij} H^+ e_{Rj} - \bar{u}_i (V \rho_d P_R - \rho_u^\dagger V P_L)^{ij} H^+ d_j + \text{h.c.}, \end{aligned} \quad (5)$$

² Sometimes, this is called the Type III two Higgs doublet model. See, for example, Refs. [48–57] for the model and its phenomenological studies. However, sometimes the Type III 2HDM is referred to as a different type of 2HDM [58], and hence we simply call it general 2HDM.

where

$$\begin{aligned}
y_{hij}^f &= \frac{m_f^i}{v} s_{\beta\alpha} \delta_{ij} + \frac{\rho_f^{ij}}{\sqrt{2}} c_{\beta\alpha}, \\
y_{Hij}^f &= \frac{m_f^i}{v} c_{\beta\alpha} \delta_{ij} - \frac{\rho_f^{ij}}{\sqrt{2}} s_{\beta\alpha}, \\
y_{Aij}^f &= \begin{cases} -\frac{i\rho_f^{ij}}{\sqrt{2}} & (\text{for } f = u), \\ \frac{i\rho_f^{ij}}{\sqrt{2}} & (\text{for } f = d, e), \end{cases}
\end{aligned} \tag{6}$$

where $c_{\beta\alpha} \equiv \cos \theta_{\beta\alpha}$ and $s_{\beta\alpha} \equiv \sin \theta_{\beta\alpha}$. Note that when $c_{\beta\alpha}$ is small, the Yukawa interactions of h are almost equal to those of the SM Higgs boson, however, there are small flavor-violating interactions ρ_f^{ij} which are suppressed by $c_{\beta\alpha}$. On the other hand, the Yukawa interactions of heavy Higgs bosons (H , A , and H^+) mainly come from the ρ_f couplings. Therefore, for the SM-like Higgs boson, the tree level flavor violation can be suppressed by the small mixing $c_{\beta\alpha}$ and for the heavy Higgs bosons, it would be suppressed by their heaviness and/or the smallness of the extra flavor violation.

Here we also stress that the interactions of the charged Higgs boson are simply parameterized by ρ_f Yukawa couplings in the Higgs basis. In order to analyze the effects on $R(D^{(*)})$, we adopt the Higgs basis in our analysis because it is convenient to effectively understand how large deviation from the SM prediction on the $R(D^{(*)})$ is possible in the 2HDM, which is the aim of this paper. To understand the effects on $R(D^{(*)})$, we can consider some simple flavor violation in the Higgs basis. On the other hand, if we consider the simple flavor violation in the original basis, it may correspond to the complex flavor violation in the Higgs basis (as shown in Appendix A), and hence it induces the effects not only on $R(D^{(*)})$ but also on other processes, which may generate strong constraints in the model. In that sense, we expect that our approach is conservative to see the possibly large effects on $R(D^{(*)})$, but consistent with other constraints. Therefore, in our analysis, using the Higgs basis, we try to clarify how large deviations are possible within the framework of the 2HDM in general.

A. Higgs mass spectrum

A scalar potential in the general 2HDM is given by

$$\begin{aligned}
V = & M_{11}^2 H_1^\dagger H_1 + M_{22}^2 H_2^\dagger H_2 - \left(M_{12}^2 H_1^\dagger H_2 + \text{h.c.} \right) \\
& + \frac{\lambda_1}{2} (H_1^\dagger H_1)^2 + \frac{\lambda_2}{2} (H_2^\dagger H_2)^2 + \lambda_3 (H_1^\dagger H_1)(H_2^\dagger H_2) + \lambda_4 (H_1^\dagger H_2)(H_2^\dagger H_1) \\
& + \frac{\lambda_5}{2} (H_1^\dagger H_2)^2 + \left\{ \lambda_6 (H_1^\dagger H_1) + \lambda_7 (H_2^\dagger H_2) \right\} (H_1^\dagger H_2) + \text{h.c.}
\end{aligned} \tag{7}$$

In the basis shown in Eq. (2), Higgs boson masses are related as follows:

$$\begin{aligned}
m_{H^+}^2 &= M_{22}^2 + \frac{v^2}{2} \lambda_3, \\
m_A^2 - m_{H^+}^2 &= -\frac{v^2}{2} (\lambda_5 - \lambda_4), \\
(m_H^2 - m_h^2)^2 &= \left\{ m_A^2 + (\lambda_5 - \lambda_1) v^2 \right\}^2 + 4\lambda_6^2 v^4, \\
\sin 2\theta_{\beta\alpha} &= -\frac{2\lambda_6 v^2}{m_H^2 - m_h^2}.
\end{aligned} \tag{8}$$

Especially, when $c_{\beta\alpha}$ is close to zero (or $\lambda_6 \sim 0$), we approximately get the following expressions for the Higgs boson masses:

$$\begin{aligned}
m_h^2 &\simeq \lambda_1 v^2, \\
m_H^2 &\simeq m_A^2 + \lambda_5 v^2, \\
m_{H^+}^2 &= m_A^2 - \frac{\lambda_4 - \lambda_5}{2} v^2, \\
m_A^2 &= M_{22}^2 + \frac{\lambda_3 + \lambda_4 - \lambda_5}{2} v^2.
\end{aligned} \tag{9}$$

Note that fixing the couplings λ_i , the heavy Higgs boson masses are expressed by the CP-odd Higgs boson mass m_A . We also note that a dangerous contribution to Peskin-Takeuchi's T-parameter are suppressed by the degeneracy between m_A and m_{H^+} or m_A and m_H as well as the small Higgs mixing parameter $c_{\beta\alpha}$.

III. $\bar{B} \rightarrow D^{(*)} l^- \bar{\nu}$ ($l = e, \mu, \tau$) IN A GENERAL 2HDM

A. $\bar{B} \rightarrow D l^- \bar{\nu}$

In the 2HDM, the charged Higgs boson generates a new contribution to $B \rightarrow D l^- \bar{\nu}$. The relevant hadronic matrix elements are parameterized by the form factors

$f_0(q^2)$ and $f_+(q^2)$ as follows [59, 60]:

$$\langle D(p_D) | \bar{c} \gamma^\mu b | \bar{B}(p_B) \rangle = \left(p_B^\mu + p_D^\mu - \frac{m_B^2 - m_D^2}{q^2} q^\mu \right) f_+(q^2) + \frac{m_B^2 - m_D^2}{q^2} q^\mu f_0(q^2), \quad (10)$$

$$\langle D(p_D) | \bar{c} b | \bar{B}(p_B) \rangle = \frac{m_B^2 - m_D^2}{m_b - m_c} f_0(q^2). \quad (11)$$

where p_B and p_D (m_B and m_D) are momenta (masses) of B and D mesons, respectively, and q is a momentum transfer $q = p_B - p_D$ ($m_l^2 \leq q^2 \leq (m_B - m_D)^2$), and m_b and m_c are b and c quark masses, respectively. In Appendix B, we summarize an information on form factors and in Appendix D, we list numerical values of various parameters we use in our numerical analysis.

Then the differential decay rate in the 2HDM is given by

$$\begin{aligned} \frac{d\Gamma(\bar{B} \rightarrow Dl^- \bar{\nu})}{dq^2} &= \frac{G_F^2 |V_{cb}|^2}{192\pi^3 m_B^3} \left(1 - \frac{m_l^2}{q^2}\right)^2 \sqrt{\lambda_D} \\ &\times \left[\lambda_D \left(1 + \frac{m_l^2}{2q^2}\right)^2 f_+(q^2) + \frac{3m_l^2}{2q^2} (m_B^2 - m_D^2)^2 f_0^2(q^2) (1 + \delta_{H^+}^{Dl}(q^2)) \right], \end{aligned} \quad (12)$$

where $\lambda_D = (m_B^2 - m_D^2 - q^2)^2 - 4m_D^2 q^2$. The charged Higgs boson induces the corrections which are proportional to the form factor $f_0^2(q^2)$, and the contributions $\delta_{H^+}^{Dl}$ are expressed by

$$\begin{aligned} \delta_{H^+}^{Dl}(q^2) &= -\frac{q^2}{m_l(m_b - m_c)} \frac{\text{Re} \left[\rho_e^u V_{cb} (\rho_d^\dagger V^\dagger - V^\dagger \rho_u)_{bc} \right]}{\sqrt{2} G_F m_{H^+}^2 |V_{cb}|^2} \\ &+ \frac{q^4}{m_l^2 (m_b - m_c)^2} \frac{(\rho_e^\dagger \rho_e)^u \left| (\rho_d^\dagger V^\dagger - V^\dagger \rho_u)_{bc} \right|^2}{8 G_F^2 m_{H^+}^4 |V_{cb}|^2}, \end{aligned} \quad (13)$$

where m_{H^+} is a charged Higgs boson mass, and ρ_f ($f = e, u, d$) are Yukawa couplings introduced in Eq. (4). The first term in Eq. (13) is an interference between the SM W-boson and charged Higgs boson contributions suppressed by $m_{H^+}^2$, and the second term comes from the charged Higgs boson contribution suppressed by $m_{H^+}^4$.

Notice that the charged Higgs boson contribution to $\Gamma(\bar{B} \rightarrow Dl^- \bar{\nu})$ is proportional to ρ_e^u or $(\rho_e^\dagger \rho_e)^u$. We also note that if $(\rho_d^\dagger V^\dagger - V^\dagger \rho_u)_{bc}$ is small, the charged Higgs boson contribution is suppressed because the scalar coupling $\bar{b}cH^+$ is small. On the other hand, if $(\rho_d^\dagger V^\dagger - V^\dagger \rho_u)_{bc}$ is sizable, the charged Higgs contribution can be significant especially in the large q^2 region.

B. $\bar{B} \rightarrow D^* l^- \bar{\nu}$

The relevant hadronic matrix elements for this process are parameterized by the form factors $V(q^2)$ and $A_i(q^2)$ ($i = 1 - 3$) [59, 60]:

$$\begin{aligned}\langle D^*(p_{D^*}, \epsilon) | \bar{c} \gamma_\mu b | \bar{B}(p_B) \rangle &= -i \epsilon_{\mu\nu\rho\sigma} \epsilon^{\nu*} p_B^\rho p_{D^*}^\sigma \frac{2V(q^2)}{m_B + m_{D^*}} \\ \langle D^*(p_{D^*}, \epsilon) | \bar{c} \gamma_\mu \gamma_5 b | \bar{B}(p_B) \rangle &= \epsilon_\mu^* (m_B + m_{D^*}) A_1(q^2) \\ &\quad - (p_B + p_{D^*})_\mu (\epsilon^* \cdot q) \frac{A_2(q^2)}{m_B + m_{D^*}} - q_\mu (\epsilon^* \cdot q) \frac{2m_{D^*}}{q^2} \{A_3(q^2) - A_0(q^2)\},\end{aligned}\quad (14)$$

$$\langle D^*(p_{D^*}, \epsilon) | \bar{c} \gamma_5 b | \bar{B}(p_B) \rangle = -\frac{1}{m_b + m_c} q_\mu \langle D^*(p_{D^*}, \epsilon) | \bar{c} \gamma^\mu \gamma_5 b | \bar{B}(p_B) \rangle \quad (15)$$

where

$$A_3(q^2) = \frac{m_B + m_{D^*}}{2m_{D^*}} A_1(q^2) - \frac{m_B - m_{D^*}}{2m_{D^*}} A_2(q^2). \quad (16)$$

Here p_{D^*} and m_{D^*} are momentum and mass of D^* , respectively, and q is a momentum transfer $q = p_B - p_{D^*}$. In Appendix B, we summarize an information on the form factors.

The differential decay rate in the 2HDM is given by

$$\begin{aligned}\frac{d\Gamma(\bar{B} \rightarrow D^* l^- \bar{\nu})}{dq^2} &= \frac{G_F^2 |V_{cb}|^2}{192\pi^3 m_B^3} \left(1 - \frac{m_l^2}{q^2}\right) \sqrt{\lambda_{D^*}} \\ &\times \left[\left(1 + \frac{m_l^2}{2q^2}\right) \left\{ q^2 (m_B + m_{D^*})^2 \left(2 + \frac{(q^2 - m_B^2 + m_{D^*}^2)^2}{4m_{D^*}^2 q^2}\right) A_1^2(q^2) \right. \right. \\ &\quad + \frac{\lambda_{D^*}^2}{4m_{D^*}^2 (m_B + m_{D^*})^2} A_2^2(q^2) + \frac{\lambda_{D^*} (q^2 - m_B^2 + m_{D^*}^2)}{2m_{D^*}^2} A_1(q^2) A_2(q^2) \\ &\quad \left. \left. + \frac{2q^2 \lambda_{D^*}}{(m_B + m_{D^*})^2} V^2(q^2) \right\} + \frac{3}{2} \frac{m_l^2 \lambda_{D^*}}{q^2} A_0^2(q^2) (1 + \delta_{H^+}^{D^* l}(q^2)) \right],\end{aligned}\quad (17)$$

where $\lambda_{D^*} = (m_B^2 - m_{D^*}^2 - q^2)^2 - 4m_{D^*}^2 q^2$. Note that compared to the process $\bar{B} \rightarrow D l^- \bar{\nu}$, various form factors contribute to $\bar{B} \rightarrow D^* l^- \bar{\nu}$. However the charged Higgs boson only generates the corrections proportional to $A_0^2(q^2)$, and the corrections $\delta_{H^+}^{D^* l}(q^2)$ are given by

$$\begin{aligned}\delta_{H^+}^{D^* l}(q^2) &= -\frac{q^2}{m_l(m_b + m_c)} \frac{\text{Re} \left[\rho_e^u V_{cb} (\rho_d^\dagger V^\dagger + V^\dagger \rho_u)_{bc} \right]}{\sqrt{2} G_F m_{H^+}^2 |V_{cb}|^2} \\ &\quad + \frac{q^4}{m_l^2 (m_b + m_c)^2} \frac{(\rho_e^\dagger \rho_e)^u \left| (\rho_d^\dagger V^\dagger + V^\dagger \rho_u)_{bc} \right|^2}{8 G_F^2 m_{H^+}^4 |V_{cb}|^2}.\end{aligned}\quad (18)$$

Notice that similar to $\bar{B} \rightarrow Dl^- \bar{\nu}$ process, the charged Higgs boson contributions to the decay rate is proportional to ρ_e^l or $(\rho_e^\dagger \rho_e)^l$. We also note that contrary to $\bar{B} \rightarrow Dl^- \bar{\nu}$ process, the charged Higgs contributions are proportional to $(\rho_d^\dagger V^\dagger + V^\dagger \rho_u)_{bc}$ since the pseudo-scalar coupling $\bar{c}\gamma_5 b H^+$ contributes to $\bar{B} \rightarrow D^* l^- \bar{\nu}$ process.

IV. $R(D^{(*)})$ IN THE GENERAL 2HDM

$R(D^{(*)})$ are defined to measure a lepton flavor universality between τ and l ($l = e, \mu$) modes in $\bar{B} \rightarrow D^{(*)} l^- \bar{\nu}$:

$$R(D^{(*)}) = \frac{\text{BR}(\bar{B} \rightarrow D^{(*)} \tau^- \bar{\nu})}{\text{BR}(\bar{B} \rightarrow D^{(*)} l^- \bar{\nu})}, \quad (19)$$

where $l = e$ or μ . So far, an apparent flavor non-universality between μ and e modes has not been reported [61]. Therefore, we expect that the deviation from the SM prediction of $R(D^{(*)})$ mainly comes from $\bar{B} \rightarrow D^{(*)} \tau^- \bar{\nu}$ mode in the 2HDM.

As we discussed in the previous section, the charged Higgs boson contributions to $\bar{B} \rightarrow D^{(*)} l^- \bar{\nu}$ are proportional to ρ_e^l or $(\rho_e^\dagger \rho_e)^l$ ($l = e, \mu, \tau$). Therefore, $\rho_e^{\tau\tau}$, $\rho_e^{e\tau}$ and $\rho_e^{\mu\tau}$ induce the corrections to $\bar{B} \rightarrow D^{(*)} \tau^- \bar{\nu}$, on the other hand, $\rho_e^{i\mu}$ and ρ_e^{ie} ($i = e, \mu, \tau$) break the lepton flavor universality between μ and e modes, and hence here we assume $\rho_e^{i\mu}$ and ρ_e^{ie} are negligibly small.

The charged Higgs boson contributions in $\bar{B} \rightarrow D^{(*)} \tau^- \bar{\nu}$ are proportional to $(\rho_d^\dagger V^\dagger \mp V^\dagger \rho_u)_{bc}$:

$$(\rho_d^\dagger V^\dagger \mp V^\dagger \rho_u)_{bc} = \sum_i (\rho_d^{ib*} V_{ci}^* \mp V_{ib}^* \rho_u^{ic}), \quad (20)$$

$$= \rho_d^{sb*} V_{cs}^* + \rho_d^{db*} V_{cd}^* + \rho_d^{bb*} V_{cb}^* \mp (V_{tb}^* \rho_u^{tc} + V_{cb}^* \rho_u^{cc} + V_{ub}^* \rho_u^{uc}). \quad (21)$$

Because of the hierarchical structure of the CKM matrix as

$$|V_{cs}| \sim |V_{tb}| \sim 1 > |V_{cd}| \sim 0.2 \gg |V_{cb}| \sim 0.04 \gg |V_{ub}| \sim 0.004, \quad (22)$$

effects of Yukawa couplings ρ_d^{bb} , ρ_u^{cc} and ρ_u^{uc} are small even if these are of the order of one. Therefore, we consider the effects of ρ_u^{tc} , ρ_d^{sb} and ρ_d^{db} .

In order to see how large deviations of $R(D^{(*)})$ from the SM prediction are possible in the 2HDM, we consider the following three typical scenarios:

- 1). non-zero ρ_u^{tc}
- 2). non-zero ρ_u^{tc} and ρ_d^{sb} (and ρ_d^{db})
- 3). non-zero ρ_u^{tc} and $\rho_e^{\mu\tau}$ (and $\rho_e^{e\tau}$)

in addition to the non-zero $\rho_e^{\tau\tau}$. We will also show the predictions in the Type II 2HDM as a comparison.

Before we study scenarios listed above, first we discuss the constraints from measurements of Higgs boson couplings, a top decay $t \rightarrow hc$ and lepton flavor violating Higgs boson decays on the relevant Yukawa couplings in these scenarios.

A. Constraints from measurements of Higgs boson couplings and a top decay $t \rightarrow hc$

1. Constraints from measurements of Higgs boson couplings

In the general 2HDM, even if the extra Yukawa couplings ρ_f are negligible, the SM-like Higgs boson couplings with the SM particles are modified and multiplied by the Higgs mixing parameter $s_{\beta\alpha}$. Therefore, the measurements of the Higgs boson couplings constrain the Higgs mixing parameter. The current limit [62] is³

$$|c_{\beta\alpha}| \leq 0.4. \quad (23)$$

If $\rho_e^{\tau\tau}$ Yukawa coupling is not negligible, it contributes to the Higgs boson decay $h \rightarrow \tau^+\tau^-$. The measurement of the signal strength μ_τ constrains the $\rho_e^{\tau\tau}c_{\beta\alpha}$:

$$\mu_\tau \equiv \frac{\text{BR}(h \rightarrow \tau^+\tau^-)}{\text{BR}(h \rightarrow \tau^+\tau^-)_{\text{SM}}} \simeq \left| s_{\beta\alpha} + \frac{\rho_e^{\tau\tau}c_{\beta\alpha}v}{\sqrt{2}m_\tau} \right|^2. \quad (24)$$

The current measurement of μ_τ is given by [63]

$$\mu_\tau = 1.11^{+0.24}_{-0.22}. \quad (25)$$

The result of the constraint on $\rho_e^{\tau\tau}c_{\beta\alpha}$ at the 95% confidence level (C.L.) is given by

$$-2 \times 10^{-3} \leq \rho_e^{\tau\tau}c_{\beta\alpha} \leq 3 \times 10^{-3}. \quad (26)$$

³ When the extra Yukawa couplings ρ are all negligible, the SM-like Higgs boson couplings with the SM particles in our 2HDM are the same as those in the Type I 2HDM with a large $\tan\beta$. See, for example, Ref. [62].

2. Constraint from the top decay $t \rightarrow hc$

Non-zero ρ_u^{tc} as well as ρ_u^{ct} generate an exotic top quark decay $t \rightarrow hc$. The decay branching ratio is obtained by

$$\text{BR}(t \rightarrow hc) = \frac{c_{\beta\alpha}^2(|\rho_u^{tc}|^2 + |\rho_u^{ct}|^2)}{64\pi} \frac{m_t}{\Gamma_t} \left(1 - \frac{m_h^2}{m_t^2}\right)^2, \quad (27)$$

$$\simeq 3 \times 10^{-3} \left(\frac{\rho_u^{tc} c_{\beta\alpha}}{0.15}\right)^2. \quad (28)$$

Here we have adopted $\Gamma_t = 1.41$ GeV for the total decay rate of the top quark and we assumed that ρ_u^{ct} is negligible in the numerical estimate of Eq. (28). The current experimental limit is set as

$$\text{BR}(t \rightarrow hc) \leq 4 \times 10^{-3}, \quad (29)$$

at the 95% C.L. [64].

3. Constraints from lepton flavor violating Higgs boson decays

A search for the lepton flavor violating Higgs boson decays $h \rightarrow e\tau$, $\mu\tau$ constrains on the lepton flavor violating Yukawa couplings $\rho_e^{e\tau}$ and $\rho_e^{\mu\tau}$. The latest data from the CMS collaboration at the LHC with an integrated luminosity of 35.9 fb^{-1} at $\sqrt{s} = 13$ TeV is given by

$$\text{BR}(h \rightarrow \mu\tau) \leq 0.25 \%, \quad (30)$$

$$\text{BR}(h \rightarrow e\tau) \leq 0.61 \%, \quad (31)$$

at 95% C.L. [18]. The branching ratio $\text{BR}(h \rightarrow \mu\tau)$ in the general 2HDM is given by

$$\text{BR}(h \rightarrow \mu\tau) = \frac{c_{\beta\alpha}^2(|\rho_e^{\mu\tau}|^2 + |\rho_e^{\tau\mu}|^2) m_h}{16\pi\Gamma_h}, \quad (32)$$

$$= 0.24\% \left(\frac{\rho_e^{\mu\tau} c_{\beta\alpha}}{2 \times 10^{-3}}\right)^2, \quad (33)$$

where Γ_h is the total decay rate of the Higgs boson and we have used $\Gamma_h = 4.1$ MeV, and we have neglected $\rho_e^{\tau\mu}$ for this numerical estimate. Similarly we get

$$\text{BR}(h \rightarrow e\tau) = 0.62\% \left(\frac{\rho_e^{e\tau} c_{\beta\alpha}}{3.2 \times 10^{-3}}\right)^2. \quad (34)$$

Note that if the Higgs mixing parameter $c_{\beta\alpha}$ is small ($|c_{\beta\alpha}| \leq 10^{-2} - 10^{-3}$), these ρ_f Yukawa couplings relevant to $R(D^{(*)})$ can be still of $O(0.1) - O(1)$.

B. Scenario (1): non-zero ρ_u^{tc} and $\rho_e^{\tau\tau}$

This scenario has been suggested by Refs. [26, 35] as an interesting solution to explain the $R(D^{(*)})$ anomalies in the effective theory language. In this scenario, the charged Higgs boson contributions $\delta_{H^+}^{D^{(*)}\tau}$ in Eqs. (13, 18) are expressed by

$$1 + \delta_{H^+}^{D^{(*)}\tau}(q^2) = \left| 1 \pm \frac{q^2 \rho_e^{\tau\tau} \rho_u^{tc} V_{cb} V_{tb}^*}{2\sqrt{2} G_F m_{H^+}^2 m_\tau (m_b \mp m_c) |V_{cb}|^2} \right|^2, \quad (35)$$

where double sign corresponds to a case for D and D^* , respectively. For the parameterization of the Cabbibo-Kobayashi-Maskawa (CKM) matrix, we use the Particle Data Group (PDG) convention. We note that in the PDG convention, V_{cb} and V_{tb} are real and positive. When $\rho_e^{\tau\tau}$ is real and negative, one can increase $R(D^*)$ by increasing ρ_u^{tc} positively, but $R(D)$ is decreased. However, as one increases ρ_u^{tc} further, $R(D)$ also starts to increase so that the current world average values of $R(D^{(*)})$ can be explained. As noticed in Ref. [35], this scenario requires relatively large Yukawa coupling ρ_u^{tc} in order to explain $R(D^{(*)})$. However, the constraints from the other processes in this scenario would be important. Therefore, we will clarify the allowed parameter space consistent with the experimental results.

1. Constraint from $B_c^- \rightarrow \tau^- \bar{\nu}$

In general, the effective operators for $\bar{B} \rightarrow D^* \tau^- \bar{\nu}$ which are generated by the charged Higgs boson also contribute to $B_c^- \rightarrow \tau^- \bar{\nu}$ process. Therefore, large extra contributions to $\bar{B} \rightarrow D^* \tau^- \bar{\nu}$ process would be strongly constrained by this process [40, 65].⁴ The branching ratio for $B_c^- \rightarrow \tau^- \bar{\nu}$ is obtained by

$$\text{BR}(B_c^- \rightarrow \tau^- \bar{\nu}) = \tau_{B_c} \frac{m_{B_c} m_\tau^2 f_{B_c}^2 G_F^2 |V_{cb}|^2}{8\pi} \left(1 - \frac{m_\tau^2}{m_{B_c}^2} \right)^2 [1 + \delta_{H^+}^{D^*\tau}(m_{B_c}^2)], \quad (36)$$

⁴ See also Ref.[66].

where τ_{B_c} is the lifetime of B_c^- meson and the charged Higgs boson contribution $\delta_{H^+}^{D^*\tau}$ is given in Eq. (18). For non-zero $\rho_e^{\tau\tau}$ and ρ_u^{tc} , the numerical estimate shows

$$\text{BR}(B_c^- \rightarrow \tau^- \bar{\nu}) = \tau_{B_c} \frac{m_{B_c} m_\tau^2 f_{B_c}^2 G_F^2 |V_{cb}|^2}{8\pi} \left(1 - \frac{m_\tau^2}{m_{B_c^2}}\right)^2 \times \left|1 - \frac{m_{B_c}^2 \rho_e^{\tau\tau} \rho_u^{tc} V_{tb}^*}{2\sqrt{2} G_F m_{H^+}^2 m_\tau (m_b + m_c) V_{cb}^*}\right|^2, \quad (37)$$

$$= (2\%) \left|1 + 3 \left(\frac{500 \text{ GeV}}{m_{H^+}}\right)^2 \left(\frac{0.04}{V_{cb}/V_{tb}}\right)^* \left(\frac{\rho_e^{\tau\tau}}{-0.5}\right) \left(\frac{\rho_u^{tc}}{0.5}\right)\right|^2. \quad (38)$$

As studied in Ref. [40], the life time of the B_c^- meson provides a constraint $\text{BR}(B_c^- \rightarrow \tau^- \bar{\nu}) \leq 30\%$. Furthermore, the recent study suggested that the LEP data taken at the Z peak requires $\text{BR}(B_c^- \rightarrow \tau^- \bar{\nu}) \leq 10\%$ [65]. We simply adopt both constraints as references.⁵ In the Scenario (1), the constraint $\text{BR}(B_c^- \rightarrow \tau^- \bar{\nu}) \leq 30\%$ (10%) corresponds to, for example, $-0.8 \leq \rho_u^{tc} \leq 0.5$ ($-0.5 \leq \rho_u^{tc} \leq 0.2$) for $m_{H^+} = 500$ GeV and $\rho_e^{\tau\tau} = -0.5$ if ρ_u^{tc} is real. In order to explain the current world average for $R(D^*)$ [$R(D^*) = 0.304$], large Yukawa coupling ρ_u^{tc} is required ($\rho_u^{tc} \sim +1$ for $m_{H^+} = 500$ GeV and $\rho_e^{\tau\tau} = -0.5$) [35]. Therefore, the constraint severely restricts the possibility to have a large deviation from the SM prediction for $R(D^*)$.

In order to study the effects of the complex phases in the Yukawa couplings, we parameterize the Yukawa coupling $\rho_e^{\tau\tau}$ as

$$\rho_e^{\tau\tau} = \rho_{\tau\tau} e^{i\delta_{\tau\tau}}, \quad (39)$$

where $\rho_{\tau\tau}$ is a real parameter and the phase $\delta_{\tau\tau}$ is assumed to be $0 \leq \delta_{\tau\tau} \leq \frac{\pi}{2}$. The phase of Yukawa coupling ρ_u^{tc} is effectively absorbed into the phase of $\delta_{\tau\tau}$ in $R(D^{(*)})$, and therefore we assume that ρ_u^{tc} is a real (positive or negative) parameter.⁶ The leading effect of $\delta_{\tau\tau}$ comes from the interference between the SM and charged Higgs contributions, and it is proportional to “ $\rho_u^{tc} \rho_{\tau\tau} \cos \delta_{\tau\tau}$ ” in $R(D^{(*)})$. Therefore, the

⁵ The constraint obtained in Ref. [65] relies on the theoretical value of $\text{BR}(B_c^- \rightarrow J/\psi l \bar{\nu})$, which may be subject to debate. Therefore, we use both constraints $\text{BR}(B_c^- \rightarrow \tau^- \bar{\nu}) \leq 30\%$ and 10% as references.

⁶ As we show in Appendix C, the phase of ρ_u^{tc} affects an imaginary part of $B_{d,s} - \bar{B}_{d,s}$ mixing. Therefore, the measurements of the imaginary part of $B_{d,s} - \bar{B}_{d,s}$ mixing have a potential to distinguish the origin of the phase.

range of $\delta_{\tau\tau}$ ($0 \leq \delta_{\tau\tau} \leq \frac{\pi}{2}$) is sufficient to see the possible predictions for the $R(D^{(*)})$ when $\rho_u^{tc}\rho_{\tau\tau}$ is allowed to be positive or negative.

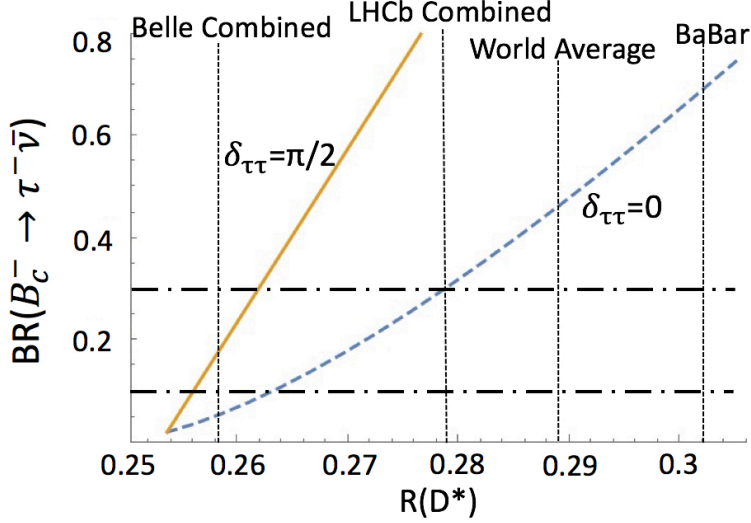


FIG. 1: The correlations between $R(D^*)$ and $\text{BR}(B_c^- \rightarrow \tau^- \bar{\nu})$ are shown in cases with $\delta_{\tau\tau} = 0$ (dashed blue line) and $\frac{\pi}{2}$ (solid orange line). Here $\delta_{\tau\tau}$ is a phase of $\rho_e^{\tau\tau}$ which is parameterized by $\rho_e^{\tau\tau} = \rho_{\tau\tau} e^{i\delta_{\tau\tau}}$. The suggested constraints $\text{BR}(B_c^- \rightarrow \tau^- \bar{\nu}) \leq 30\%$ and 10% are shown by horizontal dashed-dotted lines. The lower limits at 1σ for BaBar, Belle, LHCb and world average are also shown.

In Figure 1, the correlations between $R(D^*)$ and $\text{BR}(B_c^- \rightarrow \tau^- \bar{\nu})$ are shown for $\delta_{\tau\tau} = 0$ (dashed blue line) and $\frac{\pi}{2}$ (solid orange line). When the phase $\delta_{\tau\tau}$ is zero, the predicted value of $R(D^*)$ can not be larger than 0.279 (0.263) because of constraints $\text{BR}(B_c^- \rightarrow \tau^- \bar{\nu}) \leq 30\%$ (10%) [40, 65]. We found that when the phase $\delta_{\tau\tau}$ is non-zero, the constraint on $B_c^- \rightarrow \tau^- \bar{\nu}$ becomes much stronger. For example, for $\delta_{\tau\tau} = \frac{\pi}{2}$, the upper limit on $R(D^*)$ is about 0.262 (0.256) for $\text{BR}(B_c^- \rightarrow \tau^- \bar{\nu}) \leq 30\%$ (10%). Note that the correlations do not depend on the detail of values of model parameters other than the phase parameter $\delta_{\tau\tau}$ in the current scenario.

In Figure 2, the predicted values for $R(D)$ and $R(D^*)$ in the Scenario (1) are shown. The current experimental 1σ limits for BaBar, Belle, and world average are also shown. Here we have set $m_{H^+} = 500$ GeV and $\rho_{\tau\tau} = -0.5$ as a reference set of parameters. The value of ρ_u^{tc} is varied from the SM point ($\rho_u^{tc} = 0$) (blue star-mark)

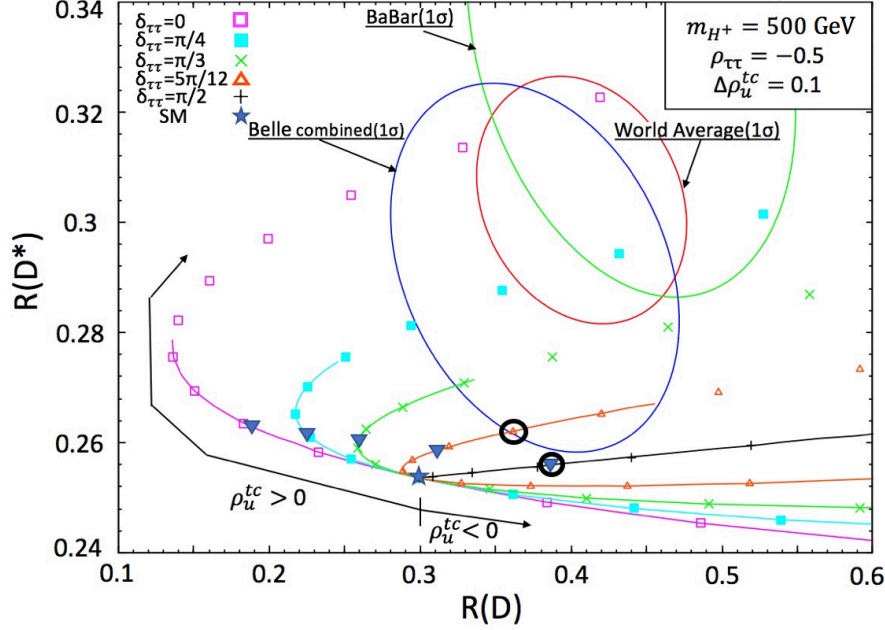


FIG. 2: The predicted values for $R(D)$ and $R(D^*)$ are shown in the scenario (1). The current experimental limits (1σ) for BaBar, Belle, and world average are also shown. Here we have set $m_{H^+} = 500$ GeV and $\rho_{\tau\tau} = -0.5$ as a reference set of parameters. The Yukawa coupling $\rho_e^{\tau\tau}$ is parameterized by $\rho_e^{\tau\tau} = \rho_{\tau\tau} e^{i\delta_{\tau\tau}}$. The value of ρ_u^{tc} is varied from the SM point ($\rho_u^{tc} = 0$) (blue star-mark) by 0.1 step positively ($\rho_u^{tc} > 0$) or negatively ($\rho_u^{tc} < 0$) with different phase parameters $\delta_{\tau\tau} = 0$ (open pink quadrangle), $\frac{\pi}{4}$ (filled cyan quadrangle), $\frac{\pi}{3}$ (green \times), $\frac{5\pi}{12}$ (orange triangle) and $\frac{\pi}{2}$ (black +). The solid line in each value of $\delta_{\tau\tau}$ shows the regions which are consistent with the constraint $\text{BR}(B_c^- \rightarrow \tau \bar{\nu}) \leq 30\%$. If we impose the constraint $\text{BR}(B_c^- \rightarrow \tau^- \bar{\nu}) \leq 10\%$, the regions above filled blue triangle in each value of $\delta_{\tau\tau}$ are excluded. The points indicated by a black circle are adopted as reference points for the LHC physics study discussed later. See the text in details.

by 0.1 step positively ($\rho_u^{tc} > 0$) or negatively ($\rho_u^{tc} < 0$) with different phase values $\delta_{\tau\tau} = 0$ (open pink quadrangle), $\frac{\pi}{4}$ (filled cyan quadrangle), $\frac{\pi}{3}$ (green \times), $\frac{5\pi}{12}$ (orange triangle) and $\frac{\pi}{2}$ (black +) as shown in Figure 2. The solid line in each phase value $\delta_{\tau\tau}$ shows the regions which are consistent with the constraint $\text{BR}(B_c^- \rightarrow \tau^- \bar{\nu}) \leq 30\%$. If we impose the constraint $\text{BR}(B_c^- \rightarrow \tau^- \bar{\nu}) \leq 10\%$, the regions above filled blue triangle in each value of $\delta_{\tau\tau}$ are excluded.

Because of the constraints on $\text{BR}(B_c^- \rightarrow \tau^- \bar{\nu})$, the predicted $R(D^*)$ are strongly restricted. When ρ_u^{tc} is positive and the phase parameter $\delta_{\tau\tau}$ is non-zero, the imaginary value of $\rho_e^{\tau\tau} \rho_u^{tc}$ can increase $R(D)$. As one increases $\delta_{\tau\tau}$ and ρ_u^{tc} , $R(D)$ can get larger before the value of $R(D^*)$ reaches the constraint from $B_c^- \rightarrow \tau^- \bar{\nu}$ as one can see in Figure 2. The predicted $R(D)$ and $R(D^*)$ can not explain the current world average values. They can (can not) be within the 1σ region of the combined Belle result if the constraint $\text{BR}(B_c^- \rightarrow \tau^- \bar{\nu}) \leq 30\%$ (10%) is imposed. Here we have fixed a charged Higgs mass to be 500 GeV ($m_{H^+} = 500$ GeV) and Yukawa coupling $\rho_{\tau\tau}$ to be -0.5 ($\rho_e^{\tau\tau} = -0.5e^{i\delta_{\tau\tau}}$). The new physics contributions to both $R(D^{(*)})$ and $\text{BR}(B_c^- \rightarrow \tau^- \bar{\nu})$ scale like

$$\left(\frac{\rho_e^{\tau\tau}}{m_{H^+}} \right) \left(\frac{\rho_u^{tc}}{m_{H^+}} \right). \quad (40)$$

Therefore, even when we change m_{H^+} and $\rho_{\tau\tau}$, the predicted values of $R(D^{(*)})$ (and $\text{BR}(B_c^- \rightarrow \tau^- \bar{\nu})$) are read from Figure 2.

For the LHC physics study discussed later, we choose two reference points shown by a black circle in Figure 2. As a reference point 1, we select a point with $\rho_u^{tc} \rho_{\tau\tau} = -0.2$, $\delta_{\tau\tau} = \frac{5\pi}{12}$ and $m_{H^+} = 500$ GeV, which satisfies the constraint $\text{BR}(B_c^- \rightarrow \tau^- \bar{\nu}) \leq 30\%$ but not $\text{BR}(B_c^- \rightarrow \tau^- \bar{\nu}) \leq 10\%$. The reference point 1 predicts $(R(D), R(D^*)) = (0.361, 0.262)$. As a reference point 2, we choose a point with $\rho_u^{tc} \rho_{\tau\tau} = -0.156$, $\delta_{\tau\tau} = \frac{\pi}{2}$ and $m_{H^+} = 500$ GeV, which satisfies the constraint $\text{BR}(B_c^- \rightarrow \tau^- \bar{\nu}) \leq 10\%$. This point predicts $(R(D), R(D^*)) = (0.385, 0.256)$.

2. q^2 distribution in $d\Gamma(\bar{B} \rightarrow D\tau^- \bar{\nu})/dq^2$

As stressed in Refs. [26, 31], the charged Higgs boson contribution significantly affects the q^2 distribution in $d\Gamma(\bar{B} \rightarrow D\tau^- \bar{\nu})/dq^2$. In Figure 3, the q^2 distributions in $d\Gamma(\bar{B} \rightarrow D\tau^- \bar{\nu})/dq^2$ are shown in cases with $(\delta_{\tau\tau}, R(D^*)) = (65^\circ, 0.270)$, $(75^\circ, 0.263)$ and $(90^\circ, 0.256)$. Here we take $m_{H^+} = 500$ GeV and $\rho_{\tau\tau} = -0.5$. The predicted value of $R(D)$ is fixed to be $R(D) = 0.375$ by adjusting the value of ρ_u^{tc} in each case. To compare the shapes of the q^2 distributions, the heights of all plots are normalized to be the same. Here we also show the q^2 distribution in the SM case ($R(D) = 0.304$, $R(D^*) = 0.254$) as a comparison. As one can see from Figure 3,

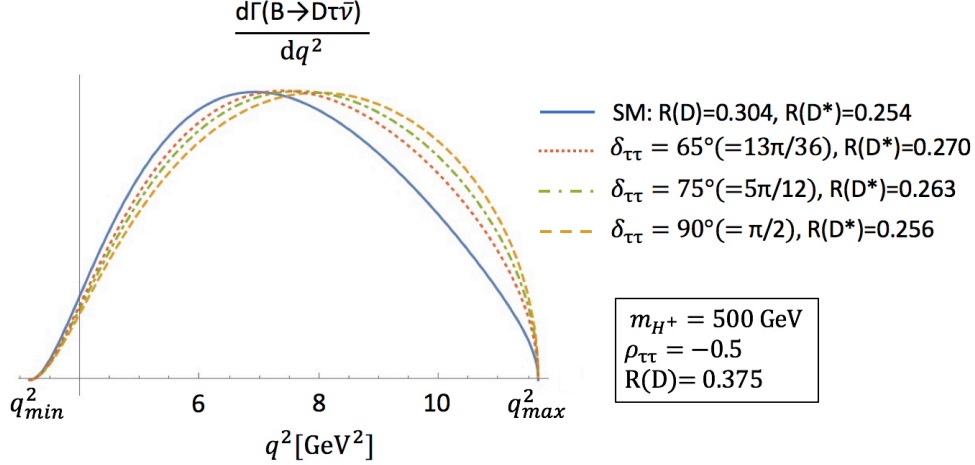


FIG. 3: The q^2 distributions in $d\Gamma(\bar{B} \rightarrow D\tau^-\bar{\nu})/dq^2$ are shown in cases with $(\delta_{\tau\tau}, R(D^*)) = (65^\circ, 0.270)$, $(75^\circ, 0.263)$ and $(90^\circ, 0.256)$. Here we have set $m_{H^+} = 500$ GeV and $\rho_{\tau\tau} = -0.5$. $R(D)$ is fixed to be $R(D) = 0.375$ by adjusting the value of ρ_u^{tc} in each case. To compare the shapes of the q^2 distributions, the heights of all plots are normalized to be the same. Here we also show the q^2 distribution in the SM case ($R(D) = 0.304$, $R(D^*) = 0.254$) as a comparison.

the difference from the SM distribution increases in large q^2 regions as the phase of $\rho_e^{\tau\tau}$ ($\delta_{\tau\tau}$) becomes larger. The BaBar [2] and Belle [3] have provided results of the q^2 distribution. However, the general 2HDM can not explain the BaBar's results of $R(D^{(*)})$, and the Belle's result for the q^2 distribution still has large uncertainty. Furthermore, their analyses for the q^2 distribution measurement rely on the theoretical models. Therefore, here we do not explicitly impose a constraint from the q^2 distributions in $d\Gamma(\bar{B} \rightarrow D\tau^-\bar{\nu})/dq^2$. However we would like to stress that the precise measurement of the q^2 distributions in $d\Gamma(\bar{B} \rightarrow D\tau^-\bar{\nu})/dq^2$ would have a significant impact on this scenario.

3. Effects on $b \rightarrow s(d)$ transition: $B_{d,s} - \bar{B}_{d,s}$ mixing, $b \rightarrow s\gamma$ and $b \rightarrow sl^+l^-$

In the existence of ρ_u^{tc} , a charged Higgs boson induces new contributions to $b \rightarrow s(d)$ transition processes such as $B_{d,s} - \bar{B}_{d,s}$ mixing, $b \rightarrow s\gamma$ and $b \rightarrow sl^+l^-$ at one-loop level.

For $B_{d,s} - \bar{B}_{d,s}$ mixing, the detail expressions of the 2HDM contributions are shown in Appendix C. The charged Higgs boson correction to $B_{d,s}$ meson mass difference is approximately expressed by

$$\begin{aligned}\Delta m_{B_{d_i}}^{2\text{HDM}} &= \Delta m_{B_{d_i}}^{\text{SM}} + \delta(\Delta m_{B_{d_i}})^{2\text{HDM}}, \\ \delta(\Delta m_{B_{d_i}})^{2\text{HDM}} &= -\frac{m_{B_{d_i}} F_{B_{d_i}}^2 B_{B_{d_i}}}{192\pi^2 m_{H^+}^2} \text{Re}[(V_{tb} V_{td_i}^*)^2] |\rho_u^{tc}|^4 G_1(x_c, x_c),\end{aligned}\quad (41)$$

where a function G_1 is defined in Eq. (C6) in Appendix C and $G_1(x_c, x_c) \simeq 1$ for $x_c = m_c^2/m_{H^+}^2 \ll 1$, and $m_{B_{d_i}}$, $F_{B_{d_i}}$ and $B_{B_{d_i}}$ are a mass, a decay constant and a bag parameter of B_{d_i} meson, respectively and their values for our numerical analysis are listed in Appendix D. The numerical estimates of the charged Higgs boson contribution are obtained by

$$\delta(\Delta m_{B_d})^{2\text{HDM}} = -0.05 \times \left(\frac{500 \text{ GeV}}{m_{H^+}}\right)^2 \left(\frac{|\rho_u^{tc}|}{1.0}\right)^4 [\text{ps}^{-1}], \quad (42)$$

$$\delta(\Delta m_{B_s})^{2\text{HDM}} = -2 \times \left(\frac{500 \text{ GeV}}{m_{H^+}}\right)^2 \left(\frac{|\rho_u^{tc}|}{1.0}\right)^4 [\text{ps}^{-1}]. \quad (43)$$

As one sees, the charged Higgs boson contributions with non-zero ρ_u^{tc} prefer the negative values. The measured values $\Delta m_{B_{d,s}}^{\text{exp}}$ [19] are

$$\Delta m_{B_d}^{\text{exp}} = 0.5064 \pm 0.0019 [\text{ps}^{-1}], \quad \Delta m_{B_s}^{\text{exp}} = 17.757 \pm 0.021 [\text{ps}^{-1}], \quad (44)$$

and the SM predictions $\Delta m_{B_{d,s}}^{\text{SM}}$ (95 % C.L. region) [67] are given by

$$0.45 [\text{ps}^{-1}] \leq \Delta m_{B_d}^{\text{SM}} \leq 0.78 [\text{ps}^{-1}], \quad 16.2 [\text{ps}^{-1}] \leq \Delta m_{B_s}^{\text{SM}} \leq 21.9 [\text{ps}^{-1}]. \quad (45)$$

Since the uncertainty of the measured values is very small in contrast to the SM predictions, we take into account the uncertainty of the SM predictions, and we apply the 95% C.L. allowed region to the 2HDM contribution as follows:

$$\begin{aligned}-0.27 [\text{ps}^{-1}] &\leq \delta(\Delta m_{B_d})^{2\text{HDM}} \leq 0.06 [\text{ps}^{-1}], \\ -4.1 [\text{ps}^{-1}] &\leq \delta(\Delta m_{B_s})^{2\text{HDM}} \leq 1.6 [\text{ps}^{-1}].\end{aligned}\quad (46)$$

Compared with Eqs. (42, 43), interesting parameter regions ($\rho_u^{tc} \sim 0.2 - 0.5$ for $m_{H^+} = 500 \text{ GeV}$) in Scenario (1) are consistent with the current limit on $\Delta m_{B_{d,s}}$.

The effective operators relevant to $b \rightarrow s\gamma$ and $b \rightarrow sl^+l^-$ are given by

$$\begin{aligned} \mathcal{L}_{\text{eff}} = & \frac{4G_F}{\sqrt{2}} V_{tb} V_{ts}^* \left[\frac{e}{16\pi^2} C_7 m_b (\bar{s} \sigma_{\mu\nu} P_R b) F^{\mu\nu} + \frac{g_3}{16\pi^2} C_8 m_b (\bar{s} \sigma_{\mu\nu} T^a P_R b) G^{a,\mu\nu} \right. \\ & \left. + \frac{e^2}{16\pi^2} C_{9(l)} (\bar{s} \gamma^\mu P_L b) (\bar{l} \gamma_\mu l) + \frac{e^2}{16\pi^2} C_{10(l)} (\bar{s} \gamma^\mu P_L b) (\bar{l} \gamma_\mu \gamma_5 l) \right], \end{aligned} \quad (47)$$

where l is a charged lepton $l = e, \mu$ or τ . We summarize the detail expressions induced by the charged Higgs boson via ρ_u Yukawa couplings for $C_{7,8,9,10}$ in Appendix C. The charged Higgs boson contributions with non-zero ρ_u^{tc} are expressed by

$$C_7^{2\text{HDM}} = \frac{1}{4\sqrt{2}G_F m_{H^+}^2} |\rho_u^{tc}|^2 G_\sigma(x_c), \quad (48)$$

$$C_8^{2\text{HDM}} = \frac{1}{4\sqrt{2}G_F m_{H^+}^2} |\rho_u^{tc}|^2 G_{\sigma 2}(x_c), \quad (49)$$

$$C_{9(l)}^{2\text{HDM}} = -\frac{1}{2\sqrt{2}G_F m_{H^+}^2} |\rho_u^{tc}|^2 G_\gamma(x_c) + \frac{-1 + 4s_W^2}{8\pi\alpha} |\rho_u^{tc}|^2 G_Z(x_c), \quad (50)$$

$$C_{10(l)}^{2\text{HDM}} = \frac{1}{8\pi\alpha} |\rho_u^{tc}|^2 G_Z(x_c), \quad (51)$$

where $x_c = m_c^2/m_{H^+}^2 \ll 1$ for $m_{H^+} = 500$ GeV and various functions are defined in Appendix C and the approximate expressions are obtained as

$$G_\sigma(x_c) = Q_u G_{\sigma 1}(x_c) + Q_{H^+} G_{\sigma 2}(x_c) \simeq -\frac{7}{36}, \quad (52)$$

$$G_{\sigma 2}(x_c) \simeq -\frac{1}{6}, \quad (53)$$

$$G_\gamma(x_c) = Q_u G_{\gamma 1}(x_c) + Q_{H^+} G_{\gamma 2}(x_c) \simeq -\frac{19 + 12 \log x_c}{54}, \quad (54)$$

$$G_Z(x_c) \simeq 0, \quad (55)$$

for $x_c \ll 1$. Here Q_u and Q_{H^+} are charges of up-type quarks (+2/3) and a charged Higgs boson (+1). We note that a term proportional to $G_\gamma(x_c)$ in $C_{9(l)}^{2\text{HDM}}$ originates from γ penguin contribution, on the other hand, terms proportional to $G_Z(x_c)$ in $C_{9,10(l)}^{2\text{HDM}}$ come from Z penguin contribution. Therefore, $C_{9,10(l)}^{2\text{HDM}}$ are universal to all lepton flavor l . We also note that in $G_\gamma(x)$ there is a log-enhancement when x is small.

For $b \rightarrow s\gamma$, Wilson coefficients $C_{7,8}^{2\text{HDM}}$ are estimated as

$$C_7^{2\text{HDM}} = -0.012 \left(\frac{500 \text{ GeV}}{m_{H^+}} \right)^2 \left(\frac{|\rho_u^{tc}|}{1.0} \right)^2, \quad (56)$$

$$C_8^{2\text{HDM}} = -0.010 \left(\frac{500 \text{ GeV}}{m_{H^+}} \right)^2 \left(\frac{|\rho_u^{tc}|}{1.0} \right)^2. \quad (57)$$

The low-energy Wilson coefficient $C_7(\mu_b)$ is evaluated by using the renormalization group equation and the charged Higgs boson contribution $C_7^{\text{2HDM}}(\mu_b)$ is expressed by

$$\begin{aligned} C_7^{\text{2HDM}}(\mu_b) &= \eta^{\frac{16}{23}} C_7^{\text{2HDM}} + \frac{8}{3} \left(\eta^{\frac{14}{23}} - \eta^{\frac{16}{23}} \right) C_8^{\text{2HDM}}, \\ &= -0.009 \left(\frac{500 \text{ GeV}}{m_{H^+}} \right)^2 \left(\frac{|\rho_u^{tc}|}{1.0} \right)^2, \end{aligned} \quad (58)$$

where $\eta = \alpha_s(\mu)/\alpha_s(\mu_b)$ and we have taken $\mu = m_W$, $\mu_b = 5 \text{ GeV}$ and $\alpha_s(m_Z) = 0.118$ in our numerical estimate. As discussed in Ref. [68], for example, the allowed regions of the new physics contributions $C_7^{\text{NP}}(\mu_b)$ from a global fit analysis of $b \rightarrow s$ transition observables are constrained as

$$-0.04 \leq C_7^{\text{NP}}(\mu_b) \leq 0.0 \quad (59)$$

at 1σ level. Therefore, the interesting regions in Scenario (1) ($\rho_u^{tc} \sim 0.2 - 0.5$ for $m_{H^+} = 500 \text{ GeV}$) are consistent with this constraint.

For $b \rightarrow sl^+l^-$ process, the contributions to $C_{9,10}$ play an important role. The numerical estimates for the charged Higgs boson contributions with non-zero ρ_u^{tc} are given by

$$C_{9(l)}^{\text{2HDM}} = -0.27 \left(\frac{500 \text{ GeV}}{m_{H^+}} \right)^2 \left(\frac{|\rho_u^{tc}|}{1.0} \right)^2, \quad (60)$$

$$C_{10(l)}^{\text{2HDM}} \simeq 0, \quad (61)$$

where the Z penguin contribution is suppressed, and hence only $C_{9(l)}^{\text{2HDM}}$ receives the non-negligible correction from the γ penguin contribution, which has a “ $\log x_c$ ” enhancement.

As we discussed in the introduction, the current experimental situation on $b \rightarrow sl^+l^-$ processes is involved. In the angular observable of $B \rightarrow K^*\mu^+\mu^-$, the discrepancies between the SM prediction and the measured value have been reported. (See Refs. [8–12].) The LHCb results have also indicated deviations from the SM predictions in lepton flavor universality measurements $R_K^{(*)} = \text{BR}(B \rightarrow K^{(*)}\mu^+\mu^-)/\text{BR}(B \rightarrow K^{(*)}e^+e^-)$. In Ref. [69], for example, a global fit analysis of angular observables in $B \rightarrow K^*\mu^+\mu^-$ as well as branching ratios of $B \rightarrow K^{(*)}\mu^+\mu^-$ and $B_s \rightarrow \phi\mu^+\mu^-$ suggests that the best fit values of new physics contributions to

$C_{9,10}$ are preferred to be away from zero, $(C_{9(\mu)}^{\text{NP}}, C_{10(\mu)}^{\text{NP}}) = (-1.15, +0.26)$. As shown in Eqs. (60, 61), the interesting regions in Scenario (1) ($\rho_u^{tc} \sim 0.2-0.5$ for $m_{H^+} = 500$ GeV) can not explain these discrepancies and the fit may be only slightly improved, compared to the SM predictions.⁷ Since the anomalies in $b \rightarrow sl^+l^-$ are still subject to discuss, we do not impose the constraints from this process in our analysis.

In addition to these $b \rightarrow s(d)$ transition processes, in the presence of ρ_u^{tc} and $\rho_e^{\tau\tau}$, $B_s \rightarrow \tau^+\tau^-$ process is induced. However, we have checked that the constraint from this process is still very weak, and hence we only list the expression of $B_s \rightarrow \tau^+\tau^-$ process in Appendix C.

C. Scenario (2): non-zero ρ_u^{tc} , $\rho_e^{\tau\tau}$ and ρ_d^{sb} (ρ_d^{db})

In addition to the non-zero $\rho_e^{\tau\tau}$ and ρ_u^{tc} , we introduce other non-zero Yukawa couplings ρ_d^{sb} (and/or ρ_d^{db}) in this scenario. This scenario has been suggested by, for example, Refs. [2, 28, 31] in the effective theory description.

To study the typical parameter space which is consistent with the other experimental data, we parameterize the Yukawa couplings as follows:

$$r_s = \frac{\rho_d^{sb}}{\rho_u^{tc*}}, \quad r_d = \frac{\rho_d^{db}}{\rho_u^{tc*}}, \quad a = r_s \frac{V_{cs}}{V_{tb}} + r_d \frac{V_{cd}}{V_{tb}}. \quad (62)$$

Note that

$$(\rho_d^\dagger V^\dagger \pm V^\dagger \rho_u)_{bc} = V_{tb}^* \rho_u^{tc} (a^* \pm 1). \quad (63)$$

Therefore for non-zero r_s (and/or r_d), it is possible to realize $\text{Re}[\rho_e^{\tau\tau}(\rho_d^\dagger V^\dagger \pm V^\dagger \rho_u)_{bc}] < 0$, so that one may increase both $R(D)$ and $R(D^*)$ without having too large Yukawa couplings.

In Figure 4, the predicted values for $R(D)$ and $R(D^*)$ are shown in the Scenario (2). The current experimental limits (1σ) for Belle and world average are also shown. Here we have assumed that the Yukawa coupling $\rho_e^{\tau\tau}$, ρ_u^{tc} and ρ_d^{sb} are all real, and we have set $m_{H^+} = m_{H/A} = 500$ GeV, $\rho_e^{\tau\tau} = -0.2$, and $c_{\beta\alpha} = 0.01$. The value of ρ_d^{sb} is varied from the SM point ($\rho_d^{sb} = 0$) (blue star-mark) by 0.1 step positively with

⁷ The Scenario (1) can not explain $R_K^{(*)}$ anomalies because the charged Higgs boson effects with non-zero ρ_u^{tc} are universal to all charged leptons l in $b \rightarrow sl^+l^-$.

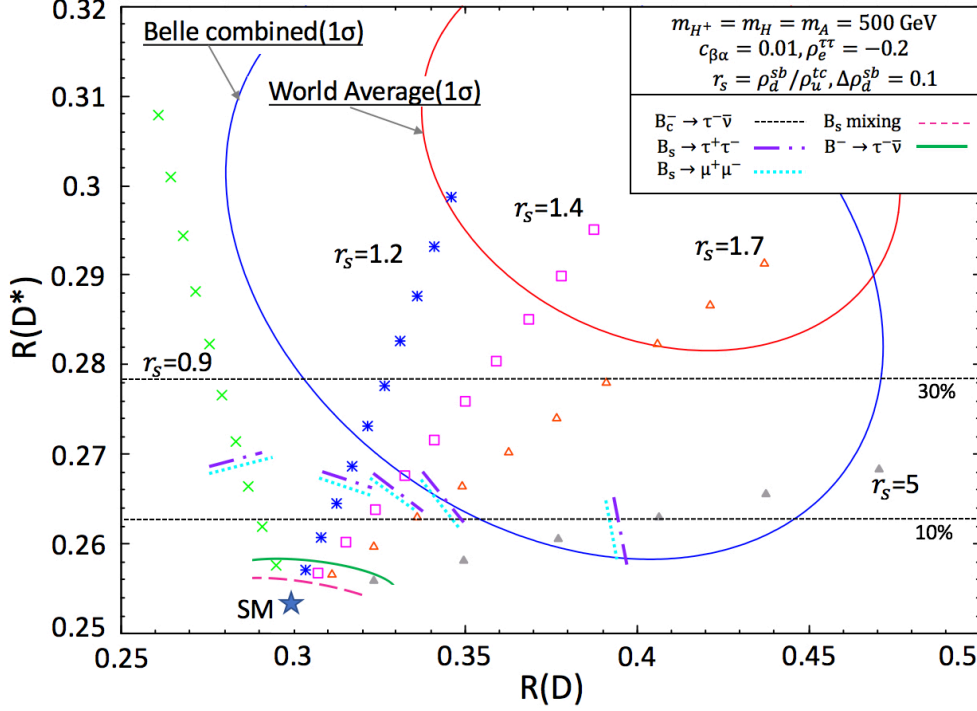


FIG. 4: The predicted values for $R(D)$ and $R(D^*)$ are shown in the Scenario (2). The current experimental limits (1σ) for Belle and world average are also shown. Here we have assumed that the relevant Yukawa couplings are all real, and we have set $m_{H^+} = m_{H/A} = 500$ GeV, $\rho_e^{\tau\tau} = -0.2$ and $c_{\beta\alpha} = 0.01$. The value of ρ_d^{sb} is varied from the SM point ($\rho_d^{sb} = 0$) (blue star-mark) by 0.1 step positively with different values of $r_s (= \rho_d^{sb}/\rho_u^{tc})$, $r_s = 0.9$ (green \times), 1.2 (blue $*$), 1.4 (open pink quadrangle), 1.7 (open orange triangle) and 5 (filled grey triangle). We also show the constraints from $B_c^- \rightarrow \tau^- \bar{\nu}$, $B_s - \bar{B}_s$ mixing, $B_s \rightarrow \tau^+ \tau^-$ and $B^- \rightarrow \tau^- \bar{\nu}$. See the text in details.

different values of $r_s (= \rho_d^{sb}/\rho_u^{tc})$, $r_s = 0.9$ (green \times), 1.2 (blue $*$), 1.4 (open pink quadrangle), 1.7 (open orange triangle) and 5 (filled grey triangle). As one can see from Figure 4, for $r_s \sim 1 - 2$ and $\rho_d^{sb} \sim 1$, the predicted values of $R(D)$ and $R(D^*)$ can be within the 1σ of the world average.

However, as we will see below, the strong constraints come from not only $B_c^- \rightarrow \tau^- \bar{\nu}$ but also $B_{d,s} - \bar{B}_{d,s}$ mixing, $B_{d,s} \rightarrow \mu^+ \mu^-$ and $\tau^+ \tau^-$, and $B^- \rightarrow \tau^- \bar{\nu}$ processes.

1. *Constraint from $B_c^- \rightarrow \tau^- \bar{\nu}$*

For non-zero $\rho_d^{sb(db)}$ as well as non-zero $\rho_e^{\tau\tau}$ and ρ_u^{tc} , the branching ratio for $B_c^- \rightarrow \tau^- \bar{\nu}$ is given by the same expression shown in Eq. (36):

$$\text{BR}(B_c^- \rightarrow \tau^- \bar{\nu}) = \tau_{B_c} \frac{m_{B_c} m_\tau^2 f_{B_c}^2 G_F^2 |V_{cb}|^2}{8\pi} \left(1 - \frac{m_\tau^2}{m_{B_c}^2}\right)^2 \times \left|1 - \frac{m_{B_c}^2 V_{tb}^* \rho_e^{\tau\tau} \rho_u^{tc} (1 + a^*)}{2\sqrt{2} m_\tau (m_b + m_c) V_{cb}^* G_F m_{H^+}^2}\right|^2. \quad (64)$$

From the constraint on $\text{BR}(B_c^- \rightarrow \tau^- \bar{\nu})$, the upper limit on ρ_u^{tc} is modified by about $1/|1 + a^*|$, compared with the Scenario (1). In Figure 4, the constraint from $B_c^- \rightarrow \tau^- \bar{\nu}$ is shown by horizontal dashed black lines (30% and 10%). As discussed in Scenario (1), we should note that $R(D^*)$ can not be larger than 0.279 (0.263) due to the constraint $\text{BR}(B_c^- \rightarrow \tau^- \bar{\nu}) \leq 30\%$ (10%) as shown in Figure 4, since $B_c^- \rightarrow \tau^- \bar{\nu}$ and $\bar{B} \rightarrow D^* \tau^- \bar{\nu}$ are correlated.

2. *Constraint from $B_{d,s} - \bar{B}_{d,s}$ mixing*

In the presence of $\rho_d^{sb,db}$, the flavor changing neutral current appears at the tree level. It would be strongly constrained by $B_{d,s} - \bar{B}_{d,s}$ mixing ($B_{d,s}$ mass differences, $\Delta m_{B_{d,s}}$). For B_s mass difference, the contributions induced by the neutral Higgs boson mediations at the tree level are given by

$$\begin{aligned} \delta(\Delta m_{B_s})^{2\text{HDM}} &= -\frac{5R}{48} m_{B_s} B_{B_s} F_{B_s}^2 \text{Re}[(\rho_d^{sb})^2] \left(\frac{c_{\beta\alpha}^2}{m_h^2} + \frac{s_{\beta\alpha}^2}{m_H^2} - \frac{1}{m_A^2} \right), \\ &\simeq 4 \left(\frac{\rho_d^{sb}}{0.1} \right)^2 \left[\left(\frac{\Delta^2/m_H^2}{10^{-3}} \right) \left(\frac{500 \text{ GeV}}{m_H} \right)^2 - 1.5 \left(\frac{c_{\beta\alpha}}{0.01} \right)^2 \right] [\text{ps}^{-1}]. \end{aligned} \quad (65)$$

(66)

The detail expression is shown in Appendix C, and numerical values of the parameters are listed in Appendix D, and here we have assumed that $\Delta^2 = m_H^2 - m_A^2 \ll m_H^2, m_A^2$.

To satisfy the constraint shown in Eq. (46), the degeneracy between H and A (that is, small Δ^2) has to be realized⁸. For example, Δ^2/m_H^2 has to be much smaller

⁸ Note that $\Delta^2 \simeq \lambda_5 v^2$. Therefore, the small Δ^2 corresponds to the small Higgs quartic coupling λ_5 .

than 10^{-3} for $m_H \simeq 500$ GeV and $\rho_d^{sb} \sim 0.1$. Therefore, we simply assume $\Delta^2 = 0$ in our studies below. To satisfy the constraint, the coupling $\rho_d^{sb} c_{\beta\alpha}$ has to be small. For example, for $c_{\beta\alpha} = 0.01$, $\rho_d^{sb} \leq 0.08$. In Figure 4, the constraints from Δm_{B_s} are shown by long dashed pink line. The regions above the long dashed pink line are excluded.

For B_d mass difference, one can get the expression from one for B_s by replacing its flavor index s with d . To satisfy the constraint on Δm_{B_d} shown in Eq. (46), the coupling $\rho_d^{db} c_{\beta\alpha}$ also has to be small. For example, for $c_{\beta\alpha} = 0.01$, $\rho_d^{db} \leq 0.02$. Since the constraint is very severe, ρ_d^{db} can not generate the significant contributions to $R(D^{(*)})$. Therefore, we do not include the effects of ρ_d^{db} in our studies.

3. Constraint from $B_s \rightarrow \mu^+ \mu^-$ and $\tau^+ \tau^-$

The measured value [70, 71] of branching ratio for $B_s \rightarrow \mu^+ \mu^-$ is

$$\text{BR}(B_s \rightarrow \mu^+ \mu^-) = 2.9_{-0.6}^{+0.7} \times 10^{-9}. \quad (67)$$

The SM prediction [72] is given by

$$\text{BR}(B_s \rightarrow \mu^+ \mu^-)_{\text{SM}} = (3.25 \pm 0.17) \times 10^{-9}, \quad (68)$$

which agrees with the current measured value, and hence the new physics contributions would be strongly constrained.

The 2HDM contributions mediated by the neutral Higgs bosons (h , H , A) at the tree level and the decay rate for $B_s \rightarrow \mu^+ \mu^-$ are presented in Appendix C. If ρ_d^{bs} and $\rho_e^{\mu\mu}$ Yukawa couplings are negligible, non-zero Wilson coefficient is obtained by

$$\frac{G_F^2 m_W^2}{\pi^2} (C_{S(\mu)}^{bs})^{2\text{HDM}} = \frac{\rho_d^{sb*} m_\mu s_{\beta\alpha} c_{\beta\alpha}}{\sqrt{2}v} \left(\frac{1}{m_h^2} - \frac{1}{m_H^2} \right), \quad (69)$$

The branching ratio for $B_s \rightarrow \mu^+ \mu^-$ in the current scenario is given by

$$\text{BR}(B_s \rightarrow \mu^+ \mu^-)_{2\text{HDM}} = \text{BR}(B_s \rightarrow \mu^+ \mu^-)_{\text{SM}} + \Delta\text{BR}(B_s \rightarrow \mu^+ \mu^-), \quad (70)$$

$$\begin{aligned} \Delta\text{BR}(B_s \rightarrow \mu^+ \mu^-) &= \frac{f_{B_s}^2 m_{B_s}^5 \tau_{B_s}}{32\pi(m_b + m_s)^2} \left(1 - \frac{4m_\mu^2}{m_{B_s}^2} \right)^{\frac{3}{2}} \left| \frac{G_F^2 m_W^2}{\pi^2} (C_{S(\mu)}^{bs})^{2\text{HDM}} \right|^2, \\ &= 1.1 \times 10^{-9} \left(\frac{\rho_d^{sb}}{0.33} \right)^2 \left(\frac{c_{\beta\alpha}}{0.01} \right)^2, \end{aligned} \quad (71)$$

Here note that the small Higgs mixing parameter $c_{\beta\alpha}$ can suppress the 2HDM contribution. In Figure 4, the constraints from $B_s \rightarrow \mu^+\mu^-$ are shown by dotted cyan lines in each r_s case. The regions above the line are excluded.

In addition to $B_s \rightarrow \mu^+\mu^-$ process, $B_s \rightarrow \tau^+\tau^-$ process could also put a strong constraint on this scenario. In the presence of non-zero ρ_d^{sb} and $\rho_e^{\tau\tau}$, the 2HDM contributions to Wilson coefficients are given by

$$\begin{aligned} \frac{G_F^2 m_W^2}{\pi^2} (C_{S(\tau)}^{bs})^{2\text{HDM}} &= \frac{\rho_d^{sb} c_{\beta\alpha}}{2m_h^2} \left(\rho_e^{\tau\tau} c_{\beta\alpha} + \frac{\sqrt{2} m_\tau s_{\beta\alpha}}{v} \right) \\ &\quad + \frac{\rho_d^{sb} s_{\beta\alpha}}{2m_H^2} \left(\rho_e^{\tau\tau} s_{\beta\alpha} - \frac{\sqrt{2} m_\tau c_{\beta\alpha}}{v} \right), \end{aligned} \quad (72)$$

$$\frac{G_F^2 m_W^2}{\pi^2} (C_{P(\tau)}^{bs})^{2\text{HDM}} = \frac{\rho_d^{sb} \rho_e^{\tau\tau}}{2m_A^2}, \quad (73)$$

where we have assumed that ρ_d^{sb} and $\rho_e^{\tau\tau}$ are real.

The current experimental bound on this process is given by the LHCb collaboration [73]:

$$\text{BR}(B_s \rightarrow \tau^+\tau^-) \leq 6.8 \times 10^{-3} \quad (74)$$

at 95% C.L. Since the SM prediction is $(7.73 \pm 0.49) \times 10^{-7}$ [74], we neglect it in our analysis below. The branching ratio is given by

$$\begin{aligned} \text{BR}(B_s \rightarrow \tau^+\tau^-)_{2\text{HDM}} &= \frac{\tau_{B_s} f_{B_s}^2 m_{B_s}^5}{128\pi(m_b + m_s)^2} \sqrt{1 - \frac{4m_\tau^2}{m_{B_s}^2} (\rho_d^{sb} \rho_e^{\tau\tau})^2} \\ &\quad \times \left[\frac{s_{\beta\alpha}^4}{m_H^4} (1 + \Delta_\tau)^2 \left(1 - \frac{4m_\tau^2}{m_{B_s}^2}\right) + \frac{1}{m_A^4} \right], \end{aligned} \quad (75)$$

where

$$\Delta_\tau = c_{\beta\alpha} \left\{ \frac{c_{\beta\alpha} m_H^2}{s_{\beta\alpha} m_h^2} + \frac{\sqrt{2} m_\tau}{\rho_e^{\tau\tau} v} \left(\frac{m_H^2}{m_h^2} - 1 \right) \right\}. \quad (76)$$

Note that Δ_τ is small when the Higgs mixing parameter $c_{\beta\alpha}$ is small ($c_{\beta\alpha} \sim 0.01$) and $\rho_e^{\tau\tau} \sim O(0.1)$. The numerical estimate shows

$$\text{BR}(B_s \rightarrow \tau^+\tau^-)_{2\text{HDM}} \simeq 6.6 \times 10^{-3} \left(\frac{\rho_d^{sb}}{0.35} \right)^2 \left(\frac{\rho_e^{\tau\tau}}{-0.2} \right)^2 \left(\frac{500 \text{ GeV}}{m_H} \right)^4, \quad (77)$$

where we have assumed $m_A = m_H$. In Figure 4, the constraints from $B_s \rightarrow \tau^+\tau^-$ are shown by dashed-dotted purple lines in each r_s case. The regions above the line are excluded.

4. Constraint from $B^- \rightarrow \tau^- \bar{\nu}$

The charged Higgs boson can also contribute to $B^- \rightarrow \tau^- \bar{\nu}$ process.⁹ The current experimental value [3, 78] is given by

$$\text{BR}(B^- \rightarrow \tau^- \bar{\nu}) = (1.09 \pm 0.24) \times 10^{-4}. \quad (78)$$

The decay branching ratio for $B^- \rightarrow \tau^- \bar{\nu}$ in the 2HDM can be obtained from one for $B_c^- \rightarrow \tau^- \bar{\nu}$ by replacing its flavor index c with u . Especially, if non-zero $\rho_d^{sb,db}$ are assumed (and $\rho_u^{iu} = 0$ for $i = u, c, t$), the branching ratio in the 2HDM is given by

$$\text{BR}(B^- \rightarrow \tau^- \bar{\nu})_{\text{2HDM}} = \text{BR}(B^- \rightarrow \tau^- \bar{\nu})_{\text{SM}} \left| 1 - \frac{m_B^2 \rho_e^{\tau\tau} Y_{ub}^*}{2\sqrt{2} m_\tau m_b G_F m_{H^+}^2} \right|^2, \quad (79)$$

where the SM ratio and Y_{ub} are expressed by

$$\text{BR}(B^- \rightarrow \tau^- \bar{\nu})_{\text{SM}} = \tau_B \frac{m_B m_\tau^2 f_B^2 G_F^2 |V_{ub}|^2}{8\pi} \left(1 - \frac{m_\tau^2}{m_B^2} \right)^2 = 0.948 \times 10^{-4}, \quad (80)$$

$$Y_{ub} = \rho_d^{sb} \frac{V_{us}}{V_{ub}} + \rho_d^{db} \frac{V_{ud}}{V_{ub}}. \quad (81)$$

Here, to calculate the SM prediction, we have used the best fitted values of the CKM matrix elements ($|V_{ub}| = 0.409 \times 10^{-2}$). Since $|V_{us}/V_{ub}| \simeq 6 \times 10$ and $|V_{ud}/V_{ub}| \simeq 3 \times 10^2$, the flavor violating couplings $\rho_d^{sb,db}$ are strongly constrained. The numerical estimate of the correction to the branching ratio ΔBR ($= \text{BR}_{\text{2HDM}} - \text{BR}_{\text{SM}}$) is given by

$$\begin{aligned} \frac{\Delta\text{BR}}{\text{BR}_{\text{SM}}} &\simeq 0.37 \left(\frac{\rho_e^{\tau\tau}}{-0.2} \right) \left(\frac{\rho_d^{sb}}{0.1} + \frac{\rho_d^{db}}{0.02} \right) \left(\frac{500 \text{ GeV}}{m_{H^+}} \right)^2 \\ &+ 0.32 \left(\frac{\rho_e^{\tau\tau}}{-0.2} \right)^2 \left(\frac{\rho_d^{sb}}{0.1} + \frac{\rho_d^{db}}{0.02} \right)^2 \left(\frac{500 \text{ GeV}}{m_{H^+}} \right)^4. \end{aligned} \quad (82)$$

For example, for $m_{H^+} = 500 \text{ GeV}$ and $\rho_e^{\tau\tau} = -0.2$, which corresponds to the same parameter set as in Figure 4, the constraint from $B^- \rightarrow \tau^- \bar{\nu}$ is given by

$$\rho_d^{sb} \leq 0.1, \quad \rho_d^{db} \leq 0.02, \quad (83)$$

⁹ An importance of the correlation between $B \rightarrow D^{(*)} \tau \bar{\nu}$ and $B \rightarrow \tau \bar{\nu}$ in some models has been discussed in Refs. [75–77].

at 95% C.L. In Figure 4, the constraint from $B^- \rightarrow \tau^- \bar{\nu}$ is shown by the solid green line. The regions above the line are excluded.

Since the experimental constraints are severe, the effects on $R(D^{(*)})$ from the Yukawa couplings $\rho_d^{sb,db}$ in the Scenario (2) are very limited. Therefore, we will not study the Scenario (2) furthermore.

D. Scenario (3): non-zero ρ_u^{tc} , $\rho_e^{\tau\tau}$ and $\rho_e^{\mu\tau}$ (and/or $\rho_e^{e\tau}$)

The lepton flavor violating Yukawa couplings $\rho_e^{\mu\tau}$ and $\rho_e^{e\tau}$ can also affect $\bar{B} \rightarrow D^{(*)}\tau^-\bar{\nu}$. Therefore we study their effects. The charged Higgs contributions are given by

$$1 + \delta_{H^+}^{D^{(*)}\tau}(q^2) = \left| 1 \pm \frac{q^2}{m_\tau(m_b \mp m_c)} \frac{V_{cb}V_{tb}^* \rho_e^{\tau\tau} \rho_u^{tc}}{2\sqrt{2}G_F m_{H^+}^2 |V_{cb}|^2} \right|^2 + \frac{q^4}{m_\tau^2(m_b \mp m_c)^2} \frac{|V_{tb}|^2 |\rho_u^{tc}|^2 (|\rho_e^{e\tau}|^2 + |\rho_e^{\mu\tau}|^2)}{8G_F^2 m_{H^+}^4 |V_{cb}|^2}, \quad (84)$$

where double sign corresponds to $R(D)$ and $R(D^*)$, respectively. As discussed in the Scenario (1), negative $\rho_e^{\tau\tau}$ and positive ρ_u^{tc} increase $R(D^*)$, but decrease $R(D)$. However, since the flavor violating contributions do not interfere with the SM contributions, the effects behave like the imaginary part of $\rho_e^{\tau\tau}$ discussed in the Scenario (1), and always increase both $R(D)$ and $R(D^*)$. Here, to study the effects of $\rho_e^{\mu\tau}$, we take $m_{H^+} = 500$ GeV and $\rho_e^{\tau\tau} = -0.15$ as a reference set of parameters. We parameterize the flavor violating coupling $\rho_e^{\mu\tau}$ as

$$r_\tau = \left| \frac{\rho_e^{\mu\tau}}{\rho_e^{\tau\tau}} \right|. \quad (85)$$

In Figure 5, the predicted values of $R(D)$ and $R(D^*)$ are shown in the Scenario (3). The current experimental limit (1σ) for Belle and world average are also shown. The value of ρ_u^{tc} is assumed to be real and is varied from $\rho_u^{tc} = 0$ (SM point, star-mark) by 0.1 step positively ($\rho_u^{tc} > 0$) and negatively ($\rho_u^{tc} < 0$) with different values of $r_\tau (= |\rho_e^{\mu\tau}/\rho_e^{\tau\tau}|)$, $r_\tau = 1.6$ (orange triangle), 2 (filled cyan quadrangle), 2.7 (open pink quadrangle), and 4 (green \times). The regions with the solid line in each r_τ are consistent with the constraint $\text{BR}(B_c^- \rightarrow \tau^- \bar{\nu}) \leq 30\%$. The regions above filled blue

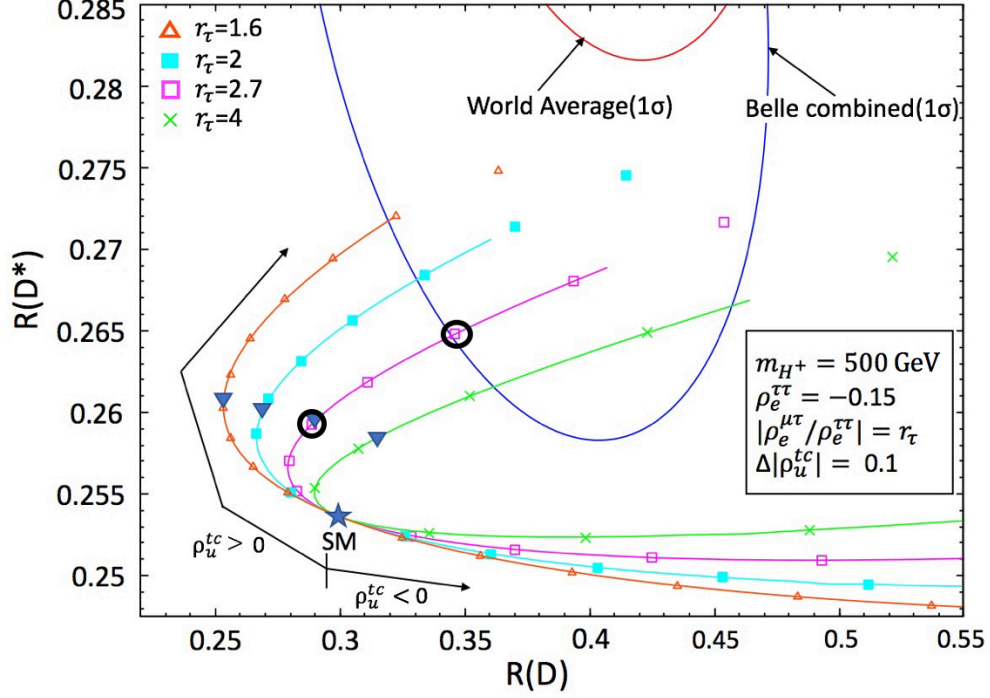


FIG. 5: The predicted values for $R(D)$ and $R(D^*)$ are shown in the scenario (3). The current experimental limits (1σ) for Belle, and world average are also shown. Here we have set $m_{H^+} = 500 \text{ GeV}$, $\rho_e^{\tau\tau} = -0.15$. The value of ρ_u^{tc} is assumed to be real and is varied from the SM point ($\rho_d^{sb} = 0$) (blue star-mark) by 0.1 step positively ($\rho_u^{tc} > 0$) and negatively ($\rho_u^{tc} < 0$) with different values of $r_\tau (= |\rho_e^{\mu\tau}/\rho_e^{\tau\tau}|)$, $r_\tau = 1.6$ (orange triangle), 2 (filled cyan quadrangle), 2.7 (open pink quadrangle), and 4 (green \times). The regions with the solid line in each r_τ are consistent with the constraint $\text{BR}(B_c^- \rightarrow \tau^- \bar{\nu}) \leq 30\%$. The regions above filled blue triangle in each value of r_τ are excluded if $\text{BR}(B_c^- \rightarrow \tau^- \bar{\nu}) \leq 10\%$ is adopted. The points indicated by a black circle are reference points for the LHC physics study discussed later.

triangle in each r_τ are excluded if $\text{BR}(B_c^- \rightarrow \tau^- \bar{\nu}) \leq 10\%$ is imposed. Similar to the effect of imaginary part of the ρ_u^{tc} in the Scenario (1), the constraint on $R(D^*)$ get stronger when $\rho_e^{\mu\tau}$ becomes larger. We see that the predicted values of $R(D^*)$ can not explain the current world average. On the other hand, they can (can not) be within 1σ region of Belle's result as shown in Figure 5 if $\text{BR}(B_c^- \rightarrow \tau^- \bar{\nu}) \leq 30\%$ (10%) is adopted. From Eq. (84), the effect of non-zero $\rho_e^{e\tau}$ on $R(D^{(*)})$ is expected

to be the same as one of $\rho_e^{\mu\tau}$.

So far we have fixed parameters $m_{H^+} = 500$ GeV and $\rho_e^{\tau\tau} = -0.15$. The predicted values of $R(D^{(*)})$ depend on parameter sets $\rho_e^{\tau\tau}\rho_u^{tc}/m_{H^+}^2$ and $|\rho_u^{tc}\rho_e^{i\tau}/m_{H^+}^2|^2$ where $i = e, \mu$. Therefore, even if we change m_{H^+} and $\rho_e^{\tau\tau}$ but these parameter sets are fixed, the predicted values do not change. For the LHC physics study discussed later, we choose two reference points in the Scenario (3). As a reference point 1, we take a point with $\rho_u^{tc}\rho_e^{\tau\tau} = -0.075$, $r_\tau = 2.7$ and $m_{H^+} = 500$ GeV, which satisfies the constraint $\text{BR}(B_c^- \rightarrow \tau^- \bar{\nu}) \leq 30\%$, but not $\text{BR}(B_c^- \rightarrow \tau^- \bar{\nu}) \leq 10\%$. As a reference point 2 in Scenario (3), we choose a point with $\rho_u^{tc}\rho_e^{\tau\tau} = -0.045$, $r_\tau = 2.7$ and $m_{H^+} = 500$ GeV, which satisfies the constraint $\text{BR}(B_c^- \rightarrow \tau^- \bar{\nu}) \leq 10\%$.

Below, we have several comments. The q^2 distribution in $d\Gamma(\bar{B} \rightarrow D\tau^- \bar{\nu})/dq^2$ is similar to the one in Scenario (1). The difference from the SM distribution increases in large q^2 regions as $\rho_e^{\mu\tau}$ becomes larger.

The effects in the $b \rightarrow s$ transition processes are also the same as one in Scenario (1).

A new interesting process is $\tau \rightarrow \mu\gamma$ ($\tau \rightarrow e\gamma$) when both $\rho_e^{\tau\tau}$ and $\rho_e^{\mu\tau}$ ($\rho_e^{e\tau}$) Yukawa couplings are non-zero. We will discuss the $\tau \rightarrow \mu\gamma$ process in the next section.

1. $\tau \rightarrow \mu\gamma$

In the presence of non-zero $\rho_e^{\tau\tau}$ and $\rho_e^{\mu\tau}$, $\tau \rightarrow \mu\gamma$ process is generated. As discussed in Ref. [16], not only 1-loop contribution but also Barr-Zee type 2-loop contribution are important. The 1-loop contribution tends to be suppressed when H and A are degenerate. On the other hand, the Barr-Zee type 2-loop contribution is affected by ρ_u^{tt} , which does not have an impact on $R(D^{(*)})$. In Figure 6, the predicted branching ratio $\text{BR}(\tau \rightarrow \mu\gamma)$ is shown as a function of ρ_u^{tt} and r_1 ($= \frac{\rho_e^{\mu\tau}}{-0.27} = \frac{\rho_e^{\tau\tau}}{-0.1}$). Here we have set $c_{\beta\alpha} = 0.001$, $m_{H/A} = m_{H^+} = 500$ GeV and $r_\tau = |\rho_e^{\mu\tau}/\rho_e^{\tau\tau}| = 2.7$. We note that this parameter set is consistent with the constraint from $h \rightarrow \mu\tau$. As seen in Figure 6, the interesting parameter region for $R(D^{(*)})$ is consistent with the current experimental upper limit on $\text{BR}(\tau \rightarrow \mu\gamma)$ [$\text{BR}(\tau \rightarrow \mu\gamma) \leq 4.4 \times 10^{-8}$] unless the

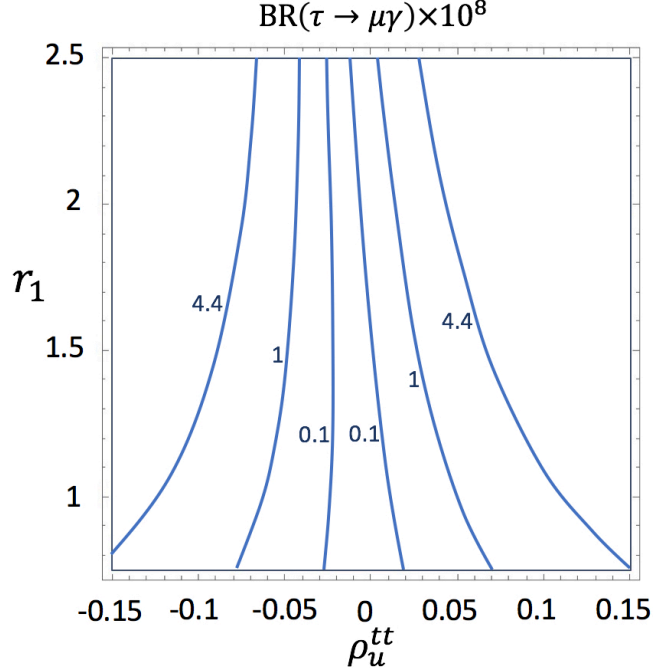


FIG. 6: $\text{BR}(\tau \rightarrow \mu\gamma)$ is shown as a function of ρ_u^{tt} and r_1 ($= \frac{\rho_e^{\mu\tau}}{-0.27} = \frac{\rho_e^{\tau\tau}}{-0.1}$). Here we have assumed that $c_{\beta\alpha} = 0.001$, $m_{H/A} = m_{H^\pm} = 500$ GeV and $r_\tau = |\rho_e^{\mu\tau}/\rho_e^{\tau\tau}| = 2.7$. Note that the current experimental upper limit on $\text{BR}(\tau \rightarrow \mu\gamma)$ is 4.4×10^{-8} .

$|\rho_u^{tt}|$ is large ($|\rho_u^{tt}| > 0.1$).¹⁰

E. Type II two Higgs doublet model

So far, we have discussed $R(D^{(*)})$ in the general 2HDM. As a comparison, here we discuss the typical prediction of $R(D^{(*)})$ in type II 2HDM. The Yukawa interactions in the type II 2HDM are restricted by the fermion masses and $\tan\beta$, which is a ratio between vacuum expectation values of two neutral Higgs components, and hence the predicted values of $R(D^{(*)})$ are very limited in contrast to those in the general 2HDM. In Figure 7, the predicted values for $R(D)$ and $R(D^*)$ are shown in the type II 2HDM. The current experimental limits (1σ) for BaBar, Belle and world

¹⁰ When ρ_u^{tt} is not zero, the charged Higgs boson contributions to $b \rightarrow s$ transition processes are modified. When ρ_u^{tt} is small ($|\rho_u^{tt}| \leq 0.1$), the effects are limited. In Appendix C, we present the effects with non-zero ρ_u^{tt} on the $b \rightarrow s$ transition processes.

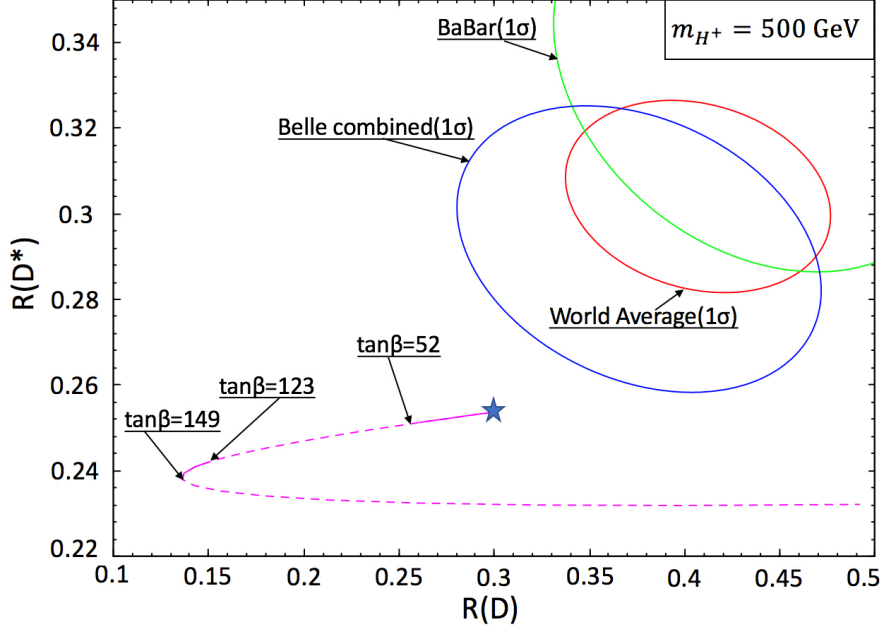


FIG. 7: The predicted values for $R(D)$ and $R(D^*)$ are shown in the type II 2HDM. The current experimental limits (1σ) for Belle, and world average are also shown. Here we have set $m_{H^+} = 500$ GeV, and $\tan\beta$ is varied from zero (SM point, star-mark). The constraint from $B^- \rightarrow \tau^- \bar{\nu}$ is imposed and the regions with solid line are allowed, on the other hand, the regions with the dashed line are excluded.

average are also shown. Here we assume that $m_{H^+} = 500$ GeV, and $\tan\beta$ is varied from zero (SM point, star-mark). The constraint from $B^- \rightarrow \tau^- \bar{\nu}$ is imposed, and the regions with solid line are allowed, on the other hand, the regions with dashed line are excluded by the $B^- \rightarrow \tau^- \bar{\nu}$ constraint. As can be seen from Figure 7, the predicted values can not reach the region within the 1σ of BaBar, Belle nor the world average. We would like to stress that the predictions of the general 2HDM would be very different from those in the type II 2HDM.

V. CONSTRAINTS AND IMPLICATIONS AT THE LHC

So far, we have discussed the possible effects on $R(D^{(*)})$ and various constraints from the flavor physics in each scenario. In this section, we study productions and decays of heavy Higgs bosons at the LHC and discuss possible constraints from the

LHC results and implications at the LHC.

A. Productions for heavy neutral Higgs bosons

1. Scenario (1)

Since the Yukawa coupling $\rho_e^{\tau\tau}$ plays a crucial role to induce the important contribution to $R(D^{(*)})$, the heavy neutral Higgs boson search in $H/A \rightarrow \tau^+\tau^-$ mode at the LHC experiment would be important [33]. When the Higgs mixing parameter $c_{\beta\alpha}$ is small, the gluon-gluon fusion production for heavy neutral Higgs bosons H and A relies on the interaction via ρ_u^{tt} , which does not affect $R(D^{(*)})$. Here we use HIGLU [79] to calculate the production cross section for H and A via the gluon-gluon fusion process at the NNLO and they are given by

$$\sigma(pp \rightarrow H) = 1.4 |\rho_u^{tt}|^2 \text{ [pb]}, \quad \sigma(pp \rightarrow A) = 2.3 |\rho_u^{tt}|^2 \text{ [pb]}, \quad (86)$$

at $\sqrt{s} = 8 \text{ TeV}$ for $m_{H/A} = 500 \text{ GeV}$, and

$$\sigma(pp \rightarrow H) = 4.9 |\rho_u^{tt}|^2 \text{ [pb]}, \quad \sigma(pp \rightarrow A) = 8.3 |\rho_u^{tt}|^2 \text{ [pb]}, \quad (87)$$

at $\sqrt{s} = 13 \text{ TeV}$ for $m_{H/A} = 500 \text{ GeV}$.

For the LHC physics study in Scenario (1), we consider reference point 1 and 2, shown by black circle points in Figure 2. As discussed in Scenario (1), the reference point 1 is defined by a point with $\rho_u^{tc} \rho_{\tau\tau} = -0.2$, $\delta_{\tau\tau} = \frac{5\pi}{12}$ and $m_{H^+} = 500 \text{ GeV}$, and the reference point 2 is $\rho_u^{tc} \rho_{\tau\tau} = -0.156$, $\delta_{\tau\tau} = \frac{\pi}{2}$ and $m_{H^+} = 500 \text{ GeV}$. The decay branching ratios of H and A are shown as a function of ρ_u^{tc} in Figure 8.¹¹ For solid lines (dashed lines), we have taken the reference point 1 (reference point 2). Here we assume that $m_{H/A} = m_{H^+}$ and $c_{\beta\alpha} = 0.001$ as a reference parameter set for Scenario (1). We also fix $\rho_u^{tt} = 0.1$.¹²

When we fix m_{H^+} ($m_{H^+} = 500 \text{ GeV}$) and a product of the Yukawa couplings $\rho_u^{tc} \rho_e^{\tau\tau}$, the predicted values of $R(D^{(*)})$ are also fixed. In the reference parameter

¹¹ When H , A and H^+ are not degenerate, two body decays such as $H \rightarrow AZ$ and $H \rightarrow H^\pm W^\mp$ may be allowed. However, we note that for the heavy Higgs boson like $m_H \simeq 500 \text{ GeV}$, non-degeneracy for such two body decays requires large Higgs quartic couplings $\lambda_{4,5}$.

¹² We note that the phase $\delta_{\tau\tau}$ does not affect the decay $H/A \rightarrow \tau^+\tau^-$.

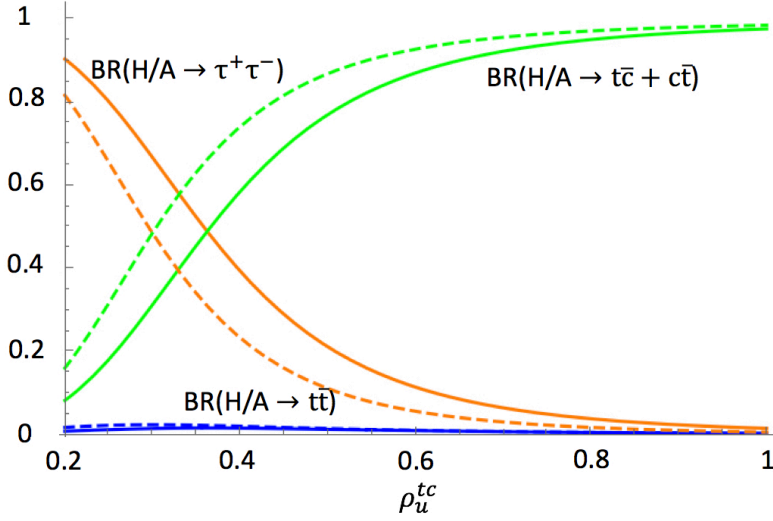


FIG. 8: The decay branching ratios of H and A are shown as a function of ρ_u^{tc} . For solid lines, we take a reference point 1 ($\rho_u^{tc}\rho_{\tau\tau} = -0.2$, $\delta_{\tau\tau} = \frac{5\pi}{12}$ and $m_{H^+} = 500$ GeV). For dashed lines, a reference point 2 ($\rho_u^{tc}\rho_{\tau\tau} = -0.156$, $\delta_{\tau\tau} = \frac{\pi}{2}$ and $m_{H^+} = 500$ GeV) is taken. We have also assumed that $m_{H/A} = m_{H^+}$ and $c_{\beta\alpha} = 0.001$ as a reference parameter set for Scenario (1). Here ρ_u^{tt} is also fixed to be 0.1 ($\rho_u^{tt} = 0.1$).

set, on the other hand, the decay branching ratios for H/A depend on ρ_u^{tc} (fixing a value of $\rho_u^{tc}\rho_e^{\tau\tau}$) as shown in Figure 8. When ρ_u^{tc} is small (large), the dominant decay mode is $H/A \rightarrow \tau^+\tau^-$ ($H/A \rightarrow t\bar{c} + c\bar{t}$) because $\rho_{\tau\tau}$ (ρ_u^{tc}) is large. For $\rho_u^{tt} = 0.1$, a decay branching ratio for $H/A \rightarrow t\bar{t}$ is always small. For a fixed value of ρ_u^{tc} , an absolute value of $\rho_e^{\tau\tau}$ in the reference point 1 ($|\rho_e^{\tau\tau}| = 0.2/\rho_u^{tc}$) is larger than one in the reference point 2 ($|\rho_e^{\tau\tau}| = 0.156/\rho_u^{tc}$), and hence the branching ratio of $H/A \rightarrow \tau^+\tau^-$ ($H/A \rightarrow t\bar{c} + c\bar{t}$) in the reference point 1 is larger (smaller) than one in the reference point 2, as seen in Figure 8.

In Figure 9, the cross sections $\sigma(pp \rightarrow H/A) \times \text{BR}(H/A \rightarrow \tau^+\tau^-)$ [pb] via the gluon-gluon fusion production at $\sqrt{s} = 8$ TeV (dashed orange line) and $\sqrt{s} = 13$ TeV (solid blue line) are shown as a function of ρ_u^{tt} . Here the sum of H and A contributions are taken into account. We have taken $\rho_u^{tc} = 0.3$ in the reference parameter set with the reference point 1, mentioned in Figure 8. We also show the regions which are excluded (95 % C.L.) by the LHC experiment at $\sqrt{s} = 7$ and 8 TeV [80, 81] (sky blue shaded region (upper)) and at $\sqrt{s} = 13$ TeV [82, 83] (lemon

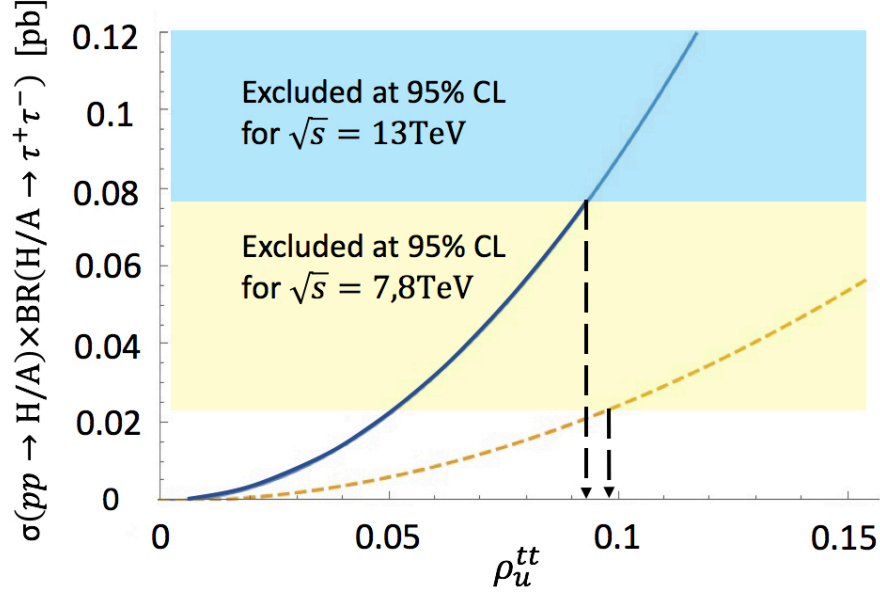


FIG. 9: The cross section $\sigma(pp \rightarrow H/A) \times \text{BR}(H/A \rightarrow \tau^+\tau^-)$ [pb] via the gluon-gluon fusion production at $\sqrt{s} = 8$ TeV (dashed orange line) and $\sqrt{s} = 13$ TeV (solid blue line) are shown as a function of ρ_u^{tt} . Here we show the sum of the H and A contributions. We have taken $\rho_u^{tc} = 0.3$ in the reference parameter set with the reference point 1, mentioned in Figure 8. We also show the regions which are excluded by the LHC experiment (95% C.L.) at $\sqrt{s} = 7$ and 8 TeV [80, 81] (lemon yellow shaded region (lower)) and at $\sqrt{s} = 13$ TeV [82, 83] (sky blue shaded region (upper)), respectively.

yellow shaded region (lower)), respectively. As can be seen from Figure 9, the Run 2 results already put a stronger constraint on ρ_u^{tt} .

In Figure 10, the cross section $\sigma(pp \rightarrow H/A) \times \text{BR}(H/A \rightarrow \tau^+\tau^-)$ [pb] via the gluon-gluon fusion production (solid green lines) at $\sqrt{s} = 13$ TeV is shown as a function of ρ_u^{tc} and ρ_u^{tt} . Here the sum of H and A contributions are shown. We have taken the reference parameter set with the reference point 1, mentioned in Figure 8, and the shaded region is excluded at 95 % C.L. by the search for $\sigma(pp \rightarrow H/A) \times \text{BR}(H/A \rightarrow \tau^+\tau^-)$ at the LHC experiment [82, 83].

In addition to the gluon-gluon fusion production for the neutral Higgs bosons (H and A), in the existence of the sizable ρ_u^{tc} Yukawa coupling, the production via ρ_u^{tc} ($gc \rightarrow t + H/A$) shown in Figure 11 would be important. We calculate

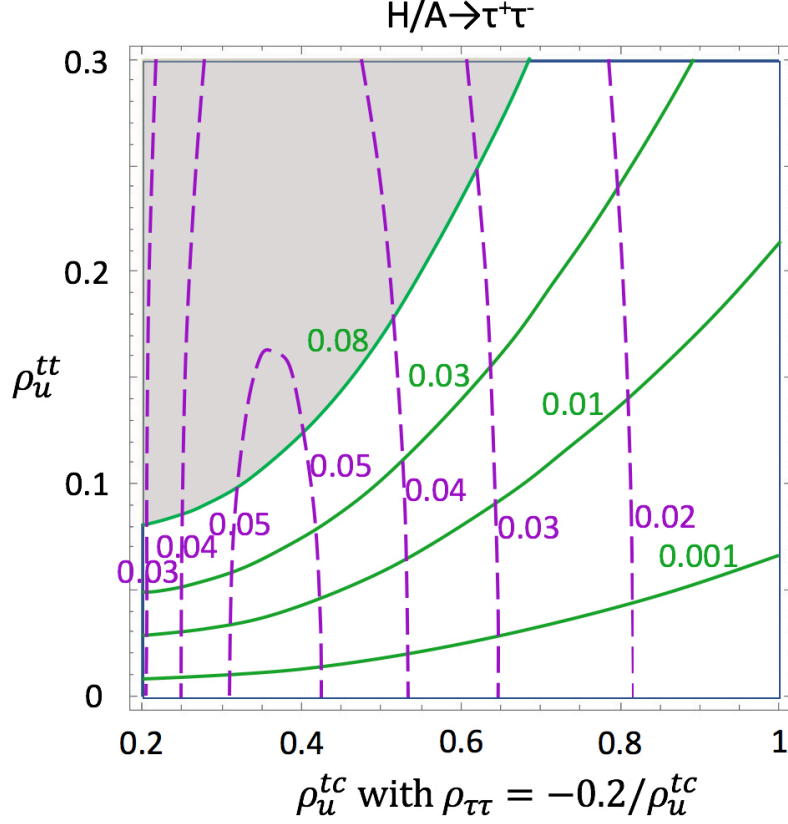


FIG. 10: The cross section $\sigma(pp \rightarrow H/A) \times \text{BR}(H/A \rightarrow \tau^+\tau^-)$ [pb] via the gluon-gluon fusion production (solid green lines) and the cross section $\sigma(pp \rightarrow t + H/A) \times \text{BR}(H/A \rightarrow \tau^+\tau^-)$ [pb] via $cg \rightarrow t + H/A$ process (dashed purple lines) at $\sqrt{s} = 13$ TeV are shown as a function of ρ_u^{tc} and ρ_u^{tt} . Here the sum of H and A contributions are shown. Here we have taken the reference parameter set with the reference point 1, mentioned in Figure 8. The shaded region is excluded at 95 % C.L. by the search for $\sigma(pp \rightarrow H/A) \times \text{BR}(H/A \rightarrow \tau^+\tau^-)$ via the gluon-gluon fusion production at the LHC experiments [82, 83].

$\sigma(pp \rightarrow t + H/A)$ via $gc \rightarrow t + H/A$ process by using the calchep [84] with CTEQ leading order PDF. The result is given by

$$\sigma(pp \rightarrow t + H/A) = 0.8 |\rho_u^{tc}|^2 \text{ [pb]}, \quad (88)$$

at $\sqrt{s} = 13$ TeV for $m_{H/A} = 500$ GeV. In Figure 10, we also show the results of $\sigma(pp \rightarrow t + H/A) \times \text{BR}(H/A \rightarrow \tau^+\tau^-)$ [pb] (dashed purple lines) as a function of ρ_u^{tc} and ρ_u^{tt} . As one can see, the cross sections are sizable. For the reference point 2 with the fixed $\rho_u^{tc,tt}$, the cross sections $\sigma(pp \rightarrow H/A) \times \text{BR}(H/A \rightarrow \tau^+\tau^-)$

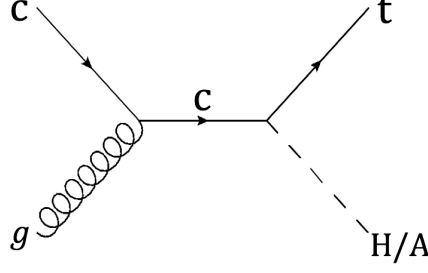


FIG. 11: A Feynman diagram for neutral Higgs boson production via $gc \rightarrow t + H/A$ process.

and $\sigma(pp \rightarrow t + H/A) \times \text{BR}(H/A \rightarrow \tau^+\tau^-)$ are slightly smaller than those for the reference point 1 because of smaller $\text{BR}(H/A \rightarrow \tau^+\tau^-)$ as shown in Figure 8.

Since the heavy neutral Higgs bosons significantly decay to top and charm quarks as shown in Figure 8, the exotic decay mode would be important. In a left figure of Figure 12, we present the cross sections $\sigma(pp \rightarrow H/A) \times \text{BR}(H/A \rightarrow t\bar{c} + c\bar{t})$ [pb] via the gluon-gluon fusion process (solid green lines) and $\sigma(pp \rightarrow t + H/A) \times \text{BR}(H/A \rightarrow t\bar{c} + c\bar{t})$ [pb] via $cg \rightarrow t + H/A$ process (dashed purple lines) as a function of ρ_u^{tc} and ρ_u^{tt} at $\sqrt{s} = 13$ TeV. The same parameter set is taken as in Figure 10. As ρ_u^{tc} gets larger, the production cross section via $cg \rightarrow t + H/A$ becomes significantly larger. For the reference point 2 with the fixed values of $\rho_u^{tc,tt}$, the cross sections $\sigma(pp \rightarrow H/A) \times \text{BR}(H/A \rightarrow t\bar{c} + c\bar{t})$ and $\sigma(pp \rightarrow t + H/A) \times \text{BR}(H/A \rightarrow t\bar{c} + c\bar{t})$ are even larger than those for the reference point 1 because of larger $\text{BR}(H/A \rightarrow t\bar{c} + c\bar{t})$, as seen in Figure 8.

On the other hand, the production cross sections $\sigma(pp \rightarrow H/A) \times \text{BR}(H/A \rightarrow t\bar{t})$ [pb] via the gluon-gluon fusion process and $\sigma(pp \rightarrow t + H/A) \times \text{BR}(H/A \rightarrow t\bar{t})$ [pb] via $cg \rightarrow t + H/A$ process tend to be smaller than other modes because of the smaller branching ratio. In a right figure of Figure 12, the cross sections $\sigma(pp \rightarrow H/A) \times \text{BR}(H/A \rightarrow t\bar{t})$ [pb] via the gluon-gluon fusion process (solid green lines) and $\sigma(pp \rightarrow t + H/A) \times \text{BR}(H/A \rightarrow t\bar{t})$ [pb] via $cg \rightarrow t + H/A$ process (dashed purple lines) are shown as a function of ρ_u^{tc} and ρ_u^{tt} at $\sqrt{s} = 13$ TeV.

So far, we have fixed the heavy neutral Higgs boson masses ($m_{H/A} = 500$ GeV). In a left figure of Figure 13, the cross sections $\sigma(pp \rightarrow H/A) \times \text{BR}(H/A \rightarrow \tau^+\tau^-)$

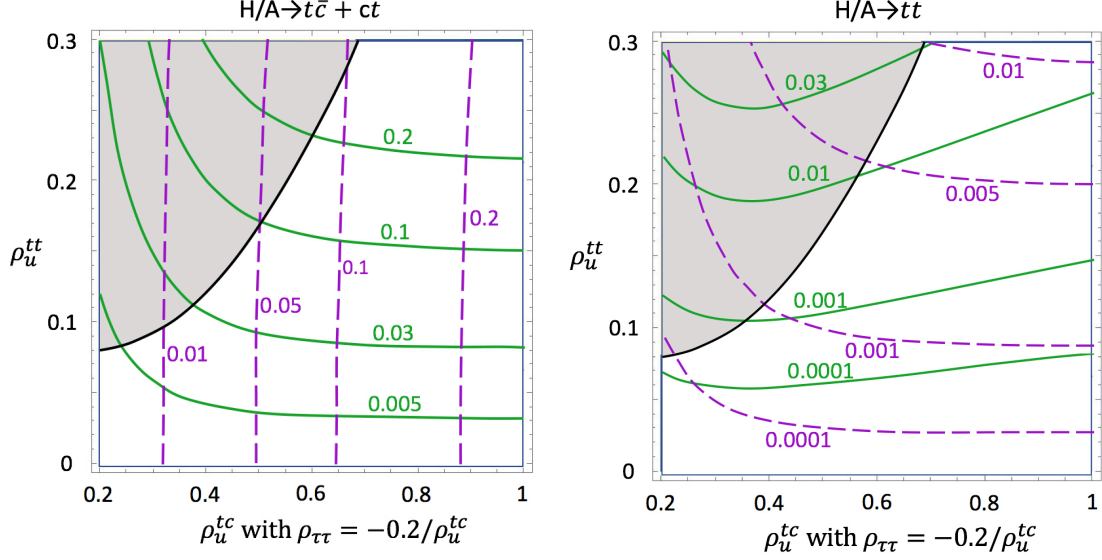


FIG. 12: **[Left]** The cross section $\sigma(pp \rightarrow H/A) \times \text{BR}(H/A \rightarrow t\bar{c} + c\bar{t})$ [pb] via the gluon-gluon fusion production (solid green lines) and the cross section $\sigma(pp \rightarrow t + H/A) \times \text{BR}(H/A \rightarrow t\bar{c} + c\bar{t})$ [pb] via $cg \rightarrow t + H/A$ process (dashed purple lines) and **[Right]** the cross section $\sigma(pp \rightarrow H/A) \times \text{BR}(H/A \rightarrow t\bar{t})$ [pb] via the gluon-gluon fusion production (solid green lines) and the cross section $\sigma(pp \rightarrow t + H/A) \times \text{BR}(H/A \rightarrow t\bar{t})$ [pb] via $cg \rightarrow t + H/A$ process (dashed purple lines) are shown as a function of ρ_u^{tc} and ρ_u^{tt} at $\sqrt{s} = 13$ TeV. The same parameter set is taken as in Figure 10. The shaded region is excluded at 95 % C.L. by the search for $\sigma(pp \rightarrow H/A) \times \text{BR}(H/A \rightarrow \tau^+\tau^-)$ via the gluon-gluon fusion production at the LHC experiment [82, 83].

[pb] via the gluon-gluon fusion process at $\sqrt{s} = 13$ TeV are shown as a function of the heavy Higgs boson mass $m_{H/A}$ [GeV]. In order to fix the predicted values of $R(D^{(*)})$, we also scale the relevant Yukawa couplings as

$$\rho_f^{ij} = \bar{\rho}_f^{ij} \left(\frac{m_{H/A}}{500 \text{ GeV}} \right), \quad (89)$$

where $\bar{\rho}_f^{ij}$ are the reference values for $m_{H/A} = 500$ GeV. Here we have assumed $m_{H/A} = m_{H^+}$. We have set $\bar{\rho}_u^{tc} = 0.3$ and $\bar{\rho}_{\tau\tau} = 0.67$ (the reference point 1). The predicted cross sections with $\bar{\rho}_u^{tt} = 0.06$, $\bar{\rho}_u^{tc} = 0.075$ and $\bar{\rho}_u^{tt} = 0.09$ as well as the ATLAS and CMS limits (95 % C.L.) are shown. As can be seen from the figure, the constraints around $m_{H/A} = 400$ GeV are somewhat stronger than one at $m_{H/A} = 500$

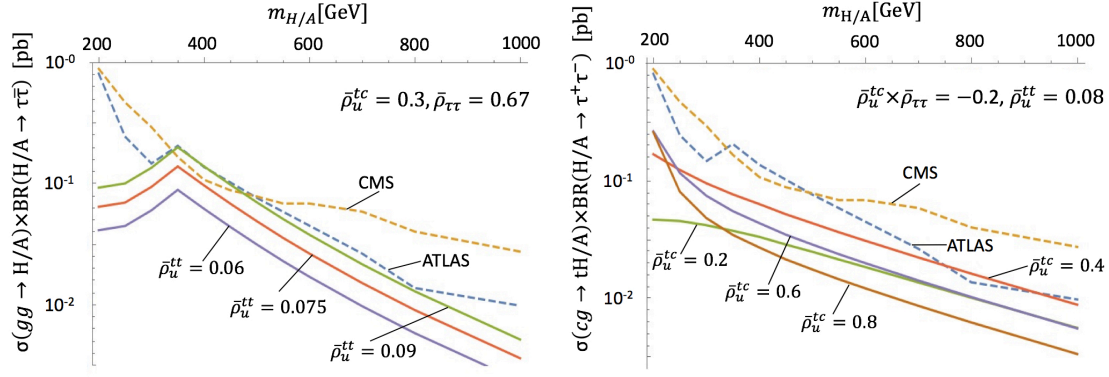


FIG. 13: **[Left]** The cross sections $\sigma(pp \rightarrow H/A) \times \text{BR}(H/A \rightarrow \tau^+\tau^-)$ [pb] via the gluon-gluon fusion production at $\sqrt{s} = 13$ TeV are shown as a function of the heavy Higgs boson mass $m_{H/A}$ [GeV]. In order to fix the predicted values of $R(D^{(*)})$, the relevant Yukawa couplings are also scaled as $\rho_f^{ij} = \bar{\rho}_f^{ij} \left(\frac{m_{H/A}}{500 \text{ GeV}} \right)$. Here $\bar{\rho}_f^{ij}$ are the reference values for $m_{H/A} = m_{H^+} = 500$ GeV, and we have set $\bar{\rho}_u^{tc} = 0.3$ and $\bar{\rho}_{\tau\tau} = 0.67$ (the reference point 1). The predicted cross sections with $\bar{\rho}_u^{tt} = 0.06$, $\bar{\rho}_u^{tt} = 0.075$ and $\bar{\rho}_u^{tt} = 0.09$ as well as the ATLAS (blue dotted line) and CMS (dotted orange line) limits (95 % C.L.) are shown. **[Right]** The cross sections $\sigma(pp \rightarrow t + H/A) \times \text{BR}(H/A \rightarrow \tau^+\tau^-)$ [pb] via $cg \rightarrow t + H/A$ process at $\sqrt{s} = 13$ TeV are shown as a function of $m_{H/A}$ [GeV]. We have taken $\bar{\rho}_u^{tt} = 0.08$ and $\bar{\rho}_u^{tc} \bar{\rho}_{\tau\tau} = -0.2$ (the reference point 1). The predicted cross sections with $\bar{\rho}_u^{tc} = 0.2$, 0.4 , 0.6 and 0.8 are shown. As a comparison, ATLAS and CMS limits (95 % C.L.) on $\sigma(pp \rightarrow H/A) \times \text{BR}(H/A \rightarrow \tau^+\tau^-)$ [pb] via the gluon-gluon fusion production at $\sqrt{s} = 13$ TeV are also shown.

GeV because of the stronger CMS limit. In the small ($m_{H/A} < 300$ GeV) and large ($m_{H/A} > 800$ GeV) mass regions, the constraints become weaker. In a right figure of Figure 13, the cross sections $\sigma(pp \rightarrow t + H/A) \times \text{BR}(H/A \rightarrow \tau^+\tau^-)$ [pb] via $cg \rightarrow t + H/A$ process at $\sqrt{s} = 13$ TeV are shown as a function of $m_{H/A}$ [GeV]. We have taken $\bar{\rho}_u^{tt} = 0.08$ and $\bar{\rho}_u^{tc} \bar{\rho}_{\tau\tau} = -0.2$ (the reference point 1). The predicted cross sections with $\bar{\rho}_u^{tc} = 0.2$, 0.4 , 0.6 and 0.8 are shown. As a comparison, ATLAS and CMS limits (95 % C.L.) on $\sigma(pp \rightarrow H/A) \times \text{BR}(H/A \rightarrow \tau^+\tau^-)$ [pb] via the gluon-gluon fusion production at $\sqrt{s} = 13$ TeV are also shown.

2. Scenario (3)

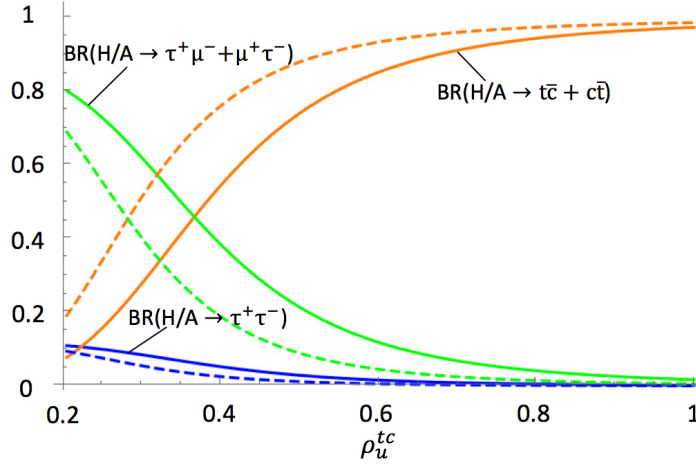


FIG. 14: The decay branching ratios of H/A are shown as a function of ρ_u^{tc} . For solid lines, the reference point 1 ($\rho_u^{tc}\rho_e^{\tau\tau} = -0.075$, $r_\tau(=|\rho_e^{\mu\tau}/\rho_e^{\tau\tau}|) = 2.7$ and $m_{H^+} = 500$ GeV) is taken. For dashed lines, the reference point 2 ($\rho_u^{tc}\rho_e^{\tau\tau} = -0.045$, $r_\tau(=|\rho_e^{\mu\tau}/\rho_e^{\tau\tau}|) = 2.7$ and $m_{H^+} = 500$ GeV) is set. Here we also assume that $m_{H/A} = m_{H^+} = 500$ GeV and $c_{\beta\alpha} = 0.001$ as a reference parameter set. Here a value of ρ_u^{tt} is fixed to be -0.1 . For this ρ_u^{tt} , $\text{BR}(H/A \rightarrow t\bar{t})$ is small (not shown in the figure).

A main difference between Scenario (1) and (3) is the existence of non-zero $\rho_e^{\mu\tau}$ coupling. Because of non-zero $\rho_e^{\mu\tau}$, the size of $\rho_e^{\tau\tau}$ coupling can be smaller than one for the Scenario (1) in the interesting regions for $R(D^{(*)})$. For the LHC study in Scenario (3), we consider two reference points, which are denoted by a black circle in Figure 5 for Scenario (3). As a reference point 1, parameters with $\rho_u^{tc}\rho_e^{\tau\tau} = -0.075$, $r_\tau(=|\rho_e^{\mu\tau}/\rho_e^{\tau\tau}|) = 2.7$ and $m_{H^+} = 500$ GeV are set, and as a reference point 2, those with $\rho_u^{tc}\rho_e^{\tau\tau} = -0.045$, $r_\tau(=|\rho_e^{\mu\tau}/\rho_e^{\tau\tau}|) = 2.7$ are taken. As a reference parameter set for Scenario (3), we also assume that $m_{H/A} = m_{H^+} = 500$ GeV and $c_{\beta\alpha} = 0.001$. In Figure 14, the decay branching ratios of H/A are shown as a function of ρ_u^{tc} . Here we have taken the reference parameter set with the reference point 1 (solid lines) and the reference point 2 (dashed lines) as mentioned above. A value of ρ_u^{tt} is fixed to be -0.1 . For this ρ_u^{tt} , $\text{BR}(H/A \rightarrow t\bar{t})$ is small (not shown in the figure). As we can see from the figure, $\text{BR}(H/A \rightarrow \tau^+\tau^-)$ can be much smaller than one in

the Scenario (1), on the other hand, $\text{BR}(H/A \rightarrow \mu^\pm \tau^\mp)$ can be of order one. Since absolute values of $\rho_e^{\tau\tau}$ and $\rho_e^{\mu\tau}$ in the reference point 1 ($|\rho_e^{\tau\tau}| = 0.075/\rho_u^{tc}$) are larger than those in the reference point 2 ($|\rho_e^{\tau\tau}| = 0.045/\rho_u^{tc}$) with the fixed value of ρ_u^{tc} , $\text{BR}(H/A \rightarrow \tau^+ \tau^-)$ and $\text{BR}(H/A \rightarrow \mu^\pm \tau^\mp)$ ($\text{BR}(H/A \rightarrow t\bar{c} + c\bar{t})$) in the reference point 1 are larger (smaller) than those in the reference point 2.

In Figure 15, the cross section $\sigma(pp \rightarrow H/A) \times \text{BR}(H/A)$ [pb] via the gluon-gluon fusion production (solid orange lines) and the cross section $\sigma(pp \rightarrow t + H/A) \times \text{BR}(H/A)$ [pb] via $cg \rightarrow t + H/A$ process (dashed-dotted purple lines) at $\sqrt{s} = 13$ TeV are shown as a function of ρ_u^{tc} and ρ_u^{tt} in cases with $\text{BR}(H/A) = \text{BR}(H/A \rightarrow \tau^+ \tau^-)$ (upper left figure), $\text{BR}(H/A) = \text{BR}(H/A \rightarrow \mu^\pm \tau^\mp)$ (upper right figure), and $\text{BR}(H/A) = \text{BR}(H/A \rightarrow t\bar{c} + c\bar{t})$ (lower figure). Here we have taken the reference parameter set with the reference point 1, mentioned in Figure 14. The dotted green lines show the branching ratio of $\tau \rightarrow \mu\gamma$ (in a unit of 10^{-8}). The shaded regions are excluded by the current limit of $\tau \rightarrow \mu\gamma$ [$\text{BR}(\tau \rightarrow \mu\gamma) \leq 4.4 \times 10^{-8}$]. In $H/A \rightarrow \tau^+ \tau^-$ mode (upper left figure of Figure 15), the cross sections are much smaller compared to those in Scenario (1) because of the smaller decay branching ratio. In $H/A \rightarrow \mu^\pm \tau^\mp$ mode (upper right figure of Figure 15), the cross section can be as large as $O(0.01)$ pb especially in $cg \rightarrow t + H/A$ production mode. On the other hand, the cross sections of $\text{BR}(H/A \rightarrow t\bar{c} + c\bar{t})$ mode can be as large as those in a case of Scenario (1). For the reference point 2 with the fixed values of $\rho_u^{tc, tt}$, the cross sections $\sigma(pp \rightarrow H/A) \times \text{BR}(H/A \rightarrow \mu^\pm \tau^\mp)$ and $\sigma(pp \rightarrow t + H/A) \times \text{BR}(H/A \rightarrow \mu^\pm \tau^\mp)$ are smaller, on the other hand, the cross sections $\sigma(pp \rightarrow H/A) \times \text{BR}(H/A \rightarrow t\bar{c} + c\bar{t})$ and $\sigma(pp \rightarrow t + H/A) \times \text{BR}(H/A \rightarrow t\bar{c} + c\bar{t})$ are larger than those for the reference point 1, because of $\text{BR}(H/A)$ shown in Figure 14.

Therefore, again, the searches for the exotic productions and exotic decay modes of the heavy neutral Higgs bosons would be important to probe the interesting parameter regions for $R(D^{(*)})$.

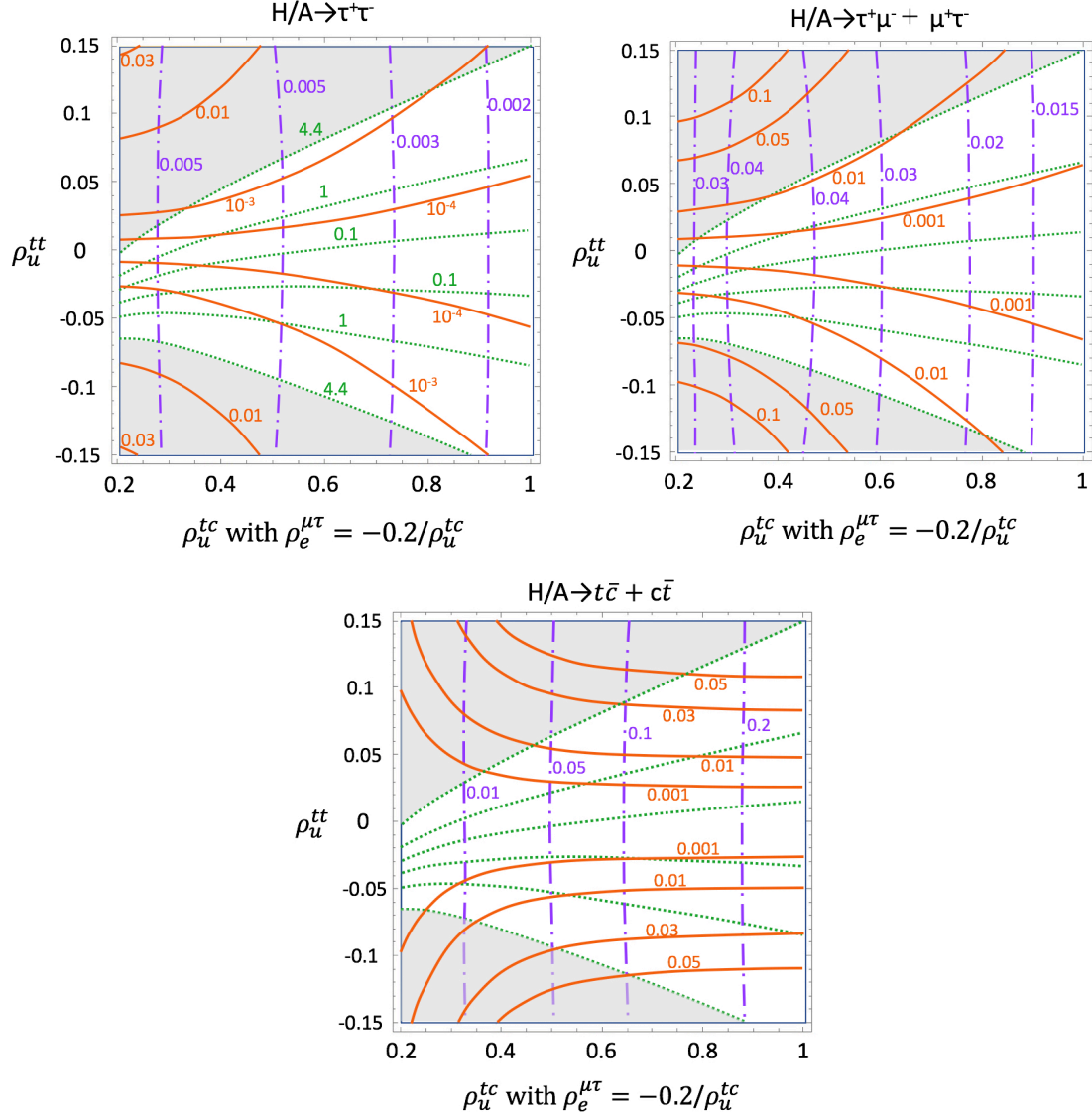


FIG. 15: The cross section $\sigma(pp \rightarrow H/A) \times \text{BR}(H/A)$ [pb] via the gluon-gluon fusion production (solid orange lines) and the cross section $\sigma(pp \rightarrow t + H/A) \times \text{BR}(H/A)$ [pb] via $cg \rightarrow t + H/A$ process (dashed-dotted purple lines) at $\sqrt{s} = 13$ TeV are shown as a function of ρ_u^{tc} and ρ_u^{tt} in cases with $\text{BR}(H/A) = \text{BR}(H/A \rightarrow \tau^+\tau^-)$ [**upper left figure**], $\text{BR}(H/A) = \text{BR}(H/A \rightarrow \mu^\pm\tau^\mp)$ [**upper right figure**], and $\text{BR}(H/A) = \text{BR}(H/A \rightarrow t\bar{c} + c\bar{t})$ [**lower figure**]. Here we have taken the reference parameter set with the reference point 1, mentioned in Figure 14. The dotted green lines show the branching ratio of $\tau \rightarrow \mu\gamma$ (in a unit of 10^{-8}). The shaded regions are excluded by the current limit of $\tau \rightarrow \mu\gamma$ [$\text{BR}(\tau \rightarrow \mu\gamma) \leq 4.4 \times 10^{-8}$].

B. Productions for charged Higgs boson

In the presence of non-zero ρ_u^{tc} and $\rho_e^{\tau\tau}$, the charged Higgs boson production via $cg \rightarrow bH^+$ shown in Figure 16, decaying into $\tau^+\nu$ ($H^+ \rightarrow \tau^+\nu$) would be very important. As pointed out in Ref. [34], this process is directly related to $\bar{B} \rightarrow D^{(*)}\tau^-\bar{\nu}$ process, and hence the search for this charged Higgs boson production and decay mode would be a crucial probe for the anomaly of $R(D^{(*)})$. The production cross section via $cg \rightarrow bH^+$ is calculated by the calchep [84] with CTEQ leading order PDF,

$$\sigma(pp \rightarrow bH^+ + \bar{b}H^-) = 19 |\rho_u^{tc}|^2 \text{ [pb]}. \quad (90)$$

Therefore the production cross section would be significantly large.

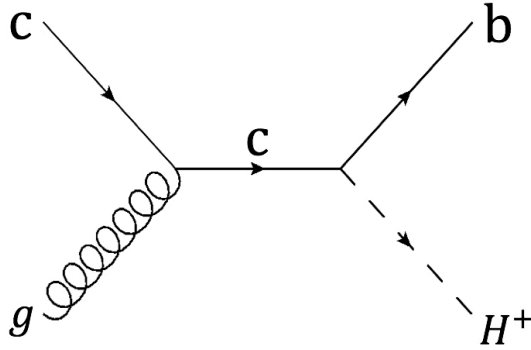


FIG. 16: A Feynman diagram for charged Higgs boson production via $cg \rightarrow b + H^+$ process.

In Figure 17, decay branching ratios for charged Higgs boson H^+ are shown as a function of ρ_u^{tc} . Here we have assumed a reference parameter set with the reference point 1 (solid lines) and the reference point 2 (dashed lines) for Scenario (1) as mentioned in Figure 8. Here the coupling ρ_u^{tt} is also fixed to be 0.1. We note that since the $\rho_e^{\tau\tau}$ coupling in the reference point 1 for Scenario (1) is larger than one for the reference point 2, $\text{BR}(H^+ \rightarrow \tau^+\nu)$ ($\text{BR}(H^+ \rightarrow c\bar{b}, t\bar{b})$) for the reference point 1 is larger (smaller) than one for the reference point 2.

We also note that in Scenario (3), in the presence of $\rho_e^{\mu\tau}$ coupling, the charged Higgs boson can decay via the $\rho_e^{\mu\tau}$ coupling. The decay product, however, is τ

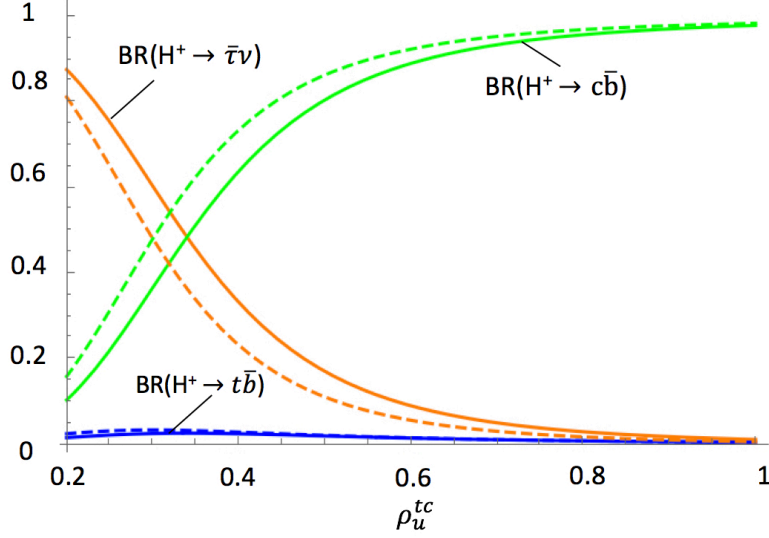


FIG. 17: Decay branching ratios for charged Higgs boson H^+ are shown as a function of ρ_u^{tc} . Here we have taken a reference parameter set with the reference point 1 (solid lines) and the reference point 2 (dashed lines) for Scenario (1) as shown in Figure 8. We also assumed $\rho_u^{tt} = 0.1$.

and ν_μ , where ν_μ can not be observed. Therefore, the decay branching ratio for $\text{BR}(H^+ \rightarrow \tau^+ \nu)$ (where a summation of neutrino flavor is taken into account) does not significantly change, compared to one in Scenario (1), and hence the result for the charged Higgs boson decay branching ratios in Scenario (1) is almost hold in Scenario (3).

We show the cross sections $\sigma(pp \rightarrow bH^+ + \bar{b}H^-) \times \text{BR}(H^\pm)$ [pb] at $\sqrt{s} = 13$ TeV as a function of ρ_u^{tc} and ρ_u^{tt} in Figure 18. In Figure 18, the size of cross sections $\sigma \times \text{BR}$ with $\text{BR}(H^\pm) = \text{BR}(H^\pm \rightarrow \tau^\pm \nu)$, $\text{BR}(H^\pm \rightarrow c\bar{b}, b\bar{c})$ and $\text{BR}(H^\pm \rightarrow t\bar{b}, b\bar{t})$ are shown in solid green lines, dashed purple lines and dotted orange lines, respectively. Here the same parameter set is taken as in Figure 10. For the reference point 2 in Scenario (1), as seen in Figure 17, the cross sections $\sigma(pp \rightarrow bH^+ + \bar{b}H^-) \times \text{BR}(H^\pm)$ with $\text{BR}(H^\pm) = \text{BR}(H^\pm \rightarrow \tau^\pm \nu)$ are slightly smaller, on the other hand, $\sigma(pp \rightarrow bH^+ + \bar{b}H^-) \times \text{BR}(H^\pm)$ with $\text{BR}(H^\pm) = \text{BR}(H^\pm \rightarrow c\bar{b}, b\bar{c})$ and $\text{BR}(H^\pm \rightarrow t\bar{b}, b\bar{t})$ are slightly larger than those for the reference point 1 with fixed values of $\rho_u^{tc, tt}$. As one can see from the figure, the cross sections are significantly large in the interesting

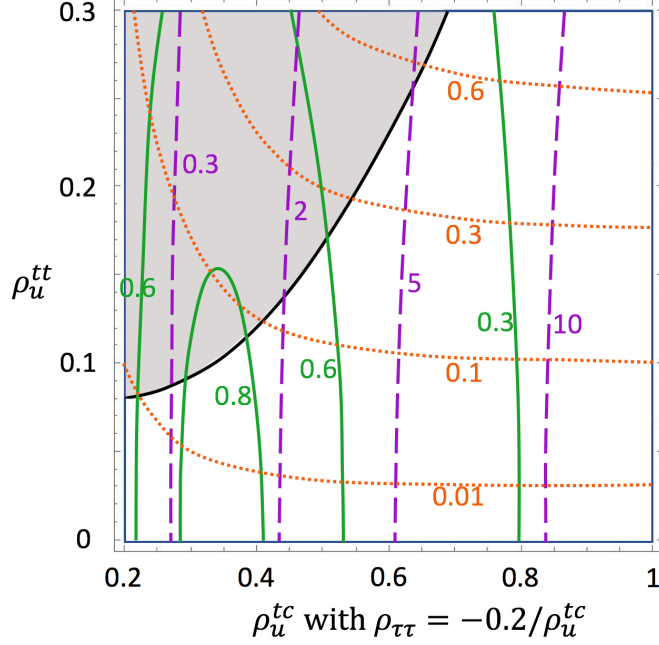


FIG. 18: The cross sections $\sigma(pp \rightarrow bH^+ + \bar{b}H^-) \times \text{BR}(H^\pm)$ (via $cg \rightarrow bH^+$ process) at $\sqrt{s} = 13$ TeV are shown as a function of ρ_u^{tc} and ρ_u^{tt} . The size of cross sections $\sigma \times \text{BR}$ with $\text{BR}(H^\pm) = \text{BR}(H^\pm \rightarrow \tau^\pm \nu)$, $\text{BR}(H^\pm \rightarrow c\bar{b}, b\bar{c})$ and $\text{BR}(H^\pm \rightarrow t\bar{b}, b\bar{t})$ are shown in solid green lines, dashed purple lines and dotted orange lines, respectively. Here the same parameter set is taken as in Figure 10.

regions for $R(D^{(*)})$.

As suggested in Ref. [34], for $pp \rightarrow bH^+ \rightarrow b\tau^+\nu$ process, the main SM background comes from $pp \rightarrow jW^+ \rightarrow j\tau^+\nu$ where j stands for a light quark or a gluon jet misidentified as a b -quark jet, and another background process is $pp \rightarrow bW^+ \rightarrow b\tau^+\nu$. Although the cross sections of these background processes are also large, the p_T distribution of τ for the signal process would be significantly different from those for the background events as discussed in Ref. [34]. In Figure 19, we show p_T distributions of τ for the signal process $pp \rightarrow bH^+ \rightarrow b\tau^+\nu$ (signal) and a background process $pp \rightarrow jW^+ \rightarrow j\tau^+\nu$ (BG1) and another background process $pp \rightarrow bW^+ \rightarrow b\tau^+\nu$ (BG2). For BG1, we have shown numbers of events multiplied by 0.015 because it is motivated by the fact that the light-parton misidentification probability is 1.5% as studied in Ref. [34]. We have imposed $p_T > 20$ GeV for all j , b and τ as motivated by experimental studies. We have taken $m_{H^+} = 500$ GeV,

$\rho_u^{tc} = 0.3$ and $\rho_{\tau\tau} = -0.67$ (the reference point 1 for Scenario (1)). As we can see from the figure, the p_T distribution for the signal events would be significantly different from those for the background events. Therefore, we expect that even current data of the LHC has a potential to discriminate the signal events from the backgrounds.

In addition to the $cg \rightarrow bH^+$ production process, the production processes $bg \rightarrow cH^-$ and $bg \rightarrow tH^-$ would be also important when we have non-zero ρ_u^{tc} and ρ_u^{tt} . The production cross sections via these processes are computed by the calchep [84],

$$\sigma(pp \rightarrow cH^- + \bar{c}H^+) = 15 |\rho_u^{tc}|^2 \text{ [pb]}, \quad (91)$$

$$\sigma(pp \rightarrow tH^- + \bar{t}H^+) = 0.46 |\rho_u^{tt}|^2 \text{ [pb]}. \quad (92)$$

In Figure 20, we show the cross sections $\sigma(pp \rightarrow cH^- + \bar{c}H^+) \times \text{BR}(H^\pm)$ [pb] (via $bg \rightarrow cH^-$ process) [Left] and $\sigma(pp \rightarrow tH^- + \bar{t}H^+) \times \text{BR}(H^\pm)$ [pb] (via $bg \rightarrow tH^-$

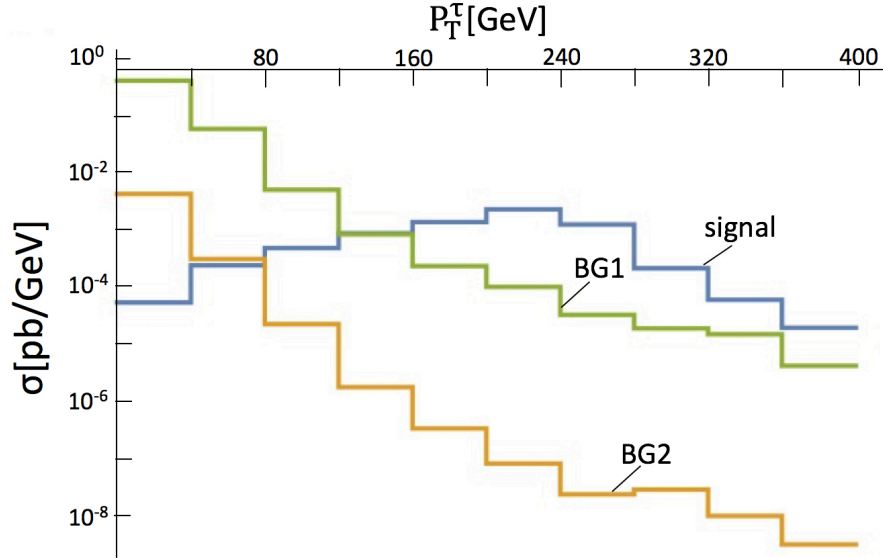


FIG. 19: p_T distributions of τ for the signal process $pp \rightarrow bH^+ \rightarrow b\tau^+\nu$ (signal) and a background process $pp \rightarrow jW^+ \rightarrow j\tau^+\nu$ where j stands for a light quark (or a gluon) jet misidentified as a b-quark jet (BG1) and another background process $pp \rightarrow bW^+ \rightarrow b\tau^+\nu$ (BG2). Here we have assumed the light-parton misidentification probability is 1.5% as studied in Ref. [34], and we have imposed $p_T > 20$ GeV for all j , b and τ . We have taken $m_{H^+} = 500$ GeV, $\rho_u^{tc} = 0.3$ and $\rho_{\tau\tau} = -0.67$ (the reference point 1 for Scenario (1)).

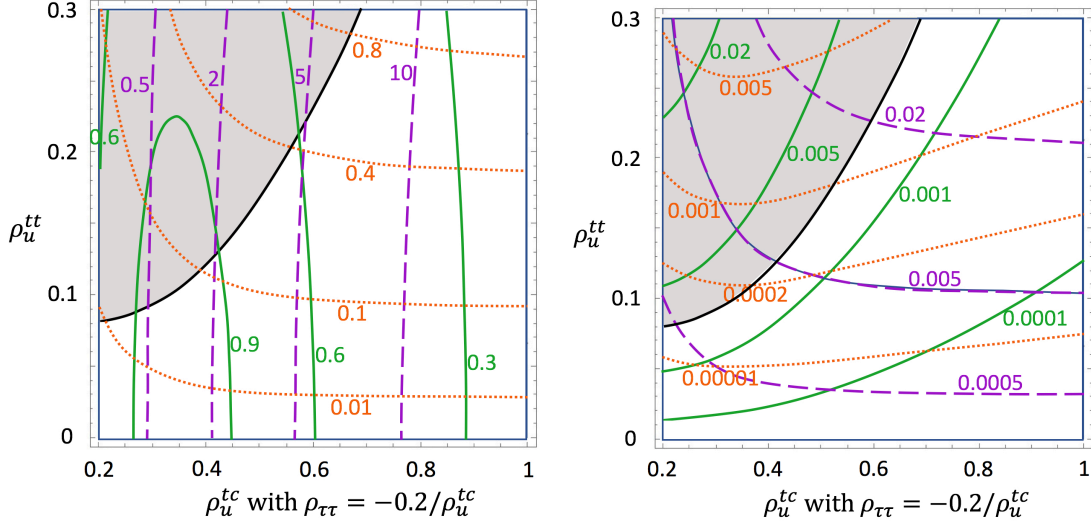


FIG. 20: **[Left]** The cross sections $\sigma(pp \rightarrow cH^- + \bar{c}H^+) \times \text{BR}(H^\pm)$ (via $bg \rightarrow cH^-$ process) and **[Right]** $\sigma(pp \rightarrow tH^- + \bar{t}H^+) \times \text{BR}(H^\pm)$ (via $bg \rightarrow tH^-$ process) at $\sqrt{s} = 13$ TeV are shown as a function of ρ_u^{tc} and ρ_u^{tt} in cases with $\text{BR}(H^\pm) = \text{BR}(H^\pm \rightarrow \tau^\pm \nu)$ (solid green lines), $\text{BR}(H^\pm) = \text{BR}(H^\pm \rightarrow c\bar{b}, b\bar{c})$ (dashed purple lines) and $\text{BR}(H^\pm) = \text{BR}(H^\pm \rightarrow t\bar{b}, b\bar{t})$ (dotted orange lines), respectively. Here the same parameter set is taken as in Figure 10.

process) [Right] at $\sqrt{s} = 13$ TeV as a function of ρ_u^{tc} and ρ_u^{tt} in cases with $\text{BR}(H^\pm) = \text{BR}(H^\pm \rightarrow \tau^\pm \nu)$ (solid green lines), $\text{BR}(H^\pm) = \text{BR}(H^\pm \rightarrow c\bar{b}, b\bar{c})$ (dashed purple lines) and $\text{BR}(H^\pm) = \text{BR}(H^\pm \rightarrow t\bar{b}, b\bar{t})$ (dotted orange lines), respectively. Here the same parameter set is taken as in Figure 10. Although the current LHC experiment has looked for the production via $bg \rightarrow tH^-$ process [85–88], we do not have any constraints from this search mode because the cross section is not so large in the general 2HDM we have discussed here. On the other hand, the cross sections via $bg \rightarrow cH^-$ process are also significantly large, compared with one via $cg \rightarrow bH^-$ process.

The charged Higgs boson production via $c\bar{b} \rightarrow H^+$ would also be significant when ρ_u^{tc} is large. The production cross section via $c\bar{b} \rightarrow H^+$ at $\sqrt{s} = 13$ TeV are calculated by the calchep [84],

$$\sigma(pp \rightarrow H^\pm) = 36 \text{ (16)} |\rho_u^{tc}|^2 \text{ [pb]}, \quad (93)$$

for $m_{H^\pm} = 500$ (600) GeV. Especially when $H^\pm \rightarrow c\bar{b}, b\bar{c}$, this production mode receives constraints from searches for dijet resonances [89]. The constraints are only available for a resonance mass larger than 600 GeV, and the CMS limit at the $\sqrt{s} = 13$ TeV using 27 fb^{-1} data is obtained by

$$\sigma \times \text{BR} \times A \leq 10 \text{ [pb]}, \quad (94)$$

for the resonance mass to be 600 GeV. Here A is the acceptance for narrow resonances with the kinematic requirements $|\Delta\eta_{ij}| < 1.3$ and $|\eta| < 2.5$ and we take $A = 0.6$ as suggested by the CMS collaboration [89]. From Eq. (93), the dijet production cross section in our 2HDM is given by

$$\sigma(pp \rightarrow H^\pm) \times \text{BR}(H^\pm \rightarrow c\bar{b} + b\bar{c}) \times A \leq 10 |\rho_u^{tc}|^2 \text{ [pb]}, \quad (95)$$

for $m_{H^\pm} = 600$ GeV. Therefore, the regions with $|\rho_u^{tc}| \leq 1$ are still consistent with this limit.¹³ The improvement of the dijet resonance search limit in future would also have important impact on this scenario.

In conclusion, the searches for these exotic production and decay processes would be crucial to probe the scenarios for the anomaly of $R(D^{(*)})$. Here we only present interesting theoretical predictions for the production cross sections of heavy neutral and charged Higgs bosons at $\sqrt{s} = 13$ TeV at the LHC. Apparently, more realistic detailed analyses for the LHC physics would be important.

¹³ Other charged Higgs boson production modes such as $\sigma(pp \rightarrow bH^\pm) \times \text{BR}(H^\pm \rightarrow c\bar{b}, b\bar{c})$ and $\sigma(pp \rightarrow cH^\pm) \times \text{BR}(H^\pm \rightarrow c\bar{b}, b\bar{c})$ also receive a constraint from the dijet resonance searches. However, the limit is weaker than one in Eq. (95), because of the smaller cross section.

VI. SUMMARY

The current experimental results have indicated a discrepancy between the measured values and the SM predictions of $R(D^{(*)})$. Since the current knowledge of the SM can not explain the discrepancy, it would be worth studying the possibilities of the extension of the SM. In this paper, we have studied the $R(D^{(*)})$ in a general 2HDM to clarify how large deviations from the SM predictions of $R(D^{(*)})$ are possible by taking into account various flavor physics constraints. We found that it is possible (impossible) to accommodate the 1σ region of the Belle's results if we adopt a constraint $\text{BR}(B_c^- \rightarrow \tau^- \bar{\nu}) \leq 30\%$ ($\text{BR}(B_c^- \rightarrow \tau^- \bar{\nu}) \leq 10\%$). To obtain the large deviations, the masses of the heavy Higgs bosons in the 2HDM should be less than $O(1)$ TeV if the size of new Yukawa couplings is less than $O(1)$. Therefore, a study for a direct production of these heavy Higgs bosons at the LHC experiment is very important.

We have studied the productions and decays of the heavy Higgs bosons at the LHC, and discussed the constraints from the current LHC results and implications at the current and future searches at the LHC. Especially we found that the exotic productions such as $cg \rightarrow t + H/A$ and $cg \rightarrow bH^+$ would be significantly large, and the searches for the exotic decay modes such as $H/A \rightarrow t\bar{c} + c\bar{t}$, $\mu^\pm \tau^\mp$ and $H^+ \rightarrow c\bar{b}$ as well as $H/A \rightarrow \tau^+ \tau^-$ and $H^+ \rightarrow \tau^+ \nu$ would be quite important to probe the interesting parameter regions which generate the sizable deviations from the SM predictions of $R(D^{(*)})$ in the general 2HDM. We have also shown that the p_T distribution of τ lepton in signal events of $pp \rightarrow bH^+ \rightarrow b\tau^+ \nu$ would be significantly different from those in the background events. Therefore, we expect that even the current data of the LHC would have a sensitivity to probe the interesting regions for $R(D^{(*)})$. Therefore, the interplay between the flavor physics and the LHC physics would play a crucial role to reveal the origin of the anomaly of $R(D^{(*)})$.

Note added

After we finished this work, we were aware of new (preliminary) LHCb result on $R_{J/\Psi} = \text{BR}(B_c \rightarrow J/\Psi \tau \bar{\nu})/\text{BR}(B_c \rightarrow J/\Psi \mu \bar{\nu})$ [90], which is another interesting

measurement of lepton flavor universality in $b \rightarrow cl\bar{\nu}$ process. The result is $R_{J/\Psi}^{\text{LHCb}} = 0.71 \pm 0.17 \pm 0.18$ and suggests about 2σ deviation from the SM prediction $R_{J/\Psi}^{\text{SM}} = 0.283 \pm 0.048$ [91]. Our study on $R_{J/\Psi}$ and $R_{\eta_c} = \text{BR}(B_c \rightarrow \eta_c \tau \bar{\nu}) / \text{BR}(B_c \rightarrow \eta_c \mu \bar{\nu})$ (which is possibly another measurement of lepton flavor universality in $b \rightarrow cl\bar{\nu}$ process, and the SM prediction is $R_{\eta_c}^{\text{SM}} = 0.31_{-0.07}^{+0.12}$ [92]) in the general 2HDM shows that $(R_{J/\Psi}, R_{\eta_c}) = (0.287, 0.37)$ at the reference point 1 and $(0.284, 0.39)$ at the reference point 2 in our Scenario (1) and $(R_{J/\Psi}, R_{\eta_c}) = (0.290, 0.35)$ at the reference point 1 and $(0.286, 0.30)$ at the reference point 2 in our Scenario (3), and hence in the general 2HDM, the large deviation for $R_{J/\Psi}$ seems difficult, similar to one for $R(D^*)$, on the other hand, the deviation for R_{η_c} might be larger.

Acknowledgments

We would like to acknowledge Yu Nakano and Masamichi Sakurai for a collaboration at the early stage. We also like to thank C.-P. Yuan for providing model files for CalcHEP and useful discussions. This work was supported in part by JSPS KAKENHI Grant Number JP16K05319.

Appendix A: Higgs (Georgi) Basis

In this Appendix, we show a relation between Higgs (Georgi) basis (which we adopt in our analysis) and general basis of Higgs boson fields in a two Higgs doublet model.

In order to break the standard model gauge symmetry $\text{SU}(3)_C \times \text{SU}(2)_L \times \text{U}(1)_Y$ to $\text{U}(1)_{\text{em}}$, both neutral Higgs boson fields in the $\text{SU}(2)_L$ doublets can get vacuum expectation values (vevs) in general. In the general basis, Yukawa interactions in quarks and leptons are written by

$$\begin{aligned} \mathcal{L}_{\text{Yukawa}} = & -\bar{Q}_L^i \Phi_1 y_{d_1}^{ij} d_R^{'j} - \bar{Q}_L^i \Phi_1 y_{d_2}^{ij} d_R^{'j} - \bar{Q}_L^i \tilde{\Phi}_2 y_{u_1}^{ij} u_R^{'j} - \bar{Q}_L^i \tilde{\Phi}_2 y_{u_2}^{ij} u_R^{'j} \\ & - \bar{L}_L^i \Phi_1 y_{e_1}^{ij} e_R^{'j} - \bar{L}_L^i \Phi_2 y_{e_2}^{ij} e_R^{'j}, \end{aligned} \quad (\text{A1})$$

where i, j denote flavor indices and the summations are taken into account. Here $\tilde{\Phi}_a = i\sigma_2 \Phi_a^*$ ($a = 1, 2$) where σ_2 is a Pauli matrix. We parameterize Higgs boson

doublet fields as follows:

$$\Phi_1 = \begin{pmatrix} \phi_1^+ \\ \frac{v_1 + \phi_1^0 + iG_1^0}{\sqrt{2}} \end{pmatrix}, \quad \Phi_2 = \begin{pmatrix} \phi_2^+ \\ \frac{v_2 + \phi_2^0 + iG_2^0}{\sqrt{2}} \end{pmatrix}, \quad (\text{A2})$$

where both Higgs boson doublets get vevs. We can always perform the following transformation:

$$\begin{pmatrix} H_1 \\ H_2 \end{pmatrix} = \begin{pmatrix} \cos \beta & \sin \beta \\ -\sin \beta & \cos \beta \end{pmatrix} \begin{pmatrix} \Phi_1 \\ \Phi_2 \end{pmatrix}, \quad (\text{A3})$$

where we define a mixing angle β to satisfy

$$\tan \beta = \frac{v_2}{v_1}, \quad v = \sqrt{v_1^2 + v_2^2}, \quad (\text{A4})$$

so that only one of Higgs boson doublets (H_1) receives the vev (v) shown in Eq. (2). This is called Higgs (Georgi) basis. Here $\phi_{1,2}^+$, $G_{1,2}^0$, $\phi_{1,2}^0$ in $\Phi_{1,2}$ are related to G^+ , H^+ , G , A , $\phi_{1,2}$ in $H_{1,2}$ (shown in Eq. (2)) via the transformation in Eq. (A3).

Under the Higgs basis, we rewrite Yukawa interactions in Eq. (A1) as follows:

$$\begin{aligned} \mathcal{L}_{\text{Yukawa}} = & -\bar{Q}_L'^i H_1 Y_{d_1}^{ij} d_R'^j - \bar{Q}_L'^i H_2 Y_{d_2}^{ij} d_R'^j - \bar{Q}_L'^i \tilde{H}_1 Y_{u_1}^{ij} u_R'^j - \bar{Q}_L'^i \tilde{H}_2 Y_{u_2}^{ij} u_R'^j \\ & - \bar{L}_L'^i H_1 Y_{e_1}^{ij} e_R'^j - \bar{L}_L'^i H_2 Y_{e_2}^{ij} e_R'^j, \end{aligned} \quad (\text{A5})$$

where Yukawa couplings $Y_{f_{1,2}}$ are written in terms of original Yukawa couplings $y_{f_{1,2}}$ for $f = d, u, e$ in Eq. (A1),

$$\begin{pmatrix} Y_{f_1} \\ Y_{f_2} \end{pmatrix} = \begin{pmatrix} \cos \beta & \sin \beta \\ -\sin \beta & \cos \beta \end{pmatrix} \begin{pmatrix} y_{f_1} \\ y_{f_2} \end{pmatrix}. \quad (\text{A6})$$

Since only H_1 receives vev, masses of quarks and leptons are induced from the Yukawa couplings Y_{f_1} ($f = d, u, e$). Therefore, we diagonalize the Yukawa couplings Y_{f_1} by biunitary transformations

$$\left(U_{f_L} Y_{f_1} U_{f_R}^\dagger \right)^{ij} = y_f^i \delta^{ij}, \quad (\text{A7})$$

for $f = d, u, e$ in order to obtain the fermion's mass eigenbasis. The mass eigenbasis for the fermions ($f_{L,R}$) is defined by

$$f_{L,R} = U_{f_{L,R}} f'_{L,R}. \quad (\text{A8})$$

Note that the CKM (V) and MNS (V_{MNS}) matrices are defined by $V = U_{u_L} U_{d_L}^\dagger$ and $V_{\text{MNS}} = U_{e_L} U_{\nu_L}^\dagger$ (where we assume that U_{ν_L} diagonalizes the 3×3 left-handed Majorana neutrino mass matrix in the low-energy effective theory), respectively. Comparing these with the Yukawa interactions in Higgs basis (Eq. (2)), the relation between Yukawa couplings in both bases are obtained by

$$\begin{aligned} y_f &= U_{f_L} [y_{f_1} \cos \beta + y_{f_2} \sin \beta] U_{f_R}^\dagger, \\ \rho_f &= U_{f_L} [-y_{f_1} \sin \beta + y_{f_2} \cos \beta] U_{f_R}^\dagger, \end{aligned} \quad (\text{A9})$$

where y_f and ρ_f ($f = d, u, e$) are defined in Higgs basis (Eq. (2)) and y_f is diagonalized and it is related to the fermion mass $y_f^i = \sqrt{2}m_f^i/v$, on the other hand, $y_{f_{1,2}}$ are defined in general basis shown in Eq. (A1).

We stress that any bases can be transferred to the Higgs basis. In general, if there is no symmetry to distinguish Higgs boson doublets Φ_1 and Φ_2 , it is difficult to define the most natural basis without considering the theory beyond the 2HDM. However, it would be useful to discuss the relations between the original basis and Higgs basis in some specific cases. For well-known type I, type II, type X (lepton-specific) and type Y (flipped) 2HDM, for example, an extra Z_2 symmetry restricts the Yukawa interactions in the model,

- Type I ($y_{d_1} = y_{u_1} = y_{e_1} = 0$),
- Type II ($y_{d_2} = y_{u_1} = y_{e_2} = 0$),
- Type X (lepton-specific) ($y_{d_1} = y_{u_1} = y_{e_2} = 0$),
- Type Y (flipped) ($y_{d_2} = y_{u_1} = y_{e_1} = 0$).

As a consequence, the flavor violating Yukawa couplings are not allowed. However, in many cases, such a Z_2 symmetry may not be exact, and hence the symmetry breaking may induce the flavor violating Yukawa couplings. For example, in the Type II 2HDM, the exact Z_2 symmetry forbids the Yukawa couplings y_{d_2} , y_{u_1} and y_{e_2} , as shown above, and hence these Yukawa couplings may be induced as corrections to the Z_2 symmetry breaking. When we write these Z_2 breaking Yukawa couplings as Δy_A ($A = d_2, u_1, e_2$), the relations between the Yukawa couplings in the original

basis and Higgs basis (Eq. (A9)) are written by

$$\begin{aligned} y_f &= U_{f_L} [y_{f_1} \cos \beta + \Delta y_{f_2} \sin \beta] U_{f_R}^\dagger, \\ \rho_f &= U_{f_L} [-y_{f_1} \sin \beta + \Delta y_{f_2} \cos \beta] U_{f_R}^\dagger, \end{aligned} \quad (\text{A10})$$

for $f = d, e$ and

$$\begin{aligned} y_f &= U_{f_L} [\Delta y_{f_1} \cos \beta + y_{f_2} \sin \beta] U_{f_R}^\dagger, \\ \rho_f &= U_{f_L} [-\Delta y_{f_1} \sin \beta + y_{f_2} \cos \beta] U_{f_R}^\dagger, \end{aligned} \quad (\text{A11})$$

for $f = u$. Therefore, we can express the flavor violating Yukawa coupling ρ_f in the Higgs basis in terms of the symmetry breaking Yukawa coupling Δy_A as follows:

$$\begin{aligned} \rho_f &= -y_f \tan \beta + U_{f_L} \Delta y_{f_2} U_{f_R}^\dagger \frac{1}{\cos \beta}, \\ &= -\frac{\sqrt{2}m_f}{v} \tan \beta + U_{f_L} \Delta y_{f_2} U_{f_R}^\dagger \frac{1}{\cos \beta}, \quad \text{for } f = d, e, \end{aligned} \quad (\text{A12})$$

$$\begin{aligned} \rho_f &= y_f \frac{1}{\tan \beta} - U_{f_L} \Delta y_{f_2} U_{f_R}^\dagger \frac{1}{\sin \beta}, \\ &= \frac{\sqrt{2}m_f}{v} \frac{1}{\tan \beta} - U_{f_L} \Delta y_{f_2} U_{f_R}^\dagger \frac{1}{\sin \beta}, \quad \text{for } f = u, \end{aligned} \quad (\text{A13})$$

where y_f is diagonalized in the Higgs basis and it is related to the fermion mass $y_f = \sqrt{2}m_f/v$. One can see that if the Z_2 symmetry is exact ($\Delta y_A = 0$), the Yukawa couplings ρ_f are diagonal and expressed by the fermion mass and $\tan \beta$, and hence the flavor violating components in ρ_f are induced by the Z_2 symmetry breaking Yukawa couplings Δy_A as well as flavor structures of the Yukawa couplings $y_{f_{1,2}}$ in the original basis (in other words, the flavor structures of $U_{f_{L,R}}$). If the mixing matrices $U_{f_{L,R}}$ are very close to the unit matrix, the flavor violating Yukawa couplings ρ_f in the Higgs basis may be directly related to the Z_2 breaking Yukawa couplings Δy_A in the original basis. In general, however, the flavor violation in the Higgs basis is realized by the complex combination of the flavor violations in the original basis.

In our analysis for $R(D^{(*)})$, we adopt the Higgs basis because the flavor violating charged Higgs interactions are simply parameterized by the flavor violating Yukawa couplings ρ_f in the Higgs basis. In order to induce the large deviation in $R(D^{(*)})$ effectively, we consider some simple flavor violation in the Higgs basis. On the other

hand, if we consider the simple flavor violation in the original basis, that may induce the very complex flavor violation in the Higgs basis, and hence that induces not only the flavor violation for $R(D^{(*)})$ but also other flavor violation which may generate strong constraints from other processes. In that sense, we expect that our approach is conservative to see the possibly large effects on $R(D^{(*)})$. Therefore, in our analysis, using the Higgs basis, we try to clarify how large deviations are possible within the framework of the 2HDM in general.

Appendix B: Hadronic matrix elements for $\bar{B} \rightarrow D^{(*)} l \bar{\nu}$

In this Appendix, we summarize hadronic matrix elements for $\bar{B} \rightarrow D^{(*)} l \bar{\nu}$ which we use in our numerical analysis. The formula we use is taken from Refs. [59, 60].¹⁴ The hadronic matrix elements relevant to $\bar{B} \rightarrow D l^- \bar{\nu}$ in the 2HDM are written as

$$\begin{aligned}\langle D(p_D) | \bar{c} \gamma^\mu b | \bar{B}(p_B) \rangle &= \left(p_B^\mu + p_D^\mu - \frac{m_B^2 - m_D^2}{q^2} q^\mu \right) f_+(q^2) + \frac{m_B^2 - m_D^2}{q^2} q^\mu f_0(q^2), \\ \langle D(p_D) | \bar{c} b | \bar{B}(p_B) \rangle &= \frac{m_B^2 - m_D^2}{m_b - m_c} f_0(q^2).\end{aligned}$$

where p_B and p_D (m_B and m_D) are momenta (masses) of B and D mesons, respectively, and q is a momentum transfer $q = p_B - p_D$ ($m_l^2 \leq q^2 \leq (m_B - m_D)^2$), and m_b and m_c are b and c quark masses, respectively. The relevant hadronic matrix elements for $\bar{B} \rightarrow D^* l^- \bar{\nu}$ are given by

$$\begin{aligned}\langle D^*(p_{D^*}, \epsilon) | \bar{c} \gamma_\mu b | \bar{B}(p_B) \rangle &= -i \epsilon_{\mu\nu\rho\sigma} \epsilon^{\nu*} p_B^\rho p_{D^*}^\sigma \frac{2V(q^2)}{m_B + m_{D^*}}, \\ \langle D^*(p_{D^*}, \epsilon) | \bar{c} \gamma_\mu \gamma_5 b | \bar{B}(p_B) \rangle &= \epsilon_\mu^* (m_B + m_{D^*}) A_1(q^2) \\ &\quad - (p_B + p_{D^*})_\mu (\epsilon^* \cdot q) \frac{A_2(q^2)}{m_B + m_{D^*}} - q_\mu (\epsilon^* \cdot q) \frac{2m_{D^*}}{q^2} \{ A_3(q^2) - A_0(q^2) \}, \\ \langle D^*(p_{D^*}, \epsilon) | \bar{c} \gamma_5 b | \bar{B}(p_B) \rangle &= -\frac{1}{m_b + m_c} q_\mu \langle D^*(p_{D^*}, \epsilon) | \bar{c} \gamma^\mu \gamma_5 b | \bar{B}(p_B) \rangle,\end{aligned}$$

where

$$A_3(q^2) = \frac{m_B + m_{D^*}}{2m_{D^*}} A_1(q^2) - \frac{m_B - m_{D^*}}{2m_{D^*}} A_2(q^2).$$

¹⁴ See also Ref. [93].

Here p_{D^*} and m_{D^*} are momentum and mass of D^* , respectively, and q is a momentum transfer $q = p_B - p_{D^*}$.

Here the form factors f_0 , f_+ , V and A_i ($i = 1 - 3$) are given by

$$\begin{aligned}
f_0(q^2) &= \frac{1}{2\sqrt{m_B m_D}} \left[\frac{(m_B + m_D)^2 - q^2}{m_B + m_D} h_+(q^2) - \frac{(m_B - m_D)^2 - q^2}{m_B - m_D} h_-(q^2) \right], \\
f_+(q^2) &= \frac{1}{2\sqrt{m_B m_D}} [(m_B + m_D) h_+(q^2) - (m_B - m_D) h_-(q^2)], \\
V(q^2) &= \frac{m_B + m_{D^*}}{2\sqrt{m_B m_{D^*}}} h_V(q^2), \\
A_0(q^2) &= \frac{1}{2\sqrt{m_B m_{D^*}}} \left[\frac{(m_B + m_{D^*})^2 - q^2}{2m_{D^*}} h_{A1}(q^2) \right. \\
&\quad \left. - \frac{m_B^2 - m_{D^*}^2 + q^2}{2m_B} h_{A2}(q^2) - \frac{m_B^2 - m_{D^*}^2 - q^2}{2m_{D^*}} h_{A3}(q^2) \right], \\
A_1(q^2) &= \frac{(m_B + m_{D^*})^2 - q^2}{2\sqrt{m_B m_{D^*}}(m_B + m_{D^*})} h_{A1}(q^2), \\
A_2(q^2) &= \frac{(m_B + m_{D^*})}{2\sqrt{m_B m_{D^*}}} [h_{3A}(q^2) + r_{D^*} h_{A2}(q^2)],
\end{aligned}$$

where $r_D^{(*)} = m_{D^{(*)}}/m_B$ and the heavy quark effective theory (HQET) form factors are given by

$$\begin{aligned}
h_+(q^2) &= \frac{1}{2[1 + r_D^2 - 2r_D w_D(q^2)]} [-(1 + r_D)^2 \{w_D(q^2) - 1\} V_1(q^2) \\
&\quad + (1 - r_D)^2 \{w_D(q^2) + 1\} S_1(q^2)], \\
h_-(q^2) &= \frac{(1 - r_D^2) \{w_D(q^2) + 1\}}{2[1 + r_D^2 - 2r_D w_D(q^2)]} [S_1(q^2) - V_1(q^2)], \\
h_V(q^2) &= R_{1D^*}(q^2) h_{A1}(q^2), \\
h_{A2}(q^2) &= \frac{R_{2D^*}(q^2) - R_{3D^*}(q^2)}{2r_{D^*}} h_{A1}(q^2), \\
h_{A3}(q^2) &= \frac{R_{2D^*}(q^2) + R_{3D^*}(q^2)}{2} h_{A1}(q^2).
\end{aligned}$$

The q^2 dependence of these form factors comes through $w_{D^{(*)}}(q^2) = \frac{m_B^2 + m_{D^{(*)}}^2 - q^2}{2m_B m_{D^{(*)}}}$,

and

$$\begin{aligned}
V_1(q^2) &= V_1(1) [1 - 8\rho_D^2 Z_D(q^2) + (51\rho_D^2 - 10)Z_D^2(q^2) - (252\rho_D^2 - 84)Z_D^3(q^2)] , \\
S_1(q^2) &= V_1(q^2) \left[1 + \Delta \left\{ -0.019 + 0.041 (w_D(q^2) - 1) - 0.015 (w_D(q^2) - 1)^2 \right\} \right] , \\
h_{A1}(q^2) &= h_{A1}(1) [1 - 8\rho_{D^*}^2 Z_{D^*}(q^2) + (53\rho_{D^*}^2 - 15)Z_{D^*}^2(q^2) - (231\rho_{D^*}^2 - 91)Z_{D^*}^3(q^2)] , \\
R_{1D^*}(q^2) &= R_1(1) - 0.12 \{w_{D^*}(q^2) - 1\} + 0.05 \{w_{D^*}(q^2) - 1\}^2 , \\
R_{2D^*}(q^2) &= R_2(1) + 0.11 \{w_{D^*}(q^2) - 1\} - 0.06 \{w_{D^*}(q^2) - 1\}^2 , \\
R_{3D^*}(q^2) &= 1.22 - 0.052 \{w_{D^*}(q^2) - 1\} + 0.026 \{w_{D^*}(q^2) - 1\}^2 , \\
Z_{D^{(*)}}(q^2) &= \frac{\sqrt{w_{D^{(*)}}(q^2) + 1} - \sqrt{2}}{\sqrt{w_{D^{(*)}}(q^2) + 1} + \sqrt{2}} .
\end{aligned}$$

The numerical values for parameters $\rho_{D^{(*)}}^2$, $R_{1,2}(1)$, Δ , $h_{A1}(1)$ and $V_1(1)$ we use in our numerical analysis are listed in Appendix D.

Appendix C: Various $b \rightarrow s(d)$ transition processes

1. $B_{d,s} - \bar{B}_{d,s}$ mixing

In the presence of $\rho_d^{sb,db}$, $b \rightarrow s(d)$ flavor transition occurs at the tree level. On the other hand, the Yukawa couplings ρ_u^{ti} ($i = t, c, u$) can induce $b \rightarrow s(d)$ transition via a charged Higgs boson mediation at the loop level. Such tree level and loop level flavor transitions would be strongly constrained from $B_{d,s} - \bar{B}_{d,s}$ mixing, such as $B_{d,s}$ meson mass differences, $\Delta m_{B_{d,s}}$. The effective Lagrangian relevant to $B_{d,s} - \bar{B}_{d,s}$ mixing is given by

$$\begin{aligned}
\mathcal{L}_{\text{eff}} &= C_{VLL}^i (\bar{d}_i \gamma^\mu P_L b) (\bar{d}_i \gamma_\mu P_L b) + C_{SLR}^i (\bar{d}_i P_L b) (\bar{d}_i P_R b) \\
&\quad + C_{SLL}^i (\bar{d}_i P_L b) (\bar{d}_i P_L b) + C_{SRR}^i (\bar{d}_i P_R b) (\bar{d}_i P_R b),
\end{aligned} \tag{C1}$$

where $i = 1$ and 2 for $B_d - \bar{B}_d$ and $B_s - \bar{B}_s$, respectively. The contributions induced by the neutral Higgs boson mediations at the tree level are given by

$$(C_{SLR}^i)^{2\text{HDM}} = - \sum_{\phi=h,H,A} \frac{y_{\phi b d_i}^{d*} y_{\phi d_i b}}{m_\phi^2}, \quad (\text{C2})$$

$$(C_{SLL}^i)^{2\text{HDM}} = - \sum_{\phi=h,H,A} \frac{(y_{\phi b d_i}^{d*})^2}{2m_\phi^2}, \quad (\text{C3})$$

$$(C_{SRR}^i)^{2\text{HDM}} = - \sum_{\phi=h,H,A} \frac{(y_{\phi d_i b}^d)^2}{2m_\phi^2}, \quad (\text{C4})$$

where $y_{\phi ij}^f$ is shown in Eqs. (6). The charged Higgs boson generates the contribution to C_{VLL} via ρ_u Yukawa couplings at the one loop level as follows:

$$(C_{VLL}^i)^{2\text{HDM}} = \frac{1}{128\pi^2 m_{H^+}^2} \sum_{k,l} (V^\dagger \rho_u)^{d_i k} (\rho_u^\dagger V)^{lb} \left[(\rho_u^\dagger V)^{kb} (V^\dagger \rho_u)^{d_i l} G_1(x_k, x_l) \right. \\ \left. - \frac{4g^2 m_{u_k} m_{u_l}}{m_{H^+}^2} V_{kb} V_{ld_i}^* G_2(x_k, x_l, x_W) + \frac{g^2 m_{u_k} m_{u_l}}{m_W^2} V_{kb} V_{ld_i}^* G_3(x_k, x_l, x_W) \right], \quad (\text{C5})$$

where $x_k = m_{u_k}^2/m_{H^+}^2$ and $x_W = m_W^2/m_{H^+}^2$. Functions G_x ($x = 1, 2, 3$) are defined by

$$G_1(x, y) = \frac{1}{x-y} \left[\frac{x^2 \log x}{(1-x)^2} + \frac{1}{1-x} - \frac{y^2 \log y}{(1-y)^2} - \frac{1}{1-y} \right], \quad (\text{C6})$$

$$G_2(x, y, z) = -\frac{1}{(x-y)(1-z)} \left[\frac{x \log x}{1-x} - \frac{y \log y}{1-y} - \frac{x \log \frac{x}{z}}{z-x} + \frac{y \log \frac{y}{z}}{z-y} \right], \quad (\text{C7})$$

$$G_3(x, y, z) = -\frac{1}{x-y} \left[\frac{1}{1-z} \left(\frac{x \log x}{1-x} - \frac{y \log y}{1-y} \right) - \frac{z}{1-z} \left(\frac{x \log \frac{x}{z}}{z-x} - \frac{y \log \frac{y}{z}}{z-y} \right) \right]. \quad (\text{C8})$$

From the effective Lagrangian, we can obtain $B_{d,s}$ mass differences, $\Delta m_{B_{d,s}}$,

$$\Delta m_{B_{d_i}} = 2\text{Re} \left[\langle \bar{B}_{d_i} | (-\mathcal{L}_{\text{eff}}) | B_{d_i} \rangle \right], \\ = -2\text{Re}(C_{VLL}) \frac{m_{B_{d_i}} F_{B_{d_i}}^2 B_{B_{d_i}}}{3} - 2\text{Re}(C_{SLR}) \left(\frac{1}{24} + \frac{R}{4} \right) m_{B_{d_i}} F_{B_{d_i}}^2 B_{B_{d_i}} \\ + 2\text{Re}(C_{SLL} + C_{SRR}) \frac{5R m_{B_{d_i}} F_{B_{d_i}}^2 B_{B_{d_i}}}{24}, \quad (\text{C9})$$

where $m_{B_{d_i}}$, $F_{B_{d_i}}$ and $B_{B_{d_i}}$ are a mass, a decay constant and Bag parameter of B_{d_i} meson, respectively, and R is

$$R = \left(\frac{m_{B_s}}{m_s + m_b} \right)^2. \quad (\text{C10})$$

The numerical values of the decay parameters are listed in Appendix D.

2. $b \rightarrow s\gamma$ and $b \rightarrow sl^+l^-$ ($l = e$ and μ)

The effective operators relevant to $b \rightarrow s\gamma$ and $b \rightarrow sl^+l^-$ are given by

$$\mathcal{L}_{\text{eff}} = \frac{4G_F}{\sqrt{2}} V_{tb} V_{ts}^* \left[\frac{e}{16\pi^2} C_7 m_b (\bar{s} \sigma_{\mu\nu} P_R b) F^{\mu\nu} + \frac{g_3}{16\pi^2} C_8 m_b (\bar{s} \sigma_{\mu\nu} T^a P_R b) G^{a,\mu\nu} \right. \\ \left. + \frac{e^2}{16\pi^2} C_{9(l)} (\bar{s} \gamma^\mu P_L b) (\bar{l} \gamma_\mu l) + \frac{e^2}{16\pi^2} C_{10(l)} (\bar{s} \gamma^\mu P_L b) (\bar{l} \gamma_\mu \gamma_5 l) \right], \quad (\text{C11})$$

where l is a charged lepton $l = e$ or μ . The charged Higgs boson contributions with non-zero ρ_u are expressed by

$$C_7^{2\text{HDM}} = \frac{1}{4\sqrt{2}G_F m_{H^+}^2 V_{tb} V_{ts}^*} \sum_i (V^\dagger \rho_u)^{si} (\rho_u^\dagger V)^{ib} [Q_u G_{\sigma 1}(x_i) + Q_{H^+} G_{\sigma 2}(x_i)], \quad (\text{C12})$$

$$C_8^{2\text{HDM}} = \frac{1}{4\sqrt{2}G_F m_{H^+}^2 V_{tb} V_{ts}^*} \sum_i (V^\dagger \rho_u)^{si} (\rho_u^\dagger V)^{ib} G_{\sigma 1}(x_i), \quad (\text{C13})$$

$$C_{9(l)}^{2\text{HDM}} = \frac{1}{2\sqrt{2}G_F m_{H^+}^2 V_{tb} V_{ts}^*} Q_l \sum_i (V^\dagger \rho_u)^{si} (\rho_u^\dagger V)^{ib} [Q_u G_{\gamma 1}(x_i) + Q_{H^+} G_{\gamma 2}(x_i)] \\ + \frac{1}{4\pi\alpha V_{tb} V_{ts}^*} (T_{3l} - 2Q_l s_W^2) \sum_i (V^\dagger \rho_u)^{si} (\rho_u^\dagger V)^{ib} G_Z(x_i), \quad (\text{C14})$$

$$C_{10(l)}^{2\text{HDM}} = \frac{1}{4\pi\alpha V_{tb} V_{ts}^*} (-T_{3l}) \sum_i (V^\dagger \rho_u)^{si} (\rho_u^\dagger V)^{ib} G_Z(x_i), \quad (\text{C15})$$

where $Q_{u,H^+,l}$ are electric charges of up-type quark, charged Higgs boson and charged lepton ($Q_{u,H^+,l} = 2/3, +1, -1$), respectively and $T_{3l} = -1/2$, and various functions are given by

$$G_{\sigma 1}(x) = -\frac{2 + 3x - 6x^2 + x^3 + 6x \log x}{12(1-x)^4}, \quad (\text{C16})$$

$$G_{\sigma 2}(x) = -\frac{1 - 6x + 3x^2 + 2x^3 - 6x^2 \log x}{12(1-x)^4}, \quad (\text{C17})$$

$$G_{\gamma 1}(x) = -\frac{16 - 45x + 36x^2 - 7x^3 + 6(2-3x) \log x}{36(1-x)^4}, \quad (\text{C18})$$

$$G_{\gamma 2}(x) = -\frac{2 - 9x + 18x^2 - 11x^3 + 6x^3 \log x}{36(1-x)^4}, \quad (\text{C19})$$

$$G_Z(x) = \frac{x(1-x+\log x)}{2(1-x)^2}. \quad (\text{C20})$$

We note that a term proportional to $G_{\gamma 1}, \gamma_2$ in $C_{9(l)}^{2\text{HDM}}$ originates from γ penguin contribution, on the other hand, terms proportional to G_Z in $C_{9,10(l)}^{2\text{HDM}}$ come from Z penguin contribution. Therefore, $C_{9,10(l)}^{2\text{HDM}}$ are universal to all lepton flavor l . We also note that in $G_{\gamma 1}(x)$ there is a log-enhancement when x is small.

3. $B_s \rightarrow l^+ l^-$ ($l = \mu$ and τ)

In a general 2HDM, the Yukawa couplings $\rho_d^{sb(bs)}$ induce $B_s \rightarrow l^+ l^-$ process at the tree level, and furthermore non-zero ρ_u Yukawa couplings also generate $B_s \rightarrow l^+ l^-$ process at the one loop level.

The effective operators for $B_s \rightarrow l^+ l^-$ ($l = \mu$ and τ) are parameterized as follows:

$$\begin{aligned} \mathcal{L}_{\text{eff}} = & \frac{G_F^2 m_W^2}{\pi^2} \left[C_{A(l)}^{bs} (\bar{b} \gamma_\mu P_L s) (\bar{l} \gamma^\mu \gamma_5 l) + C_{A(l)}^{bs'} (\bar{b} \gamma_\mu P_R s) (\bar{l} \gamma^\mu \gamma_5 l) \right. \\ & \left. + C_{S(l)}^{bs} (\bar{b} P_L s) (\bar{l} l) + C_{S(l)}^{bs'} (\bar{b} P_R s) (\bar{l} l) + C_{P(l)}^{bs} (\bar{b} P_L s) (\bar{l} \gamma_5 l) + C_{P(l)}^{bs'} (\bar{b} P_R s) (\bar{l} \gamma_5 l) \right]. \end{aligned} \quad (\text{C21})$$

The decay rate is given by

$$\begin{aligned} \Gamma(B_s \rightarrow l^+ l^-) = & \frac{G_F^4 m_W^4}{8\pi^5} f_{B_s}^2 m_{B_s} m_l^2 \sqrt{1 - \frac{4m_l^2}{m_{B_s}^2}} \\ & \times \left[\left| C_{A(l)}^{bs} - C_{A(l)}^{bs'} + \frac{m_{B_s}^2}{2m_l(m_b + m_s)} (C_{P(l)}^{bs} - C_{P(l)}^{bs'}) \right|^2 \right. \\ & \left. + \left| \frac{m_{B_s}^2}{2m_l(m_b + m_s)} (C_{S(l)}^{bs} - C_{S(l)}^{bs'}) \right|^2 \left(1 - \frac{4m_l^2}{m_{B_s}^2} \right) \right]. \end{aligned} \quad (\text{C22})$$

The 2HDM contributions mediated by the neutral Higgs bosons $\phi = h, H, A$ at the tree level are

$$\frac{G_F^2 m_W^2}{\pi^2} (C_{S(l)}^{bs})^{2\text{HDM}} = \sum_\phi \frac{y_{\phi sb}^{d*} \text{Re}(y_{\phi ll}^e)}{m_\phi^2}, \quad (\text{C23})$$

$$\frac{G_F^2 m_W^2}{\pi^2} (C_{S(l)}^{bs'})^{2\text{HDM}} = \sum_\phi \frac{y_{\phi bs}^d \text{Re}(y_{\phi ll}^e)}{m_\phi^2}, \quad (\text{C24})$$

$$\frac{G_F^2 m_W^2}{\pi^2} (C_{P(l)}^{bs})^{2\text{HDM}} = \sum_\phi \frac{i y_{\phi sb}^{d*} \text{Im}(y_{\phi ll}^e)}{m_\phi^2}, \quad (\text{C25})$$

$$\frac{G_F^2 m_W^2}{\pi^2} (C_{P(l)}^{bs'})^{2\text{HDM}} = \sum_\phi \frac{i y_{\phi bs}^d \text{Im}(y_{\phi ll}^e)}{m_\phi^2}. \quad (\text{C26})$$

At the one loop level, the charged Higgs boson via non-zero ρ_u Yukawa couplings can induce the contribution to $C_{A(l)}^{bs}$ which is the same as the effective operator proportional to $C_{10(l)}^{2\text{HDM}}$ discussed in $b \rightarrow sl^+ l^-$ process [Eq. (C15)]:

$$\frac{G_F^2 m_W^2}{\pi^2} (C_{A(l)}^{bs})^{2\text{HDM}} = \frac{4G_F}{\sqrt{2}} V_{tb}^* V_{ts} \frac{\alpha}{4\pi} C_{10(l)}^{2\text{HDM}*}, \quad (\text{C27})$$

which is induced by Z penguin contribution. We note that the expression in Eq. (C15) is correct for $l = \tau$ because it is lepton flavor universal. In addition, in the presence of $\rho_e^{\tau\tau, \mu\tau}$ Yukawa couplings, the box diagram generates the following contribution to $C_{A(\tau)}^{bs}$:

$$\frac{G_F^2 m_W^2}{\pi^2} (C_{A(\tau)}^{bs})^{2\text{HDM}} = -\frac{(\rho_e^\dagger \rho_e)^{\tau\tau} (V^\dagger \rho_u)^{bi} (\rho_u^\dagger V)^{is}}{128\pi^2 m_{H^+}^2} B(x_i), \quad (\text{C28})$$

where $x_i = m_{u_i}^2/m_{H^+}^2$ and the function $B(x)$ is defined by

$$B(x) = \frac{1 - x + x \log x}{(1 - x)^2}. \quad (\text{C29})$$

Appendix D: Various parameters for our numerical analysis

Here we summarize numerical values of various parameters we use in our numerical calculation below.

Quantity	Value	Reference	Quantity	Value	Reference
CKM parameters			parameters for hadronic matrix elements		
λ	0.22506	[94]	ρ_D^2	1.128	[19]
A	0.811	[94]	$\rho_{D^*}^2$	1.205	[19]
$\bar{\rho}$	0.124	[94]	$R_1(1)$	1.404	[19]
$\bar{\eta}$	0.356	[94]	$R_2(1)$	0.854	[19]
B and D meson parameters			Δ	1	[98]
m_{Bd}	5.280 [GeV]	[94]	$h_{A1}(1)$	0.908	[99]
m_{B^-}	5.279 [GeV]	[94]	$V_1(1)$	1.07	[100]
m_{Bs}	5.367 [GeV]	[94]	SM particle masses and G_F		
M_{Bc}	6.275 [GeV]	[94]	m_μ	0.105676 [GeV]	[94]
m_D	1.865 [GeV]	[94]	m_τ	1.77686 [GeV]	
m_{D^*}	2.007 [GeV]	[94]	$m_c(m_c)$	1.27 [GeV]	
τ_{Bd}	2.309×10^{12} [GeV $^{-1}$]	[94]	m_t	173.21 [GeV]	
$f_{Bd}\sqrt{B_{Bd}}$	227.7 [MeV]	[95]	$m_d(2\text{GeV})$	0.0047 [GeV]	
τ_{B^-}	2.489×10^{12} [GeV $^{-1}$]	[94]	$m_s(2\text{GeV})$	0.096 [GeV]	
f_{B^-}	186 [MeV]	[96]	$m_b(m_b)$	4.18 [GeV]	
τ_{Bs}	2.294×10^{12} [GeV $^{-1}$]	[94]	m_W	80.385 [GeV]	
$f_{Bs}\sqrt{B_{Bs}}$	274.6 [MeV]	[95]	m_Z	91.188 [GeV]	
τ_{Bc}	7.703×10^{11} [GeV $^{-1}$]	[94]	m_h	125.09 [GeV]	
f_{Bc}	0.434 [GeV]	[97]	G_F	1.166×10^{-5} [GeV $^{-2}$]	

-
- [1] J. P. Lees *et al.* [BaBar Collaboration], “Evidence for an excess of $\bar{B} \rightarrow D^{(*)}\tau^-\bar{\nu}_\tau$ decays,” Phys. Rev. Lett. **109**, 101802 (2012) [arXiv:1205.5442 [hep-ex]].

- [2] J. P. Lees *et al.* [BaBar Collaboration], “Measurement of an Excess of $\bar{B} \rightarrow D^{(*)}\tau^-\bar{\nu}_\tau$ Decays and Implications for Charged Higgs Bosons,” Phys. Rev. D **88**, no. 7, 072012 (2013) [arXiv:1303.0571 [hep-ex]].
- [3] M. Huschle *et al.* [Belle Collaboration], “Measurement of the branching ratio of $\bar{B} \rightarrow D^{(*)}\tau^-\bar{\nu}_\tau$ relative to $\bar{B} \rightarrow D^{(*)}\ell^-\bar{\nu}_\ell$ decays with hadronic tagging at Belle,” Phys. Rev. D **92**, no. 7, 072014 (2015) [arXiv:1507.03233 [hep-ex]].
- [4] Y. Sato *et al.* [Belle Collaboration], “Measurement of the branching ratio of $\bar{B}^0 \rightarrow D^*\tau^-\bar{\nu}_\tau$ relative to $\bar{B}^0 \rightarrow D^*\ell^-\bar{\nu}_\ell$ decays with a semileptonic tagging method,” Phys. Rev. D **94**, no. 7, 072007 (2016) [arXiv:1607.07923 [hep-ex]].
- [5] S. Hirose *et al.* [Belle Collaboration], “Measurement of the τ lepton polarization and $R(D^*)$ in the decay $\bar{B} \rightarrow D^*\tau^-\bar{\nu}_\tau$,” Phys. Rev. Lett. **118**, no. 21, 211801 (2017) [arXiv:1612.00529 [hep-ex]].
- [6] R. Aaij *et al.* [LHCb Collaboration], “Measurement of the ratio of branching fractions $\mathcal{B}(\bar{B}^0 \rightarrow D^*\tau^-\bar{\nu}_\tau)/\mathcal{B}(\bar{B}^0 \rightarrow D^*\mu^-\bar{\nu}_\mu)$,” Phys. Rev. Lett. **115**, no. 11, 111803 (2015) Erratum: [Phys. Rev. Lett. **115**, no. 15, 159901 (2015)] [arXiv:1506.08614 [hep-ex]].
- [7] Talk by Guy Wormster, on behalf of the BaBar and LHCb Collaborations at “The 15th meeting in the conference series of Flavor Physics & CP Violation (FPCP 2017)” in June 2017, at Prague, Czech Republic.
- [8] S. Wehle *et al.* [Belle Collaboration], “Lepton-Flavor-Dependent Angular Analysis of $B \rightarrow K^*\ell^+\ell^-$,” Phys. Rev. Lett. **118**, no. 11, 111801 (2017) [arXiv:1612.05014 [hep-ex]].
- [9] The ATLAS collaboration [ATLAS Collaboration], “Angular analysis of $B_d^0 \rightarrow K^*\mu^+\mu^-$ decays in pp collisions at $\sqrt{s} = 8$ TeV with the ATLAS detector,” ATLAS-CONF-2017-023.
- [10] CMS Collaboration [CMS Collaboration], “Measurement of the P_1 and P_5' angular parameters of the decay $B^0 \rightarrow K^{*0}\mu^+\mu^-$ in proton-proton collisions at $\sqrt{s} = 8$ TeV,” CMS-PAS-BPH-15-008.
- [11] J. P. Lees *et al.* [BaBar Collaboration], “Measurement of angular asymmetries in the decays $B \rightarrow K^*l^+l^-$,” Phys. Rev. D **93**, no. 5, 052015 (2016) [arXiv:1508.07960 [hep-ex]].
- [12] R. Aaij *et al.* [LHCb Collaboration], “Angular analysis of the $B^0 \rightarrow K^{*0}\mu^+\mu^-$ decay

- using 3 fb^{-1} of integrated luminosity,” JHEP **1602**, 104 (2016) [arXiv:1512.04442 [hep-ex]].
- [13] R. Aaij *et al.* [LHCb Collaboration], “Test of lepton universality using $B^+ \rightarrow K^+ \ell^+ \ell^-$ decays,” Phys. Rev. Lett. **113**, 151601 (2014) [arXiv:1406.6482 [hep-ex]]; R. Aaij *et al.* [LHCb Collaboration], “Test of lepton universality with $B^0 \rightarrow K^{*0} \ell^+ \ell^-$ decays,” [arXiv:1705.05802 [hep-ex]].
- [14] For the current status, for example, see M. Davier, A. Hoecker, B. Malaescu and Z. Zhang, “Reevaluation of the hadronic vacuum polarisation contributions to the Standard Model predictions of the muon g-2 and $\alpha(m_Z)$ using newest hadronic cross-section data,” [arXiv:1706.09436 [hep-ph]]; K. Hagiwara, A. Keshavarzi, A. D. Martin, D. Nomura and T. Teubner, “g-2 of the muon: status report,” Nucl. Part. Phys. Proc. **287-288**, 33 (2017); F. Jegerlehner, “Muon g-2 Theory: the Hadronic Part,” [arXiv:1705.00263 [hep-ph]].
- [15] Y. Omura, E. Senaha and K. Tobe, “Lepton-flavor-violating Higgs decay $h \rightarrow \mu\tau$ and muon anomalous magnetic moment in a general two Higgs doublet model,” JHEP **1505**, 028 (2015) [arXiv:1502.07824 [hep-ph]].
- [16] Y. Omura, E. Senaha and K. Tobe, “ τ - and μ -physics in a general two Higgs doublet model with $\mu - \tau$ flavor violation,” Phys. Rev. D **94**, no. 5, 055019 (2016) [arXiv:1511.08880 [hep-ph]].
- [17] K. Tobe, “Michel parameters for τ decays $\tau \rightarrow l\nu\bar{\nu}$ ($l = e, \mu$) in a general two Higgs doublet model with $\mu - \tau$ flavor violation,” JHEP **1610**, 114 (2016) doi:10.1007/JHEP10(2016)114 [arXiv:1607.04447 [hep-ph]].
- [18] The CMS Collaboration, “Search for lepton flavor violating decays of the Higgs boson to $\mu\tau$ and $e\tau$ in proton-proton collisions at $\sqrt{s} = 13 \text{ TeV}$,” CMS Physics Analysis Summary, CMS PAS HIG-17-001. See also V. Khachatryan *et al.* [CMS Collaboration], “Search for Lepton-Flavour-Violating Decays of the Higgs Boson,” Phys. Lett. B **749**, 337 (2015) [arXiv:1502.07400 [hep-ex]]; G. Aad *et al.* [ATLAS Collaboration], “Search for lepton-flavour-violating decays of the Higgs and Z bosons with the ATLAS detector,” Eur. Phys. J. C **77**, no. 2, 70 (2017) [arXiv:1604.07730 [hep-ex]].
- [19] Y. Amhis *et al.*, “Averages of b -hadron, c -hadron, and τ -lepton properties as of

- summer 2016,” [arXiv:1612.07233 [hep-ex]]. See also Heavy Flavor Averaging Group web page for the latest average: “<http://www.slac.stanford.edu/xorg/hfag/>”
- [20] S. Fajfer, J. F. Kamenik and I. Nisandzic, “On the $B \rightarrow D^* \tau \bar{\nu}_\tau$ Sensitivity to New Physics,” Phys. Rev. D **85**, 094025 (2012) [arXiv:1203.2654 [hep-ph]].
 - [21] J. A. Bailey *et al.* [MILC Collaboration], “ $B \rightarrow Dl$ form factors at nonzero recoil and $|V_{cb}|$ from 2+1-flavor lattice QCD,” Phys. Rev. D **92**, no. 3, 034506 (2015) [arXiv:1503.07237 [hep-lat]].
 - [22] H. Na *et al.* [HPQCD Collaboration], “ $B \rightarrow Dl\nu$ form factors at nonzero recoil and extraction of $|V_{cb}|$,” Phys. Rev. D **92**, no. 5, 054510 (2015) Erratum: [Phys. Rev. D **93**, no. 11, 119906 (2016)] [arXiv:1505.03925 [hep-lat]].
 - [23] D. Bigi and P. Gambino, “Revisiting $B \rightarrow D\ell\nu$,” Phys. Rev. D **94**, no. 9, 094008 (2016) [arXiv:1606.08030 [hep-ph]].
 - [24] D. Bigi, P. Gambino and S. Schacht, “ $R(D^*)$, $|V_{cb}|$, and the Heavy Quark Symmetry relations between form factors,” [arXiv:1707.09509 [hep-ph]].
 - [25] S. Jaiswal, S. Nandi and S. K. Patra, “Extraction of $|V_{cb}|$ from $B \rightarrow D^{(*)} \ell \nu_\ell$ and the Standard Model predictions of $R(D^{(*)})$,” [arXiv:1707.09977 [hep-ph]].
 - [26] M. Tanaka and R. Watanabe, “New physics in the weak interaction of $\bar{B} \rightarrow D^{(*)} \tau \bar{\nu}$,” Phys. Rev. D **87**, no. 3, 034028 (2013) [arXiv:1212.1878 [hep-ph]].
 - [27] P. Biancofiore, P. Colangelo and F. De Fazio, “On the anomalous enhancement observed in $B \rightarrow D^{(*)} \tau \bar{\nu}_\tau$ decays,” Phys. Rev. D **87**, no. 7, 074010 (2013) [arXiv:1302.1042 [hep-ph]].
 - [28] M. Freytsis, Z. Ligeti and J. T. Ruderman, “Flavor models for $\bar{B} \rightarrow D^{(*)} \tau \bar{\nu}$,” Phys. Rev. D **92**, no. 5, 054018 (2015) [arXiv:1506.08896 [hep-ph]].
 - [29] A. K. Alok, D. Kumar, S. Kumbhakar and S. U. Sankar, “ D^* polarization as a probe to discriminate new physics in $\bar{B} \rightarrow D^* \tau \bar{\nu}$,” Phys. Rev. D **95**, no. 11, 115038 (2017) [arXiv:1606.03164 [hep-ph]].
 - [30] D. Bardhan, P. Byakti and D. Ghosh, “A closer look at the R_D and R_{D^*} anomalies,” JHEP **1701**, 125 (2017) [arXiv:1610.03038 [hep-ph]].
 - [31] A. Celis, M. Jung, X. Q. Li and A. Pich, “Scalar contributions to $b \rightarrow c(u) \tau \nu$ transitions,” [arXiv:1612.07757 [hep-ph]].
 - [32] D. Choudhury, A. Kundu, R. Mandal and R. Sinha, “Minimal unified resolution to

- $R_{K^{(*)}}$ and $R(D^{(*)})$ anomalies with lepton mixing,” [arXiv:1706.08437 [hep-ph]].
- [33] D. A. Faroughy, A. Greljo and J. F. Kamenik, “Confronting lepton flavor universality violation in B decays with high- p_T tau lepton searches at LHC,” Phys. Lett. B **764**, 126 (2017) [arXiv:1609.07138 [hep-ph]].
 - [34] W. Altmannshofer, P. S. B. Dev and A. Soni, “ $R_{D^{(*)}}$ anomaly: A possible hint for natural supersymmetry with R -parity violation,” [arXiv:1704.06659 [hep-ph]].
 - [35] A. Crivellin, C. Greub and A. Kokulu, “Explaining $B \rightarrow D\tau\nu$, $B \rightarrow D^*\tau\nu$ and $B \rightarrow \tau\nu$ in a 2HDM of type III,” Phys. Rev. D **86**, 054014 (2012) [arXiv:1206.2634 [hep-ph]].
 - [36] A. Celis, M. Jung, X. Q. Li and A. Pich, “Sensitivity to charged scalars in $B \rightarrow D^{(*)}\tau\nu_\tau$ and $B \rightarrow \tau\nu_\tau$ decays,” JHEP **1301**, 054 (2013) [arXiv:1210.8443 [hep-ph]].
 - [37] A. Crivellin, A. Kokulu and C. Greub, “Flavor-phenomenology of two-Higgs-doublet models with generic Yukawa structure,” Phys. Rev. D **87**, no. 9, 094031 (2013) [arXiv:1303.5877 [hep-ph]].
 - [38] A. Crivellin, J. Heeck and P. Stoffer, “A perturbed lepton-specific two-Higgs-doublet model facing experimental hints for physics beyond the Standard Model,” Phys. Rev. Lett. **116**, no. 8, 081801 (2016) [arXiv:1507.07567 [hep-ph]].
 - [39] J. M. Cline, “Scalar doublet models confront τ and b anomalies,” Phys. Rev. D **93**, no. 7, 075017 (2016) [arXiv:1512.02210 [hep-ph]].
 - [40] R. Alonso, B. Grinstein and J. Martin Camalich, “The lifetime of the B_c^- meson and the anomalies in $B \rightarrow D^{(*)}\tau\nu$,” Phys. Rev. Lett. **118**, no. 8, 081802 (2017) [arXiv:1611.06676 [hep-ph]].
 - [41] H. Georgi and D. V. Nanopoulos, “Suppression of Flavor Changing Effects From Neutral Spinless Meson Exchange in Gauge Theories,” Phys. Lett. **82B**, 95 (1979).
 - [42] J. F. Donoghue and L. F. Li, “Properties of Charged Higgs Bosons,” Phys. Rev. D **19**, 945 (1979).
 - [43] L. Lavoura and J. P. Silva, “Fundamental CP violating quantities in a $SU(2) \times U(1)$ model with many Higgs doublets,” Phys. Rev. D **50**, 4619 (1994) [hep-ph/9404276].
 - [44] L. Lavoura, “Signatures of discrete symmetries in the scalar sector,” Phys. Rev. D **50**, 7089 (1994) [hep-ph/9405307].

- [45] F. J. Botella and J. P. Silva, “Jarlskog - like invariants for theories with scalars and fermions,” *Phys. Rev. D* **51**, 3870 (1995) [hep-ph/9411288].
- [46] G. C. Branco, L. Lavoura and J. P. Silva, “CP Violation,” *Int. Ser. Monogr. Phys.* **103**, 1 (1999).
- [47] S. Davidson and H. E. Haber, “Basis-independent methods for the two-Higgs-doublet model,” *Phys. Rev. D* **72**, 035004 (2005) Erratum: [*Phys. Rev. D* **72**, 099902 (2005)] [hep-ph/0504050].
- [48] J. Liu and L. Wolfenstein, “Spontaneous CP Violation in the $SU(2)_L \times U(1)_Y$ Model with Two Higgs Doublets,” *Nucl. Phys. B* **289**, 1 (1987).
- [49] T. P. Cheng and M. Sher, “Mass Matrix Ansatz and Flavor Nonconservation in Models with Multiple Higgs Doublets,” *Phys. Rev. D* **35**, 3484 (1987).
- [50] M. J. Savage, “Constraining flavor changing neutral currents with $B \rightarrow \mu^+ \mu^-$,” *Phys. Lett. B* **266**, 135 (1991).
- [51] W. S. Hou, “Tree level $t \rightarrow ch$ or $h \rightarrow t\bar{c}$ decays,” *Phys. Lett. B* **296**, 179 (1992).
- [52] A. Antaramian, L. J. Hall and A. Rasin, “Flavor changing interactions mediated by scalars at the weak scale,” *Phys. Rev. Lett.* **69**, 1871 (1992) [hep-ph/9206205].
- [53] L. J. Hall and S. Weinberg, “Flavor changing scalar interactions,” *Phys. Rev. D* **48**, R979 (1993) [hep-ph/9303241].
- [54] M. E. Luke and M. J. Savage, “Flavor changing neutral currents in the Higgs sector and rare top decays,” *Phys. Lett. B* **307**, 387 (1993) [hep-ph/9303249].
- [55] D. Atwood, L. Reina and A. Soni, “Probing flavor changing top - charm - scalar interactions in e^+e^- collisions,” *Phys. Rev. D* **53**, 1199 (1996) [hep-ph/9506243].
- [56] D. Atwood, L. Reina and A. Soni, “Phenomenology of two Higgs doublet models with flavor changing neutral currents,” *Phys. Rev. D* **55**, 3156 (1997) [hep-ph/9609279].
- [57] M. Aoki, S. Kanemura, K. Tsumura and K. Yagyu, “Models of Yukawa interaction in the two Higgs doublet model, and their collider phenomenology,” *Phys. Rev. D* **80**, 015017 (2009) [arXiv:0902.4665 [hep-ph]].
- [58] V. D. Barger, J. L. Hewett and R. J. N. Phillips, “New Constraints on the Charged Higgs Sector in Two Higgs Doublet Models,” *Phys. Rev. D* **41**, 3421 (1990).
- [59] I. Caprini, L. Lellouch and M. Neubert, “Dispersive bounds on the shape of $\bar{B} \rightarrow D^* l \bar{\nu}$ form-factors,” *Nucl. Phys. B* **530**, 153 (1998) [hep-ph/9712417].

- [60] Y. Sakaki, M. Tanaka, A. Tayduganov and R. Watanabe, “Testing leptoquark models in $\bar{B} \rightarrow D^{(*)}\tau\bar{\nu}$,” Phys. Rev. D **88**, no. 9, 094012 (2013) [arXiv:1309.0301 [hep-ph]].
- [61] A. Abdesselam *et al.* [Belle Collaboration], “Precise determination of the CKM matrix element $|V_{cb}|$ with $\bar{B}^0 \rightarrow D^{*+}\ell^-\bar{\nu}_\ell$ decays with hadronic tagging at Belle,” [arXiv:1702.01521 [hep-ex]].
- [62] H. Belusca-Maio, A. Falkowski, D. Fontes, J. C. Romao and J. P. Silva, “Higgs EFT for 2HDM and beyond,” Eur. Phys. J. C **77**, no. 3, 176 (2017) [arXiv:1611.01112 [hep-ph]].
- [63] The ATLAS and CMS Collaborations, “Measurements of the Higgs boson production and decay rates and constraints on its couplings from a combined ATLAS and CMS analysis of the LHC pp collision data at $\sqrt{s} = 7$ and 8 TeV” JHEP **08** (2016) 045 [arXiv:1606.02266 [hep-ex]].
- [64] V. Khachatryan *et al.* [CMS Collaboration], “Search for top quark decays via Higgs-boson-mediated flavor-changing neutral currents in pp collisions at $\sqrt{s} = 8$ TeV,” JHEP **1702**, 079 (2017) [arXiv:1610.04857 [hep-ex]].
- [65] A. G. Akeroyd and C. H. Chen, “Constraint on the branching ratio of $B_c \rightarrow \tau\nu$ from LEP1 and consequences for $R(D^*)$ anomaly,” [arXiv:1708.04072 [hep-ph]].
- [66] X. Q. Li, Y. D. Yang and X. Zhang, “Revisiting the one leptoquark solution to the $R(D^{(*)})$ anomalies and its phenomenological implications,” JHEP **1608**, 054 (2016) [arXiv:1605.09308 [hep-ph]].
- [67] C. Bobeth, A. J. Buras, A. Celis and M. Jung, “Patterns of Flavour Violation in Models with Vector-Like Quarks,” JHEP **1704**, 079 (2017) [arXiv:1609.04783 [hep-ph]].
- [68] S. Descotes-Genon, L. Hofer, J. Matias and J. Virto, “Global analysis of $b \rightarrow s\ell\ell$ anomalies,” JHEP **1606**, 092 (2016) [arXiv:1510.04239 [hep-ph]].
- [69] W. Altmannshofer, C. Niehoff, P. Stangl and D. M. Straub, “Status of the $B \rightarrow K^*\mu^+\mu^-$ anomaly after Moriond 2017,” Eur. Phys. J. C **77**, no. 6, 377 (2017) [arXiv:1703.09189 [hep-ph]].
- [70] S. Chatrchyan *et al.* [CMS Collaboration], “Measurement of the $B_s \rightarrow \mu^+\mu^-$ branching fraction and search for $B_0 \rightarrow \mu^+\mu^-$ with the CMS Experiment,” Phys. Rev. Lett. **111**, 101804 (2013) [arXiv:1307.5025 [hep-ex]].

- [71] R. Aaij *et al.* [LHCb Collaboration], “Measurement of the $B_s^0 \rightarrow \mu^+ \mu^-$ branching fraction and effective lifetime and search for $B^0 \rightarrow \mu^+ \mu^-$ decays,” *Phys. Rev. Lett.* **118**, no. 19, 191801 (2017) [arXiv:1703.05747 [hep-ex]].
- [72] A. J. Buras, R. Fleischer, J. Girrbach and R. Knegjens, “Probing New Physics with the B_s to $\mu + \mu^-$ Time-Dependent Rate,” *JHEP* **1307**, 77 (2013) [arXiv:1303.3820 [hep-ph]].
- [73] R. Aaij *et al.* [LHCb Collaboration], “Search for the decays $B_s^0 \rightarrow \tau^+ \tau^-$ and $B^0 \rightarrow \tau^+ \tau^-$,” [arXiv:1703.02508 [hep-ex]] *Phys. Rev. Lett.* **118** (2017) 251802.
- [74] C. Bobeth, M. Gorbahn, T. Hermann, M. Misiak, E. Stamou and M. Steinhauser, “ $B_{s,d} \rightarrow l^+ l^-$ in the Standard Model with Reduced Theoretical Uncertainty,” *Phys. Rev. Lett.* **112**, 101801 (2014) [arXiv:1311.0903 [hep-ph]].
- [75] H. Itoh, S. Komine and Y. Okada, “Tauonic B decays in the minimal supersymmetric standard model,” *Prog. Theor. Phys.* **114**, 179 (2005) [hep-ph/0409228].
- [76] U. Nierste, S. Trine and S. Westhoff, “Charged-Higgs effects in a new $B \rightarrow D$ tau nu differential decay distribution,” *Phys. Rev. D* **78**, 015006 (2008) [arXiv:0801.4938 [hep-ph]].
- [77] S. Nandi, S. K. Patra and A. Soni, “Correlating new physics signals in $B \rightarrow D^{(*)} \tau \nu_\tau$ with $B \rightarrow \tau \nu_\tau$,” arXiv:1605.07191 [hep-ph].
- [78] I. Adachi *et al.* [Belle Collaboration], “Evidence for $B^- \rightarrow \tau^- \bar{\nu}_\tau$ with a Hadronic Tagging Method Using the Full Data Sample of Belle,” *Phys. Rev. Lett.* **110**, no. 13, 131801 (2013) [arXiv:1208.4678 [hep-ex]].
- [79] M. Spira, “HIGLU: A program for the calculation of the total Higgs production cross-section at hadron colliders via gluon fusion including QCD corrections,” [hep-ph/9510347].
- [80] G. Aad *et al.* [ATLAS Collaboration], “Search for neutral Higgs bosons of the minimal supersymmetric standard model in pp collisions at $\sqrt{s} = 8$ TeV with the ATLAS detector,” *JHEP* **1411**, 056 (2014) [arXiv:1409.6064 [hep-ex]].
- [81] CMS Collaboration, “Search for additional neutral Higgs bosons decaying to a pair of tau leptons in pp collisions at $\sqrt{s} = 7$ and 8 TeV,” CMS-PAS-HIG-14-029.
- [82] The ATLAS collaboration, “Search for additional heavy neutral Higgs and gauge bosons in the ditau final state produced in 36.1 fb $^{-1}$ of pp collisions at $\sqrt{s} = 13$ TeV

with the ATLAS detector,” ATLAS-CONF-2017-050.

- [83] CMS Collaboration, “Search for a neutral MSSM Higgs boson decaying into $\tau\tau$ with 12.9 fb $^{-1}$ of data at $\sqrt{s} = 13$ TeV,” CMS-PAS-HIG-16-037.
- [84] A. Belyaev, N. D. Christensen and A. Pukhov, “CalcHEP 3.4 for collider physics within and beyond the Standard Model,” Comput. Phys. Commun. **184**, 1729 (2013) [arXiv:1207.6082 [hep-ph]].
- [85] G. Aad *et al.* [ATLAS Collaboration], “Search for charged Higgs bosons decaying via $H^\pm \rightarrow \tau^\pm \nu$ in fully hadronic final states using pp collision data at $\sqrt{s} = 8$ TeV with the ATLAS detector,” JHEP **1503**, 088 (2015) [arXiv:1412.6663 [hep-ex]].
- [86] V. Khachatryan *et al.* [CMS Collaboration], “Search for a charged Higgs boson in pp collisions at $\sqrt{s} = 8$ TeV,” JHEP **1511**, 018 (2015) [arXiv:1508.07774 [hep-ex]].
- [87] The ATLAS collaboration, “Search for charged Higgs bosons in the τ +jets final state using 14.7 fb $^{-1}$ of pp collision data recorded at $\sqrt{s} = 13$ TeV with the ATLAS experiment,” ATLAS-CONF-2016-088.
- [88] CMS Collaboration, “Search for charged Higgs bosons with the $H^\pm \rightarrow \tau^\pm \nu_\tau$ decay channel in the fully hadronic final state at $\sqrt{s} = 13$ TeV,” CMS-PAS-HIG-16-031.
- [89] CMS Collaboration [CMS Collaboration], “Searches for dijet resonances in pp collisions at $\sqrt{s} = 13$ TeV using data collected in 2016.,” CMS-PAS-EXO-16-056.
- [90] Presentation by M. Fontana, on behalf of LHCb Collaboration, LHCC open session CERN, Geneva, 13 September 2017.
- [91] R. Watanabe, “New Physics effect on $B_c \rightarrow J/\psi \tau \bar{\nu}$ in relation to the $R_{D^{(*)}}$ anomaly,” [arXiv:1709.08644 [hep-ph]].
- [92] R. Dutta and A. Bhol, “ $B_c \rightarrow (J/\Psi, \eta_c) \tau \nu$ semileptonic decays within Standard model and beyond,” Phys. Rev. D **96**, no. 7, 076001 (2017) [arXiv:1701.08598 [hep-ph]].
- [93] M. A. Ivanov, J. G. Korner and C. T. Tran, “Analyzing new physics in the decays $\bar{B}^0 \rightarrow D^{(*)} \tau^- \bar{\nu}_\tau$ with form factors obtained from the covariant quark model,” Phys. Rev. D **94**, no. 9, 094028 (2016) [arXiv:1607.02932 [hep-ph]].
- [94] C. Patrignani *et al.* (Particle Data Group), Chin. Phys. C, 40, 100001 (2016).
- [95] A. Bazavov *et al.* [Fermilab Lattice and MILC Collaborations], “ $B_{(s)}^0$ -mixing matrix elements from lattice QCD for the Standard Model and beyond,” Phys. Rev. D **93**,

- no. 11, 113016 (2016) [arXiv:1602.03560 [hep-lat]].
- [96] R. J. Dowdall *et al.* [HPQCD Collaboration], “B-Meson Decay Constants from Improved Lattice Nonrelativistic QCD with Physical u , d , s , and c Quarks,” Phys. Rev. Lett. **110**, no. 22, 222003 (2013) [arXiv:1302.2644 [hep-lat]].
- [97] B. Colquhoun *et al.* [HPQCD Collaboration], “B-meson decay constants: a more complete picture from full lattice QCD,” Phys. Rev. D **91**, no. 11, 114509 (2015) [arXiv:1503.05762 [hep-lat]].
- [98] M. Tanaka and R. Watanabe, “Tau longitudinal polarization in $B \rightarrow D\tau\nu$ and its role in the search for charged Higgs boson,” Phys. Rev. D **82**, 034027 (2010) [arXiv:1005.4306 [hep-ph]].
- [99] J. A. Bailey *et al.* [Fermilab Lattice and MILC Collaborations], “Update of $|V_{cb}|$ from the $\bar{B} \rightarrow D^*\ell\bar{\nu}$ form factor at zero recoil with three-flavor lattice QCD,” Phys. Rev. D **89**, no. 11, 114504 (2014) [arXiv:1403.0635 [hep-lat]].
- [100] M. Okamoto *et al.*, “Semileptonic $D \rightarrow \pi/K$ and $B \rightarrow \pi/D$ decays in 2+1 flavor lattice QCD,” Nucl. Phys. Proc. Suppl. **140**, 461 (2005) [hep-lat/0409116].